ABSOLUTE THERMAL-NEUTRON FISSION YIELDS OF U^{233}

by

Dallas C. Santry, M.Sc.(Dalhousie)

Thesis submitted to the Faculty of Graduate Studies and Research of McGill University in partial fulfilment of the requirements for the Degree of Doctor of Philosophy.

From the Radiochemistry Laboratory,
Department of Chemistry, McGill University,
under the supervision of Dr. Leo Yaffe.

McGill University,
Montreal, Canada

April 1958

ACKNOWLEDGEMENTS

The author wishes to express his sincere gratitude to Professor Leo Yaffe for the stimulating direction and many helpful suggestions offered during the course of this work.

Acknowledgement is made to the National Research Council of Canada for financial assistance in the form of a Studentship and grants-in-aid.

Thanks are also due to the Atomic Energy Control Board and Defense Research Board for additional grants-in-aid.

TABLE OF CONTENTS

Page

ACTIVITIES ISOLATED AND RESULTS

INTRODUCTION

1. The Fission Process

The splitting of a nucleus into roughly equal parts is termed nuclear fission. Although ternary and quaternary fission events have been reported (1), these would be extremely rare. Usually fission implies binary fission and this meaning will apply throughout this thesis.

The fission process was first discovered in 1939 by Hahn and Strassmann (2) who studied the products formed when natural uranium was bombarded with low-energy (thermal) neutrons. Since then fission has been produced by irradiating with protons (3), deuterons (4), alpha particles (5), carbon ions (6), gamma rays (7), and even with π^- mesons (8,9). Lighter elements such as mercury, gold, and platinum (10) have been shown to undergo fission at higher bombarding energies. In general, it is found that the fissionability of a nucleus decreases with decreasing atomic number, and increases with increasing energy of the incident particle.

Most important of the fission reactions is that produced by neutrons. The species U^{232}, U^{233}, U^{235}, Pu^{239}, Am^{241}, and Am^{242} undergo fission with either fast or thermal neutrons, whereas the fission of Th^{232}, Pa^{231}, U^{238}, and presumably other heavy nuclides require fast neutrons.

It is of interest to note that shortly after the discovery of fission, spontaneous fission was detected

experimentally in uranium (11). Later it was found to occur in other heavy nuclides (12). This phenomenon was shown not to be due to cosmic radiation, or to any other known external cause.

A general survey of the early work done on fission was given in 1940 by Turner (13), and then in 1951 by Whitehouse (14), Coryell and Sugarman (15). More recently high-energy fission was reviewed by Spence and Ford (16), and low-energy fission by Glendenin and Steinberg (17). In this thesis we shall be concerned only with the low-energy (thermal) neutron fission of uranium 233.

Uranium 233 is a radioactive nuclide which decays by alpha particle emission with a half-life of 1.62×10^5 years. It does not occur in nature, but can be produced artificially by neutron bombardment of thorium 232, followed by β^- decay processes (18).

$$_{90}Th^{232} + {}_0n^1 \longrightarrow {}_{90}Th^{233} \xrightarrow[23.3\ m.]{\beta^-} {}_{91}Pa^{233} \xrightarrow[27.4\ d.]{\beta^-} {}_{92}U^{233}$$

When U^{233} is placed near a thermal-neutron source, some of the nuclei absorb neutrons to form a highly excited compound nucleus (U^{234}). This then de-excites ($< 10^{-14}$ seconds) in either of two ways. It may get rid of its excess energy through gamma-ray emission, forming the nuclide U^{234}. This nuclide decays by alpha emission with a half-life of 2.48×10^5 years.

$$_{92}U^{233} + {}_{0}n^{1} \longrightarrow (_{92}U^{234}) \longrightarrow {}_{92}U^{234} + \gamma$$

The other alternative for de-excitation of the compound nucleus is by splitting apart into fragments*.

$$_{92}U^{233} + {}_{0}n^{1} \longrightarrow (_{92}U^{234}) \longrightarrow {}_{Z1}X_{1}^{A1} + {}_{Z2}X_{2}^{A2} + \nu\, {}_{0}n^{1} + Q + \gamma,$$

where $_{Z1}X_{1}^{A1}$ is a primary light fission fragment,

$_{Z2}X_{2}^{A2}$ is a primary heavy fission fragment,

ν is the total number of prompt neutrons released in the fission process,

Q is the kinetic energy of the fragments and the neutrons released, and

γ is the electromagnetic energy released in the fission process.

The primary fission fragments X_1^{A1} and X_2^{A2} are so formed that the sum of the mass numbers plus the integral number of neutrons emitted must, for a given pair, be equal to the mass of the compound nucleus.

$$\nu + A1 + A2 = 234$$

Also the sum of the nuclear charges of the complementary fission fragments must be equal to the nuclear charge of the fissioning nucleus.

---

* The probability of a nucleus capturing a neutron and de-exciting by γ-ray emission is called the neutron capture cross section (σ_c), whereas the probability of de-exciting by undergoing fission is the neutron fission cross section (σ_f). With U 233 both modes of de-excitation occur. The sum of σ_c and σ_f equals the neutron absorption cross section ($\sigma_{abs.}$), which gives the total probability of U 233 interacting with a neutron.

$$Z1 + Z2 = 92$$

The most probable mode of thermal neutron fission leads to two fragments with unequal masses, i.e., asymmetric fission (15,19). Physical and chemical studies on the products produced in fission have resulted in the identification of elements ranging from Z = 30 (zinc) to Z = 65 (terbium), and covering the mass range 72 to 161.

The heavy uranium nucleus which undergoes fission contains a greater neutron-to-proton ratio than the stable nuclides with masses corresponding to the nuclei into which it splits. Therefore, the primary fission fragments have an excess of neutrons. They attain nuclear stability by a series of β^- decay processes during which the mass number remains constant.

$$ {}_{Z}X^{A} \xrightarrow{\beta^-} {}_{Z+1}Y^{A} \xrightarrow{\beta^-} {}_{Z+2}Z^{A} $$

Thus, each primary fission fragment gives rise to a decay chain which ends with a stable nuclide. All the products formed in fission, including both those formed directly and those formed from decay of primary fragments, are termed fission products.

2. Fission Yields

Of prime interest in the study of the fission process is the probability of a given nuclide being formed in fission. This is known as fission yield. Since decay chains are produced following fission, it is obvious that all

members of a particular chain, except the first, may be formed in two ways; either by decay of a parent nuclide, or as a primary fragment. Therefore, two types of fission yields can be defined. The total or cumulative fission yield is the percentage of fission events which produce the nuclide in question by direct formation and through decay of its precursors. The independent fission yield is the percentage of fissions which produce the nuclide in question by direct formation as a fission fragment.

3. Charge Distribution in Thermal-Neutron Fission

Independent fission yield measurements provide information on the primary nuclear charge division in the fission process. Such measurements involve:

(a) A determination of which member of a decay chain of a given mass number has the greatest probability of being a primary fission fragment.

(b) A quantitative measure of the variation of charge among fission products of the same mass number.

Independent yields are difficult to measure. At the beginning of a chain where the yields are large, the half-lives of the nuclides are very short. Close to the end of a chain where the half-lives are conveniently long, the yields are usually very small.

There are three methods which may be used to measure independent yields.

(1) Isolate a given fission activity as quickly as possible to minimize formation from β^- decay of a parent. By correcting for what growth does occur from a parent, an independent yield can often be determined.

(2) Determine the cumulative yield of two successive members of a chain and obtain the independent yield of the latter member as the difference between the two.

(3) There are formed in fission several nuclides of one charge higher than a stable nuclide of the same mass number. Independent yields of these "shielded" nuclides can be measured since they should only occur in fission as primary fragments. Their formation by β^- decay in the chain is blocked by the preceding stable member.

The various possibilities for charge distribution in low-energy fission were reviewed by Glendenin (21,22). By assuming that the charge distribution curve is the same for different masses, Glendenin was able to collect the known independent yields for various masses and establish a nuclear charge distribution. It appears as if a redistribution of charge takes place during the fission process. The most probable split results in an equal charge displacement for the light and heavy fragments from the most stable charge for their respective masses.

$$(Z_A - Z_P)_{\text{light fragment}} = (Z_A - Z_P)_{\text{heavy fragment}}$$

The charge (Z_P) for which the yield of a given chain of mass A is a maximum, can be obtained from

$$Z_P = Z_A - 0.5(Z_A + Z_{(A'-\nu-A)} - Z') ,$$

where Z_A is considered to be the value of the most stable charge for nuclides of mass A,

ν is the average number of neutrons emitted per fission, and

A' and Z' are the mass number and charge of the fissioning nucleus.

A modification to the Glendenin hypothesis was proposed by Pappas (23). It had been shown that the prompt neutrons emitted in fission were not emitted from the compound nucleus, but from the fission fragments after the occurrence of the fissioning act (24). Pappas pointed out that the charge distribution must be decided at the moment of fission and that the primary fragments must be considered just after their separation, rather than after the emission of prompt neutrons. In addition, Pappas suggested that the Z_A values used should be those corrected for shell effects*. Consequently, the most probable primary charge (Z_P) for a given mass A would be obtained from

---

* Nuclear shell structure and its effects on fission are discussed later.

$$Z_P = Z_A - 0.5(Z_A + Z_{(A'+1-A)} - Z')$$

where Z_P, A', A and Z' are as before, but Z_A and $Z_{(A'+1-A)}$ values are taken from the curves of maximum stability as given by Coryell et. al. (25,26). The results of Pappas are similar to those of Glendenin except slightly different Z_P values are obtained at shell boundaries. A further modification to the equal charge displacement hypothesis has been given by Kennett and Thode (27). They propose that shell effects should also be considered in the evaluation of Z_P. This was done by postulating a Z_P which would yield the maximum energy release in the fission process. They have calculated $(Z - Z_P)$ for several modes of fission near closed shell configurations and reported that Z_P was shifted near shell closures. The maximum energy release condition, however, predicts shorter chain lengths in the light fragments than in the heavy fragments. It has been suggested (28) that the difference in chain lengths might result from an asymmetric charge distribution near shell closures in both the light and heavy mass region.

It appears as if further independent yield studies are required before the charge distribution in fission can be fully described. An overall picture of the charge distribution in low-energy neutron fission is such that for a given chain, the point of highest yield would represent the most probable primary charge (Z_P) for that mass number. The yield would decrease in either direction in some sort of a symmetrical

probability curve. The indication is that

50 % of the total chain yield occurs for $Z = Z_p$,

25 % of the total chain yield occurs for $Z = Z_p \pm 1$,

2 % of the total chain yield occurs for $Z = Z_p \pm 2$,

and much less for the others. Consequently, the independent fission yield of the last one or two members of any chain may be small compared with the gross yield of the chain. It appears that for all fissile nuclides thus far investigated, a single charge distribution curve is applicable for low-energy fission.

4. Mass Distribution in Thermal-Neutron Fission

The distribution of mass in fission can be studied by measuring the gross yields of the various fission product decay chains. Although the mass yield is the sum of all the independent yields along a chain, the distribution of charge in fission indicates that the yield of any given mass usually may be found by measuring the abundance of a nuclide near the end of the chain. Mass identification is made by separating individual elements and determining the mass number either by using a mass spectrometer or by comparing the nuclide's decay characteristics with those of isotopes of known mass number. A semilogarithmic plot of cumulative yield of a given mass number as a function of mass, gives the characteristic double-humped mass distribution curve. Broad maxima appear near mass 95 (light mass peak) and near mass 135

(heavy mass peak). Between these maxima is a deep central minimum (trough), which shows the low probability of symmetric fission. The curve should be symmetric about the central minimum at a mass

$$\frac{A + 1 - \nu}{2},$$

where A is the mass of the original nucleus, and ν is the number of prompt neutrons emitted. The area under the curve equals 200 %, since two fission fragments are formed per fission.

A review of the earlier yield-mass distribution measurements was given by Coryell and Sugarman (30). More recent data on mass distribution in fission has been collected by Glendenin and Steinberg (31), and Katcoff (20). Figure 1 shows the mass distribution curves as given by Katcoff (March 1956) for the thermal-neutron fission of U^{233} and U^{235}.

5. Delayed-Neutron Emission

Besides finding neutrons which were emitted at the instant of fission, there were also found a small number of neutrons, referred to as delayed neutroms, which continued to come from the uranium after the cessation of neutron bombardment (32). The delayed-neutron emitters are actually β^- emitters which decay to nuclides that are unstable with respect to instantaneous neutron emission. The precursors of the two longest lived emitters have been identified on

Figure 1

Yield-Mass Data for the Fission of
U^{233} and U^{235} by Thermal Neutrons.
(Katcoff's Tabulated Values, March 1956)

● Uranium 233

o Uranium 235

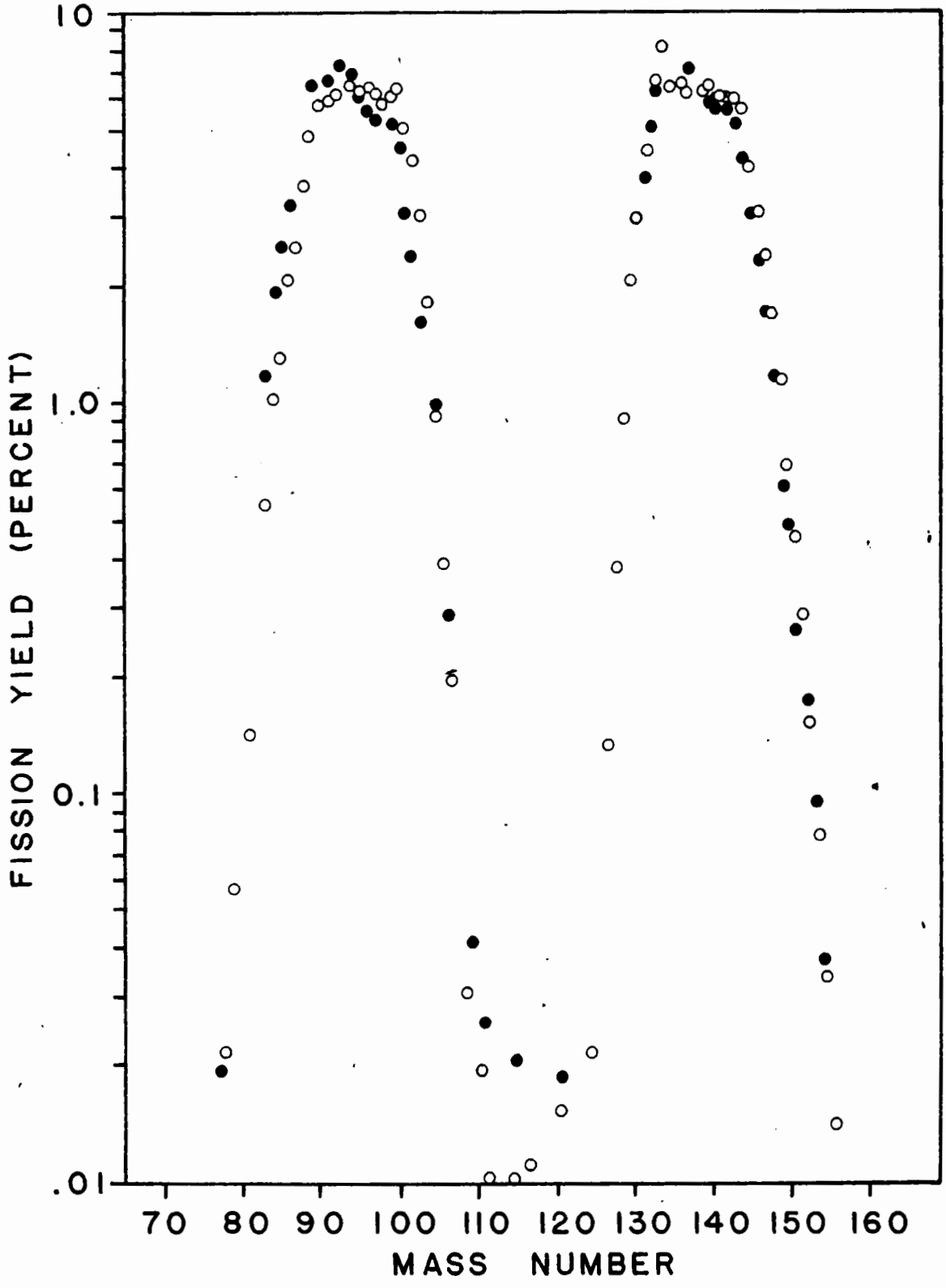
10
1.0
0.1
.01
FISSION YIELD (PERCENT)
70 80 90 100 110 120 130 140 150 160
MASS NUMBER

the basis of chemical separations and observed half-lives as Br^{87}- 54.8 seconds and I^{137}- 22.0 seconds (33). A 5.36 second emitter has chemically been shown to be an isotope of bromine. Studies on the fission fragment range indicated the mass for this nuclide lay in the range 89 to 91 (60). Three other unidentified delayed-neutron emitters have been observed with half-lives of 1.81 seconds, 0.48 seconds, and about 0.18 seconds. On the basis of yield measurements the first has been suggested to be I^{139} and the second Sb^{137} or As^{85} (23).

6. Nuclear Shell Structure

Experimental and theoretical studies have shown that certain numbers of neutrons and protons inside a nucleus constitute stable configurations called closed shells (34). Nuclei with 2, 8, 20, 28, 50, 82 and 126 neutrons or protons are said to possess stable closed shells.

7. Fine Structure in Fission

Early investigators (35,36) supposed that the fission yield curve was a smooth function of mass. In 1947 Thode and Graham (37), and Stanley and Katcoff (38) found that certain measured yields were either too high or too low to lie on the smooth mass distribution curve. Since then other anomalous yields have been reported. These perturbations in the yield-mass curve are referred to as "fine structure". Figure 2 is a magnified section of the yield-mass curves

Figure 2

Fine Structure in the Yield-Mass Data

(Katcoff's Tabulated Values, March 1956)

● Uranium 233

o Uranium 235

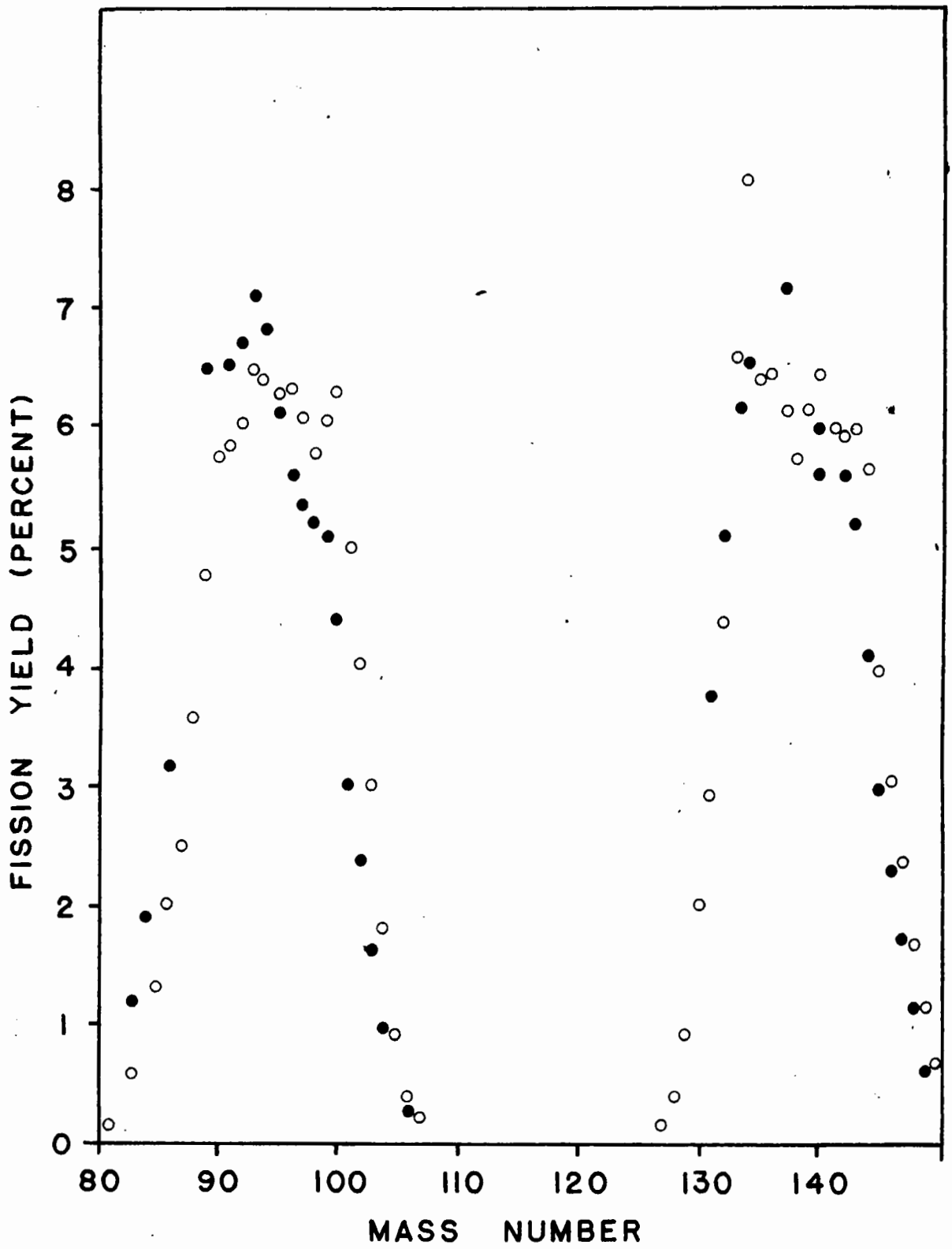
FISSION YIELD (PERCENT)
0
1
2
3
4
5
6
7
8
80
90
100
110
120
130
140
MASS NUMBER

for U^{233} and U^{235}. The yield values, as tabulated by Katcoff (20), suggest that fine structure occurs in the light and heavy mass peaks for both U^{233} and U^{235}. On the basis of the stability of closed nuclear shells, Glendenin (21) explained the observed fine structure in terms of delayed-neutron emission. He postulated that primary fission fragments containing one neutron in excess of a closed shell (i.e., contains 51 or 83 neutrons) may emit this loosely bound neutron rather than undergo β^- emission. This process of extra neutron emission would result in a decrease in the yield of the mass of the shell-plus-one fragment, and an equal increase in yield at the mass of the closed shell fragment.

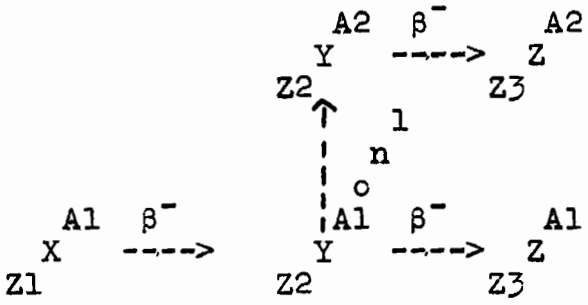

In general, nuclei with 51 or 83 neutrons might be expected to form the majority of the delayed-neutron emitters. Wiles (39) then postulated that fission fragments having closed shells of 50 protons and 82 neutrons must be especially favoured in the fission act itself. Pappas (23) extended post fission emission of neutrons to include nuclei with 83, 85, 87 and 89 neutrons.

8. The Determination of Fission Yields

A. Physical Method

A thin foil of fissionable material is placed between two parallel-plate ionization chambers. This is irradiated with neutrons, and the ionization produced by oppositely directed fission fragment recoils is observed in each chamber. Assuming that the ionization produced by a fission fragment is proportional to its energy, it may be shown that the masses of the recoil fragments are in the inverse ratio of the ionization produced in each. Since the sum of the masses is known, the individual masses of the fragments may be calculated. After observing many fissions, the frequency of occurrence of a given mass may be determined. The double ionization chamber has been used in the study of the fission process by Jentschke (19), Flammersfeld et. al. (40), Deutsch and Ramsey (41). The physical method provides only a qualitative description of the yield-mass curve. The yield measurements have rather large experimental errors, and mass resolution is poor since it represents an average over several mass units.

B. Chemical Method

A sample of fissionable material is irradiated for a period of time and the total number of fissions is measured in some manner. The sample is then analyzed to determine how many atoms of a nuclide have been produced. The number of atoms formed divided by the number of fissions which occurred,

gives a measure of the fission yield. The chemical method has been found to give the best information on fission yield measurements both for charge and mass distribution. Yield measurements may be accurately obtained and mass resolution is certain. The determination of fission yields requires two basic measurements; the number of fissions which have occurred, and the amount of the various nuclides produced in fission.

(a) Fission Rate

The fission rate can be measured either by counting the number of fission events occurring, or by "monitoring" the neutron flux to which the sample is subjected.

(i) Fission Counting

A fission-counter chamber is used in which a thin film and a thick sample of the fissile material are irradiated simultaneously. The fissions occurring in the film during the irradiation are counted in a pulse ionization chamber. The fission products, whose yields are to be determined, are chemically isolated after the end of the irradiation from the thick target. Fission counting has been used by Freedman and Steinberg (42), as well as Engelkemeir, Novey and Schrover (43). The only disadvantages of fission counting are that it is not possible to count for more than a few hours, nor is it possible to place a fission chamber in the high-flux positions of a nuclear reactor.

(ii) Fission Monitors

The first systematic absolute fission yield measurements

by a chemical method were carried out by Anderson, Fermi, and Grosse (44). They irradiated manganese under identical conditions to the uranium sample. Radioactive manganese was produced by the reaction $Mn^{55}(n\gamma)Mn^{56}$. A measurement of the manganese activity and a knowledge of the cross sections for the various reactions involved, enabled the fission rate to be calculated.

Yaffe et. al. (45) have determined the fission rate by using the B^{10} $(n\alpha)$ Li^{7} reaction as a flux monitor. Boron trifluoride was irradiated simultaneously in the same neutron flux as the uranium sample. The change in the B^{10} content was determined with a mass spectrometer by measuring the B^{10}/B^{11} ratio before and after the irradiation. Recently, workers (135) (136) have determined the number of fissions which occurred by measuring the depletion of uranium in a heavily irradiated sample. The indirect determination of fission rates by the use of flux monitors, although simple and accurate, has seldom been used.

(b) Isotopic Abundance Measurements of Fission Products

The chemical method for the study of fission yields has been subdivided on the basis of the analytical procedure used to determine the number of atoms of a fission product formed.

(i) Mass-Spectrometric Analysis

The mass-spectrographic method has been applied to relative isotopic abundance measurements of the fission products. Fairly accurate relative chain yields were determined by measuring stable and very long-lived products

after the decay of essentially all radioactive members of the mass chain. The relative abundances could then be evaluated with the aid of radiochemically determined yields. The earlier mass-spectrometer yields were therefore no more accurate than the yields to which they were normalized. By using an isotope-dilution technique (46), mass spectrometry has been adapted to the determination of absolute yields. Under satisfactory conditions, fission yields determined by the isotope-dilution method are believed reliable to five percent (31). Unfortunately, many of the fission product mass chains cannot be determined by mass-spectrometric methods. This is true of chains which decay to stable or long-lived members which are mono-isotopic, or are abundant in nature and lead to contamination problems. In addition, the bulk of the fission products are radioactive and are not conveniently studied by mass-spectrometric methods. New techniques in mass spectrometry are now being developed which may permit analysis of such nuclides as 50 d- Sr^{89}, 40 d- Ru^{103} and 32 d- Ce^{141} (29).

(ii) Radiochemical Analysis

The different nuclear species of each element present in the sample may be identified by observation of the decay periods of the sample and by analysis of its radiation. The nuclides found have been previously characterized, thus enabling definite mass assignments to be made. The number of atoms of each nuclide formed is calculated from its

disintegration rate and its half-life. Compared to the mass-spectrometric method, fission yields determined radiochemically have been considered more susceptible to errors. The errors are associated with the determination of disintegration rates, and inaccuracies in half-lives, decay schemes, analysis of complex decay curves and chemical stoichiometry. Another possible source of error would be the direct formation of the stable members of the chain which could not be determined radiochemically. By far the most serious error was introduced in the calculation of a disintegration rate from the observed counting rate. Most of the published radiochemical yields have been obtained by the use of end-window Geiger counters. To obtain disintegration rates of the fission product nuclides, it was necessary to apply many absorption and scattering corrections. Such corrections at their best accounted for most of the 10 to 20 % errors quoted for the fission yields. It was therefore realized that accurate fission yields could be obtained radiochemically only by the development of a more precise means for determining disintegration rates.

(c) Relative Fission Yields

Most investigators avoided the direct determination of the fission rate by measuring yields relative to that of another nuclide of known yield. If two nuclides, A and B, are separated from a sample of fissionable material, the yields, Y_A and Y_B, will be related to one another by

$$y_A \propto y_B \frac{N_A}{N_B} ,$$

Where N_A and N_B are the measured amounts of A and B produced. If y_B is known from an absolute determination, the yield y_A can be calculated. Yaffe et. al. (45) have measured the absolute fission yield of Ba^{140} for the thermal-neutron fission of U^{235}. Their value of 6.32 % has an accuracy of about four percent. Most of the U^{235} radiochemical yields were determined relative to Ba^{140}. With the exception of a few absolute measurements, mass-spectrometric yields have been normalized to a radiochemical value determined relative to Ba^{140}. The same is true for the yields of U^{233} with the exception that no accurate yield has been measured to which other yields could be normalized.

9. Disintegration-Rate Determination by 4π-Counting

Recent developments in 4π-counting techniques now make possible the accurate determination of disintegration rates. Pate and Yaffe (48-52) have performed a systematic study of 4π-absolute β counting of solid sources and have reported that for moderate or high-energy emitters, an accuracy of ± 0.5 % may be obtained (53). The improved accuracy in the disintegration-rate determination was made possible by placing the radioactive material inside a gas-ion counter rather than external to it, as was the case with an end-window Geiger counter. The 4π-counting chamber commonly used

is divided symmetrically into two halves, each of which is a self-contained counter unit. The two halves are separated from one another by a film of conducting material. The source is mounted at the center of the film, the central portion of which is thin in order to reduce absorption of the radiation emitted. Thus the radiation enters one half-counter directly without any intervening material, and the other half-counter through a thin layer of source-mounting material. Such a counter is sensitive to radiation emitted over an angle of 4π steradians and is said to have a "4π-geometry". The counter is used as a "flow type" in which the counting gas is constantly replaced. The resolving time of the counter, i.e., the minimum time in which two consecutive ionizing events will be counted, can be made small (~ 5 microseconds). This can be accomplished by operating the counter at a reduced voltage where the amount of ionization collected by the counter is directly proportional to the number of ions formed by the emission of the original ionizing event. The small resolving time makes possible the determination of high counting rates, yet still ensures that any event, subsequent to charged particle emission which occurs within the resolving time of the counter, will not be registered separately. Scattering of radiation either by source material, source mount, gas or counter wall has no effect on the observed counting rate. Secondary radiation such as γ-ray emission or annihilation radiation following

positron emission is not counted provided the secondary radiation occurs within the counter resolving time. The stability and sensitivity of 4π-counting leads to more accurate determinations of half-lives and decay characteristics for active materials. In addition, smaller samples may be measured with better statistical accuracy than with the conventional low-geometry counters. The only sources of error still to be considered in the calculation of a disintegration rate from 4π-counting data are due to:

1. Failure of the counter to respond once to every ionizing particle arising from a nuclear disintegration which reaches the counter gas.
2. Absorption of radiation by the material on which the source is deposited (source-mount absorption).
3. Absorption of radiation by the source material itself (self-absorption).
4. Statistical fluctuations in the disintegration rate of the source and in the background counting rate of the counter.

All the above factors have been studied in this laboratory and the corrections when applicable can accurately be applied for the determination of disintegration rates.

10. Present Work

Fission data provide important information for many cognate studies. Yield measurements have provided the basis

for much of the theoretical work in nuclear physics. Information on the actual fission process can readily be obtained by a study of the resulting fission products. Data describing fine structure in fission provide information directly related to nuclear structure and stability. In addition to many theoretical problems, the yields of fission products are of practical importance in problems relating to the design and operation of nuclear reactors and processing plants. Studies on fine structure make possible an identification of the delayed-neutron emitters. The abundance of these neutron emitters is of great importance in reactor operation. Also the abundance of nuclides having high neutron cross sections is important since they act as reactor "poisons". Such problems as artificial nuclide production, shielding requirements, decontamination and waste disposal, require a knowledge of the distribution of radioactivity in fission.

The thermal neutron fission yields for U^{235} have been investigated extensively. Although the data present an overall picture of the resulting mass distribution in fission, it is probably not accurate enough to permit a detailed examination of the complete yield-mass curve. The large uncertainties in yield measurements make it difficult to determine whether the abnormal yields at certain mass numbers are significant or not. In comparison, data relating to the thermal-neutron fission yields for U^{233} are few and

inconsistent. Fine structure has been reported, but in view of unconfirmed investigations, the uncertainties are probably greater than with the U^{235} studies. One notable example of this is that although an enhanced yield at mass 134 has been reported for U^{235} fission, there is apparently no observed fine structure in this region for U^{233} fission (54,55). This disappearance of fine structure would not have been predicted by any of the hypotheses postulated to explain fine structure in U^{235} fission. It has been assumed that the mass-yield curves for U^{233} and U^{235} are similar in gross structure, but that the most probable yield of the light-mass fragment for U^{233} is displaced, while there is little change in the yields of the heavy fragments (31). Recent investigations indicate that the yields for U^{233} fission are displaced one unit lower in mass for both the light and heavy fragments (56). It was apparent then that much more accurate fission yield measurements were required.

The purpose of this thesis is to establish, radiochemically, accurate fission yields for various nuclides along the yield-mass curve. It was felt that by using 4π β-counting techniques and determining absolute rather than relative yields, the errors associated with radiochemical determinations could be greatly reduced. In addition to indicating fine structure in fission, the absolute yields would enable all previously measured relative yields to be compared on the same basis. Fission studies on U^{233} were chosen since so

few measurements have been made on its fission products. It was also of interest to see if the fine structure for U^{233} fission differed from that reported for U^{235} fission.

EXPERIMENTAL

1. Preparation and Irradiation of Samples

a) Fissile Material

The uranium 233 was obtained on loan from Atomic Energy of Canada Limited in the form of a sulphate solution. An isotopic analysis of the sample was given as

U^{233} ... 97.746 %

U^{238} ... 2.254 %

A spectrographic analysis of impurities was given together with the limits of detection for elements looked for but not found. Results of the analysis are described later for each of the elements separated.

It was desirable to convertthe uranium to the oxide, free from sulphur, to avoid the formation of long-lived activities produced by neutron capture. The uranium solution was first evaporated to dryness in a quartz crucible under an infra-red lamp. The crucible and its contents were placed in an oven and heated for several hours at 110° C., then at 350° C., and finally at 1000° C. until a constant weight was obtained. The final weight of the black oxide (U_3O_8) corresponded exactly to the amount of fissionable material loaned.

Accurately weighed * amounts (2.30 to 6.18 mgm.) of the uranium oxide were sealed into thin quartz capsules for irradiation purposes.

(b) Flux Monitor

Since absolute fission yields were to be measured, the number of fissions which occurred in the uranium during an irradiation had to be known. It was decided that this could best be done radiochemically by simultaneously irradiating the fissile uranium together with a material which would monitor the neutron flux. In choosing a flux monitor the following characteristics were desired.

(i) A mono-isotopic element which could be obtained in pure form.

(ii) The element should have a significant accurately known thermal-neutron capture cross section.

(iii) Upon capturing a neutron the element should form a radioactive nuclide whose decay characteristics are such that an accurate disintegration rate could be determined.

Two elements which adequately met these requirements were Co^{59} and Au^{197} (see Table 1). The use of cobalt as a fission

---

*All weighings in this work were performed on a six decimal place Sartorius MPR5 microbalance.

monitor would require only a very small correction for radio-active decay if counted soon after the irradiation. On the other hand, the cross section for gold is probably more accurately known, since the cobalt cross section was determined relative to that of gold. In the present work cobalt was chosen as the flux monitor. It was felt that the cobalt cross section was sufficiently accurate. If a a better value for the cross section were determined later, it could easily be applied to the results obtained.

TABLE 1

Characteristics of Thermal-Neutron Flux Monitors

Element	Cobalt	Gold
Isotopic Mass	59	197
Isotopic Abundance	100 %	100 %
Thermal-Neutron Cross Section	36.3 barns*	98.7 barns*
Neutron Reaction	$Co^{59}(n\gamma)Co^{60}$	$Au^{197}(n\gamma)Au^{198}$
Half-Life	Co^{60}=5.24-years	Au^{198} = 2.68-days
β End-Point Energy	306 Kev.	963 Kev.

The monitor material was Johnson and Matthey "spec. pure", 0.005 in. cobalt wire. From 1.0 to 1.5 mgm. amounts of the cobalt wire were accurately weighed and sealed into

* σCo^{59} was taken as 36.3 barns (57) after correcting for the more recent value of σAu^{197} = 98.7 barns (58).

thin quartz tubes.

(c) Irradiations with Neutrons

For each irradiation two quartz capsules containing the flux monitors and one containing the fissionable uranium were wrapped individually in a layer of aluminum foil. The three were placed together in an aluminum irradiation container which was then sealed. Irradiations were carried out in a number three, self-serve position of the NRX reactor at Chalk River, Ontario. After an irradiation period of 24 hours, the material was allowed to "cool" for about 36 hours before being treated.

Since the purpose of these experiments was to obtain thermal-neutron fission yields, it was necessary to determine what fraction of fissions may have been caused by the presence of high-energy neutrons. To do this, two separate experiments were performed. The first involved a irradiation in which the quartz vial containing the fissile uranium was completely encased in about 1/2 mm. thickness of cadmium foil. Cadmium strongly absorbs low-energy neutrons. Its thermal-neutron capture cross section is 2.4×10^3 barns. Consequently, thermal neutrons were prevented from reaching the uranium sample when it was surrounded with cadmium. Any fissions which occurred in the shielded sample must have been caused by the presence of fast neutrons. A correction factor, if applicable, is called the fast fission factor. In a second

experiment two capsules were irradiated, each of which contained a known amount of the cobalt wire. One capsule was surrounded by cadmium foil. The effect of this irradiation was to activate one monitor with thermal and fast neutrons, and the other shielded monitor with fast neutrons only.

2. Chemical Procedures

(a) Dissolution of Irradiated Samples

(i) Fissile Material

Great care was taken in dissolving the irradiated uranium. To reduce the loss of volatile halogens, the quartz capsule was placed in a small beaker and covered with a warm nitric acid solution. Before the vial was crushed, one milligram each of appropriate inactive ions was added. The ions used were combinations of Cs^{+}, Ba^{++}, La^{+++} and I^{-} which served to reduce the adsorption loss of activities on the surfaces of glassware. Adsorption losses were further reduced by applying a water repellent coating of Desicote* to all glass which was to come into contact with the concentrated fission produce solution. After the sample had dissolved, it was decanted into a volumetric flask. To recover recoil fission products which may have been embedded in the quartz, the finely crushed remains of the vial were washed several

---

* Desicote is an organo-silicon compound produced by Beckman Instruments, Inc., Fullerton, California.

times with small portions of nitric acid. The washings were added to the dissolved sample which was then made up to a known volume. Measured aliquots of this solution were removed for the chemical separation of the fission products.

(ii) Flux Monitor

The vial containing the flux monitor was opened and the cobalt wire was transferred to a volumetric flask. A few drops of hot concentrated nitric acid were added and the wire dissolved. Enough water was then added to make a known volume of solution. Measured aliquots of the solution were used to determine the disintegration rate of the Co^{60} formed.

(b) Chemical Separations Involving Carrier Techniques

The weight of a product formed in fission is much too small to allow chemical separations by ordinary analytical methods. Usually an inert "carrier" element is added to carry along the activities through the various chemical procedures. In this work a measured amount (from 10 to 20 mgm.) of the element, whose yield was sought, was added to an aliquot of the irradiated sample. Chemical separations were of the semi-micro type which involved analytical methods adapted to the needs of radiochemistry. The use of organic or organo-metallic precipitants and solvent extraction techniques made it possible to pick out rapidly only the particular element of interest. Complete chemical exchange is essential between the inactive carrier and the active element. This presents no problem when the element to be separated has only one valence state. For elements such as iodine or tellurium which have several oxidation states, a series of oxidation-reduction cycles are

performed to get all of the activity and carrier into one valence state. After complete exchange has occurred, the carrier is separated. High chemical recovery is desirable only so that enough carrier plus activity is obtained to make possible accurate counting of activities and determination of the amount of the carrier recovered. The percent recovery of the carrier represents the percent recovery of the active species. In the separation of fission products, decontamination from other elements must be good. Repeated cycles of precipitations or extractions make possible radiochemically pure separations. The addition of soluble carriers, isotopic with the impurities, reduces the amount of undesired activities carried down by co-precipitation or adsorption. These "holdback" carriers merely act as inactive diluents. Further purification can be obtained by the use of scavengers. These are non-specific carriers which show a great tendency to coprecipitate or adsorb. The lower the concentration of impurity, the greater is the scavenging effect. In practice, the scavenger and carrier for the element to be separated are added. Precipitation of the scavenger then removes most of the trace impurities leaving the carrier and activities of interest in solution.

(c) Chemical Yields

The use of carriers in the chemical separation of fission products is generally advisable. It ensures a correction will be made for the loss of any activity which occurs during the separation procedures. There are several factors which control the amount of carrier used in separations.

Accurate disintegration-rate determinations require the counting of sources with high specific activity, i.e., sources with high counting rates but with low solid content. Since the radiation emitted might be absorbed in the source material itself, it is desirable to use "weightless" sources. Therefore, the maximum amount of carrier used in separations is limited by self-absorption considerations. The minimum amount of carrier used is also limited. The least amount of carrier which would permit easy gravimetric determinations is usually 10 to 20 mgm. Smaller amounts of carrier could be used if other methods of separation were employed, such as ion exchange, chromatography, or solvent extraction. The limiting factor then becomes the ability to determine accurately chemical yields at the reduced concentrations. Although special instrumental methods have been developed for the accurate micro determination of some elements, no such methods are known for many of the fission products. Usually the accuracy obtainable by gravimetric analysis in the semimicro region is at least as good as that possible in the micro region. After considering the various factors involved, it was decided that gravimetric chemical yields would be determined. Although the amount of carrier required in the separations would not produce "weightless" sources, self-absorption corrections, when applicable, could be accurately applied. In the procedure used a fission-product

element was separated, dissolved and made up to a known volume. Small aliquots of this solution were removed periodically to be counted. Larger aliquots were also removed and the carrier precipitated. The chemical yield of the carrier was determined by collecting, drying and weighing the precipitate on porcelain micro filtering crucibles. The weight of carrier recovered was compared to the weight of a measured aliquot of the original carrier solution which had been precipitated, dried and weighed under identical conditions. The chemical yield for each separation was determined in triplicate. All carrier stock solutions were standardized periodically.

3. Source Mounting

One of the errors in the determination of disintegration rates by 4π- counting may be due to absorption of radiation in the material used to support the active source. The amount of absorption may be reduced by the use of films of very low superficial density. Pate and Yaffe (48) have described a material and technique suitable for the fabrication of thin films with good chemical and mechanical stability. Their procedure was adopted for the preparation of thin source mounts. Films were made from VYNS resin (polyvinyl-chloride-acetate copolymer) and mounted on aluminum rings 1 mm. thick. The diameter of the mounted films was either 2.5 cm. or 5.0 cm. Each film was made conducting by the gold coating of one side by distillation from a tungsten filament heated to about

1200° C. and at a pressure less than one micron of mercury. Superficial densities of films and gold deposits were determined by optical transmission measurements at 600 m.μ with a Beckman Model DU Spectrophotometer. The method and calibration curves used to relate optical transmission to film and gold thicknesses were those of Pate and Yaffe (48). Superficial densities of films used ranged from 5 to 14 μgm./cm.^{2} Each film had a gold coating of about 5 μgm./cm.^{2}

Active sources were mounted on films by evaporating a measured aliquot of a fission product solution under an infrared lamp. A more evenly spread deposit was obtained by rendering the film surface hydrophilic by treatment with a dilute insulin solution. Under these conditions deposits were distributed uniformly over an area of about 1 cm.^{2} in the center of the film. The use of 20, 50 or 100 λ calibrated micro pipettes together with the above technique permitted source mounting which was reproducible to within the statistical counting errors (usually < 0.5 %).

Gold-plated films, when observed by reflected light from the reverse side to that coated, have a red-purple coloration. Occasionally it was noticed that upon evaporation of a source material, a transparent circle resulted where the source had been deposited. These sources gave erratic counting rates. By applying an additional 3 μgm./cm.^{2} of gold to these sources, normal counting rates were obtained. It was found advisable to mount and dry such sources on the film before adding the gold layer.

4. Counting of Active Samples

For an identification and determination of fission product activities a complete knowledge of nuclear decay schemes is required. As discussed earlier, low-energy neutron fission leads to the formation of nuclides with an excess of neutrons. The active nuclides decay mainly by the emission of β^- particles. Beta-decay processes usually leave nuclei in excited states. The nuclei give up their excitation energy and return to the ground state by the emission of γ radiation. Frequently the transition does not proceed directly from an upper state to the ground state, but may go in several steps involving intermediate excited states. This effect gives rise to the emission of more than one γ-ray. Usually the excited states have a very short life time ($\sim 10^{-14}$ seconds) and the γ-ray emission is said to be in coincidence with the β^- emission. States which have detectable half-lives are called nuclear isomers. The γ transitions from these states are isomeric transitions. Nuclear isomers have the same atomic number as well as mass number but differ in their radioactive properties. Isomeric states other than the ground state are designated by a superscript m (for metastable). In addition to β^- and γ-ray emission, one other decay process is possible with the fission products. Gamma-ray emission may be accompanied or even replaced by the emission of internal-conversion electrons (e^-). Internal conversion is an alternative process for the de-excitation of

a nucleus. It can be thought of as the emission by an active atom of one of its extranuclear electrons rather than a γ-ray. The kinetic energy of the ejected electron is equal to the difference between the γ energy and the binding energy of the electron. The ratio of the rate of the internal conversion process to the rate of γ-ray emission is known as the internal conversion coefficient (α). It was therefore realized that any combination of β^-, e^-, and γ radiations would occur amoung the products to be studied. To count the β^- and e^- radiation a 4π - proportional counter was used. The γ radiation was measured by means of a γ-ray scintillation spectrometer.

A. 4π-Counting

(a) Equipment

The 4π-counting equipment used in this work was essentially that described by Pate and Yaffe (49). Figure 3 shows the counting chamber which consisted of two hemispherical brass cathodes of 7 cm. diameter and two ring shaped anodes of 0.001 in. diameter tungsten wire, Both anodes were insulated from the cathodes by large teflon insulators. A Nichols high voltage supply (AEP 1007B) was used to apply a large positive potential to the anodes, while the cathodes were kept at ground potential. The anodes of the chamber were connected in parallel to an Atomic Instrument pre-amplifier (205-B). The output from this was fed into an Atomic Energy of Canada Ltd. amplifier-discriminator (AEP 1448). The

Figure 3

4π- Counting Chamber

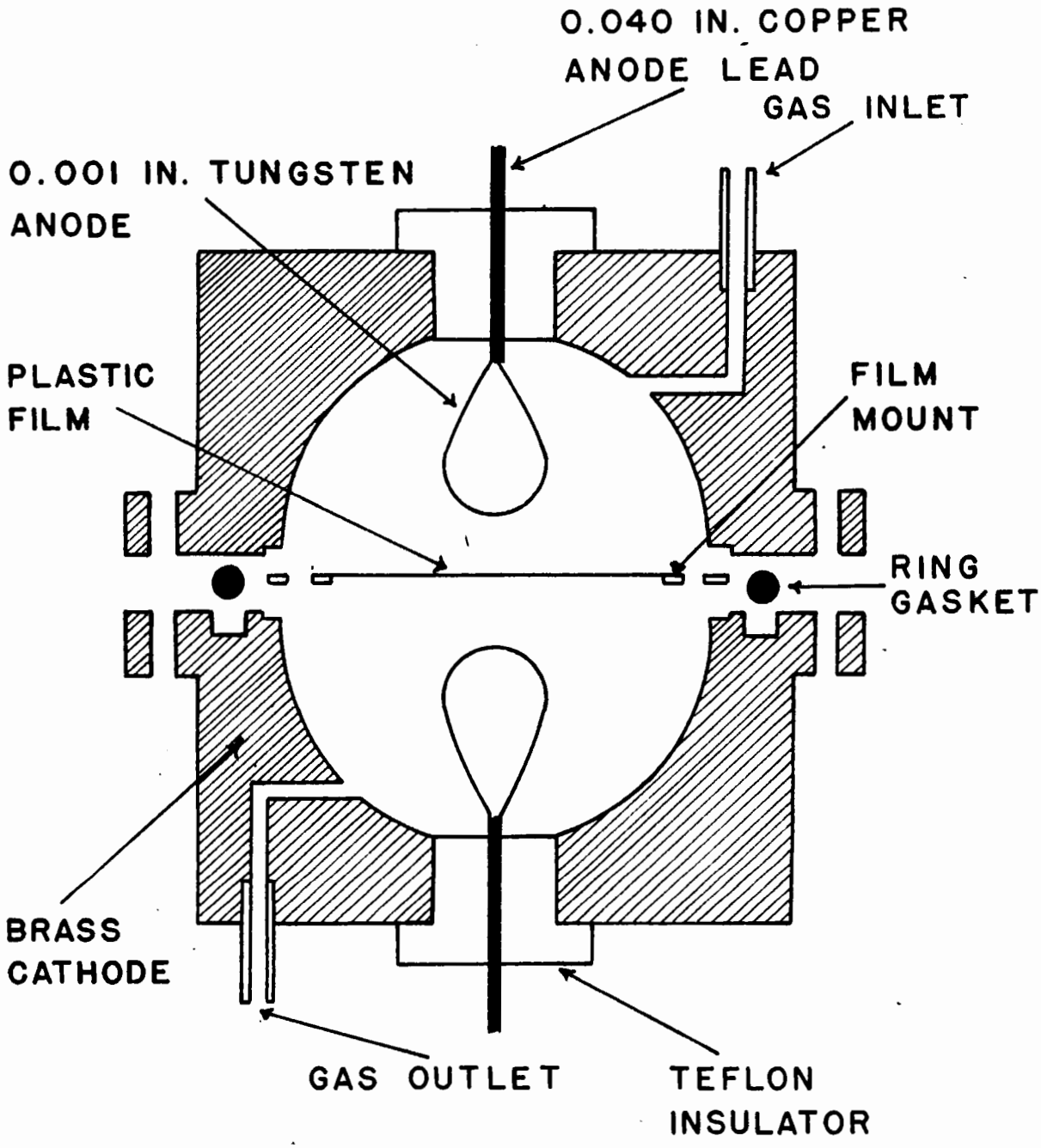
0.040 IN. COPPER
ANODE LEAD
GAS INLET
0.001 IN. TUNGSTEN
ANODE
PLASTIC
FILM
FILM
MOUNT
RING
GASKET
BRASS
CATHODE
GAS OUTLET
TEFLON
INSULATOR

overall gain of the amplifying system was 30,000 and a bias voltage up to 50 volts could be applied to the output signal by the discriminator. Counting rates were recorded on a Marconi scaling unit (AEP 908). Other auxiliary equipment included a Sola constant voltage transformer and a Lambda regulated power supply (model 28). Figure 4 shows a block diagram of the assembled equipment. The counting chamber was operated in the proportional region, the counting gas used being C. P. methane at atmospheric pressure. After insertion of a sample, the counter was flushed for several minutes at a rapid flow rate and then at a rate of about 0.5 ml. of methane per second as measured by a simple flowmeter.

(b) Counter Characteristics

High voltage characteristic curves were obtained for all fission product activities studied in this work. Figure 5 shows curves for a series of sources with increasing maximum β^- energy, taken at a constant discriminator bias. Standard deviations on the measured quantities lie within the areas of the points (this applies to all graphs which follow unless otherwise stated). The plateaus obtained were at least 400 volts long and had a slope less than o.1 % per 100 volts. For disintegration-rate measurements a polarization potential of 2600 volts was chosen. Typical discriminator bias characteristic curves are shown in Figure 6 for nuclides of different maximum β^- energies. These results were taken at a polarization potential of 2600 volts.

Figure 4

Block Diagram of 4π-Counting Assembly

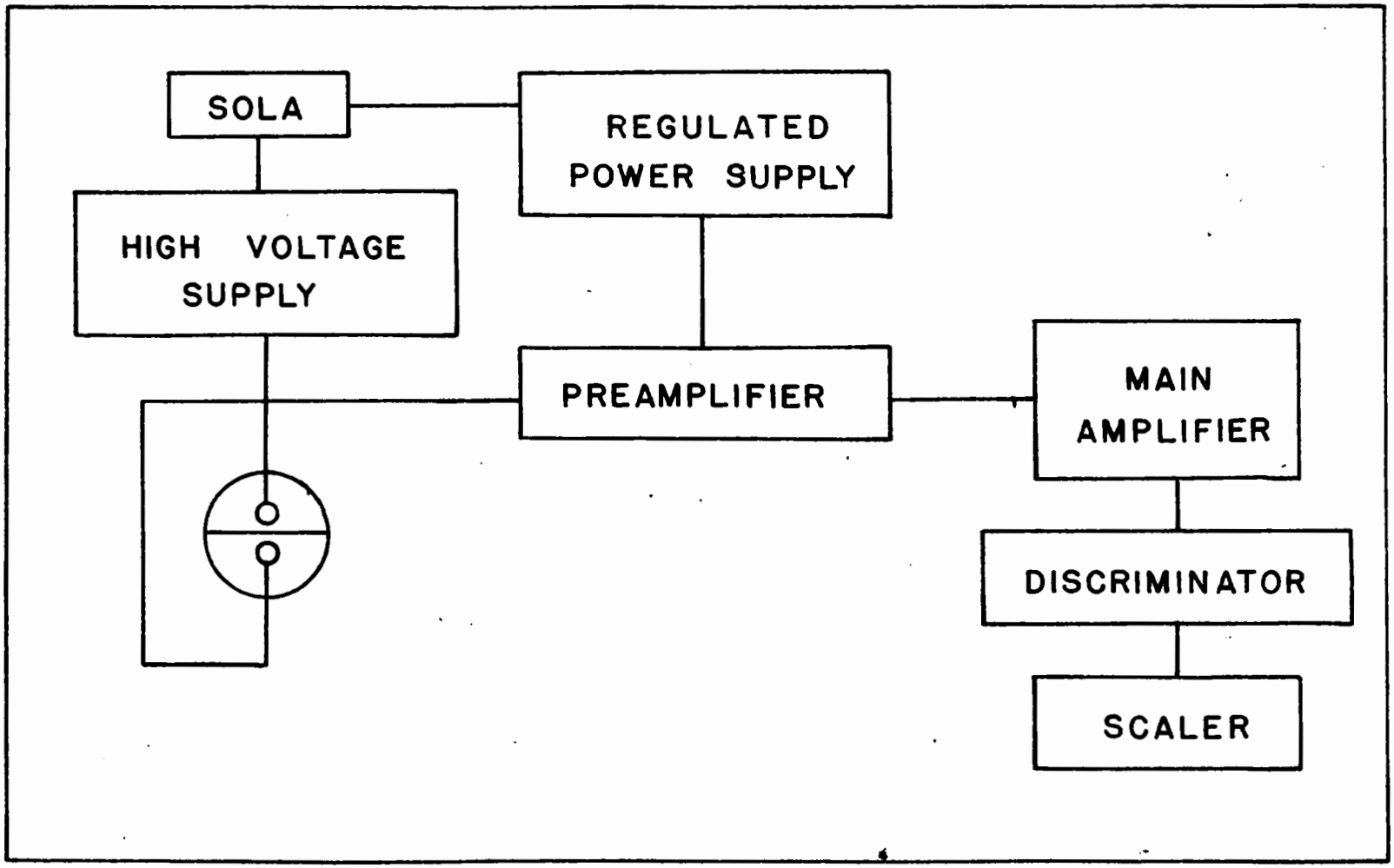
SOLA
REGULATED POWER SUPPLY
HIGH VOLTAGE SUPPLY
PREAMPLIFIER
MAIN AMPLIFIER
DISCRIMINATOR
SCALER

Figure 5

High Voltage Characteristics of the 4π-Counter for β^- Radiation of Increasing Maximum Energy.

2.26 Mev — $(Ba\text{-}La)^{140}$

1.46 Mev — Sr^{89}

1.17 Mev — Ra D+E

317 Kev — Co^{60}

160 Kev — Nb^{95}

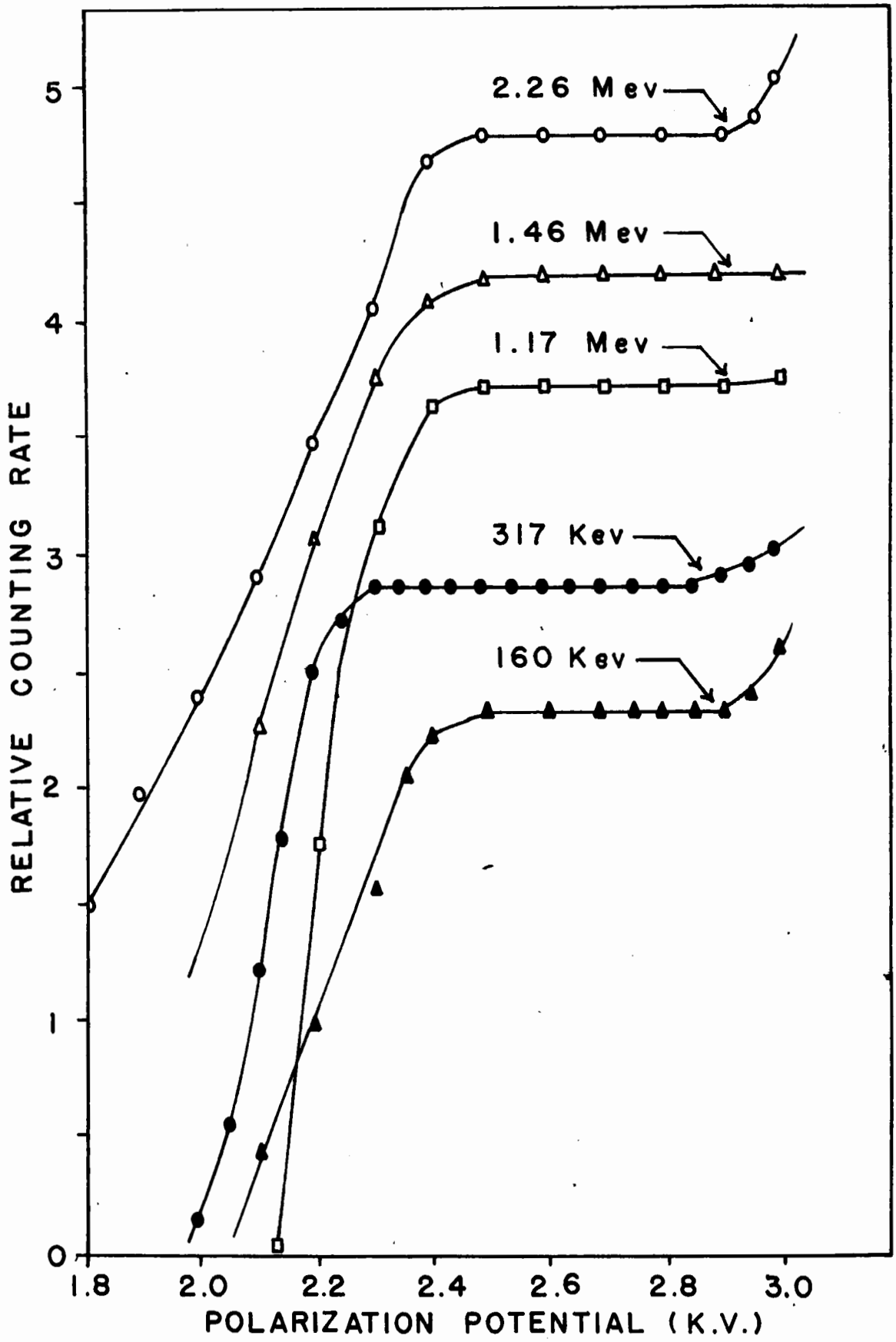
2.26 Mev
1.46 Mev
1.17 Mev
317 Kev
160 Kev
RELATIVE COUNTING RATE
0
1
2
3
4
5
1.8
2.0
2.2
2.4
2.6
2.8
3.0
POLARIZATION POTENTIAL (K.V.)

Figure 6

Discriminator Bias Characteristics for β^- Radiation of Increasing Maximum Energy at a Polarization Potential of 2.6 KV.

1.17 Mev – Ra D + E

317 Kev – Co^{60}

160 Kev – Nb^{95}

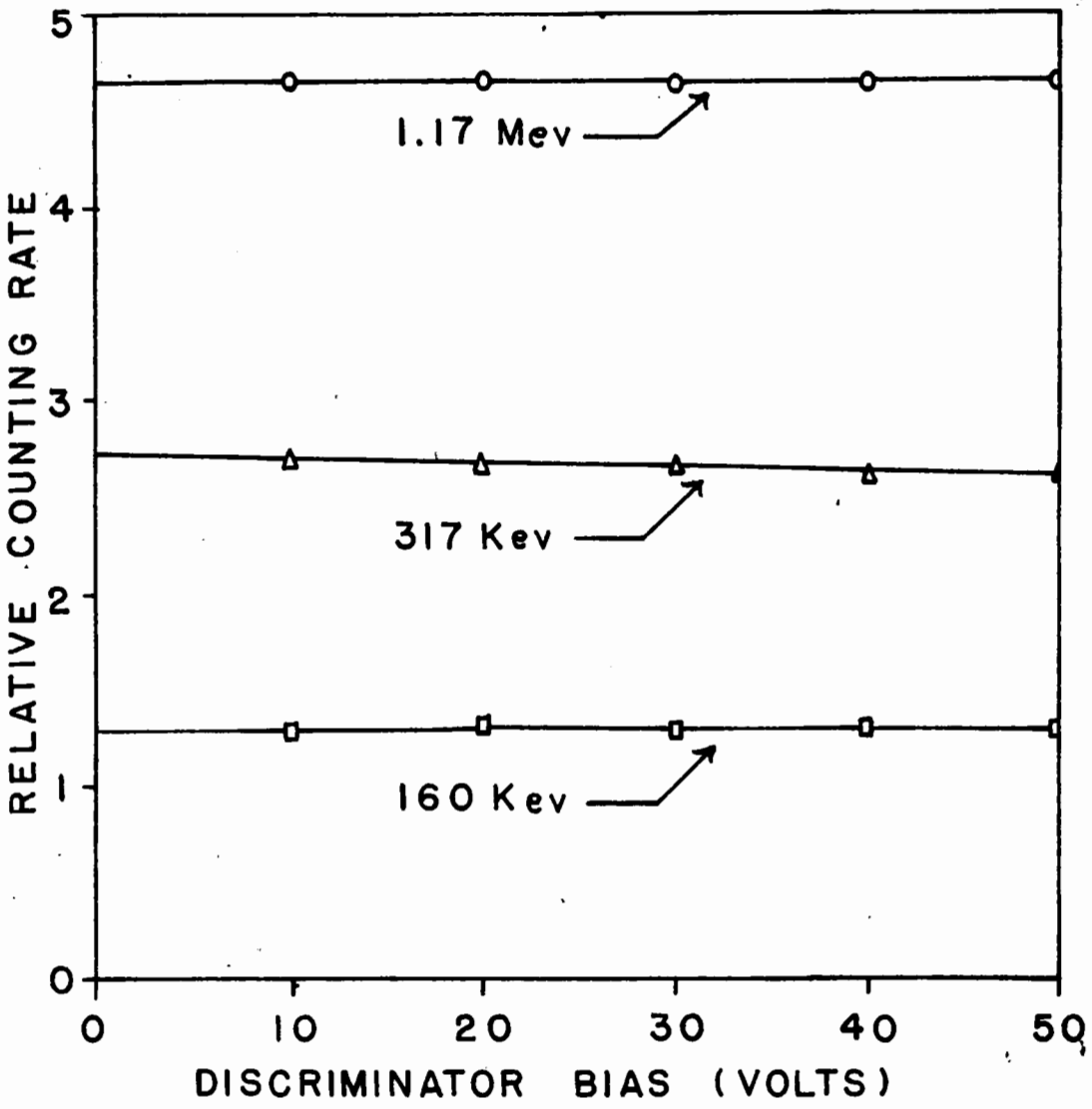
5
4
3
2
1
0
RELATIVE COUNTING RATE
1.17 Mev
317 Kev
160 Kev
0
10
20
30
40
50
DISCRIMINATOR BIAS (VOLTS)

The constant counting rate up to a bias of 50 volts shows the absence of low amplitude spurious pulses (53). Discriminator bias settings of 20 and 30 volts were chosen for general counting of the fission produce activities. The stability of the counter was checked daily by following the decay of a long-lived Ra D + E standard source.

The counting chamber was enclosed in a lead castle with walls 1 1/4 in. thick. The background counting rate varied between 42 and 60 counts per minute.

(c) Counting Corrections

(i) Resolution Losses

Although the reduced resolving time of proportional counters permits higher counting rates to be measured, it is necessary to know at what counting rates resolution losses occur and what is the magnitude of such losses. Due to the variety of processes which may cause resolution losses in proportional counters, Pate and Yaffe have suggested that this loss if best determined empirically (49,53). A modification of the multiple source technique can be used to determine resolution losses. A series of P^{32} sources was prepared on thin films and counted. The counting rates were low enough so that resolution losses could be ignored. The P^{32} sources were then laminated and the counting rates were again measured. The laminates were still so thin that absorption losses were negligible. The differences between the counting

rates of single and laminated sources represent a resolution loss at that counting rate. A "log-log" plot of the resolution loss as a function of the observed counting rate is given in Figure 7. The loss at 10^5 counts per minute was found to be only 1.8 %.

(ii) Source-Mount Absorption

The use of very thin films as source mounts usually requires no correction for the absorption of source radiation. However, with weaker β emitters the absorption loss may be important and an accurate correction factor must be known. Pate and Yaffe have proposed an "absorption curve" type method for determining accurate source-mount absorption (50). The source material is mounted on the thinnest film available, and the counting rate is measured as a function of increasing mount thickness. The disintegration rate can be obtained by extrapolating to zero mount thickness. In the present work the superficial density of film plus gold ranged from 10 to 19 μgm./cm^2. Pate and Yaffe have presented a set of curves which give source-mount absorption as a function of β energy and film thickness. A replotting of their values in the region 0 to 50 μgm./cm.^{2} enabled source-mount absorption corrections to be made in this work. A β^- emitter with a maximum end-point energy of 176 Kev shows only a 0.9 % absorption loss in a film 20 μgm./cm.^{2} thick.

Figure 7

Resolution Correction for the

4π-Counter.

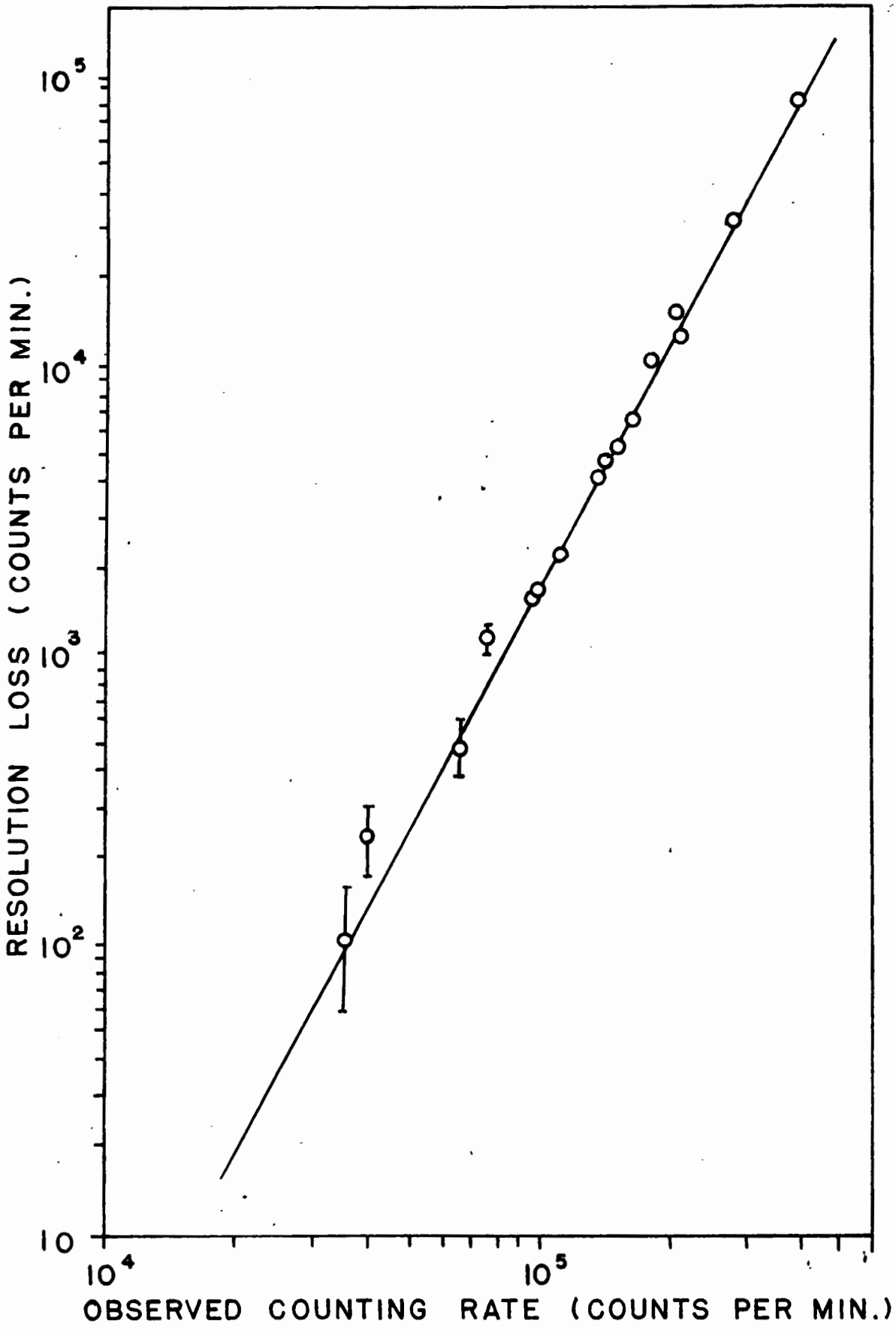
RESOLUTION LOSS (COUNTS PER MIN.)
10
10^2
10^3
10^4
10^5
10^4
10^5
OBSERVED COUNTING RATE (COUNTS PER MIN.)

(iii) Self-Absorption

By far the largest error introduced into disintegration rate determinations of solid samples by 4π-counting is the absorption of radiation in the source material itself. As expected, self-absorption effects become more important as source thickness increases and as the energy of the emitted radiation decreases. Self-absorption losses would be small for sources of moderate or high-energy β radiation with high specific activity. A preliminary study on self-absopption corrections for 4π-counting was made by Pate and Yaffe (52,53). They realized that accurate self-absorption corrections could be accurately applied only to thin uniform source deposits. Consequently, they used a technique whereby active nuclides were formed into organic compounds which were then distilled, under vacuum, on to thin VYNS films. Counting rates were obtained as a function of deposit thickness. The observed specific activity for each deposit was plotted againhst source superficial density. Extrapolation of the curve to zero source thickness enabled the absorption correction to be determined. Fishman and Yaffe (59) have extended the studies on self-absorption in 4π-counting and have prepared corrections for several nuclides of different maximum β^- energies. The self-absorption data of Pate and Yaffe and Fishman and Yaffe

have been combined and are shown in Figures 8 and 9. All self-absorption corrections used were obtained from these curves. The accuracy involved in using such absorption corrections depends on many factors. Small errors in the determinations of source thickness appear to produce very large errors in the chosen absorption factor for the weaker emitters. Although no limit has yet been set on the analytical errors involved in source thickness measurements, it was felt that error effects would be small for thin sources of moderate or high-energy emitters.

The process of β^- emission produces a continuous distribution of particle energies. Often nuclides decay by the emission of more than one β^- energy so that several β spectra are produced. Absorption corrections were taken for each maximum β^- energy and weighed according to its abundance in emission. Figures 8 and 9 seem to indicate that self-absorption effects are similar for different nuclides with the same maximum β^- energies.

(iv) Statistical Counting Errors

Nuclear disintegration is a random phenomenon subject to methods of statistical analysis. The statistical dependability of a measured counting rate can be given in terms of a standard deviation. If the counting time is short compared with the half-life of the activity being measured, the standard deviation for a reasonably large number of counts can be shown to approximate the square root of the number of counts recorded.

Figure 8

Self-Absorption Correction for a

4π-Proportional Counter.

Source Thickness as a Function of

β End-Point Energy.

Pate and Yaffe (52)

Fishman and Yaffe (59)

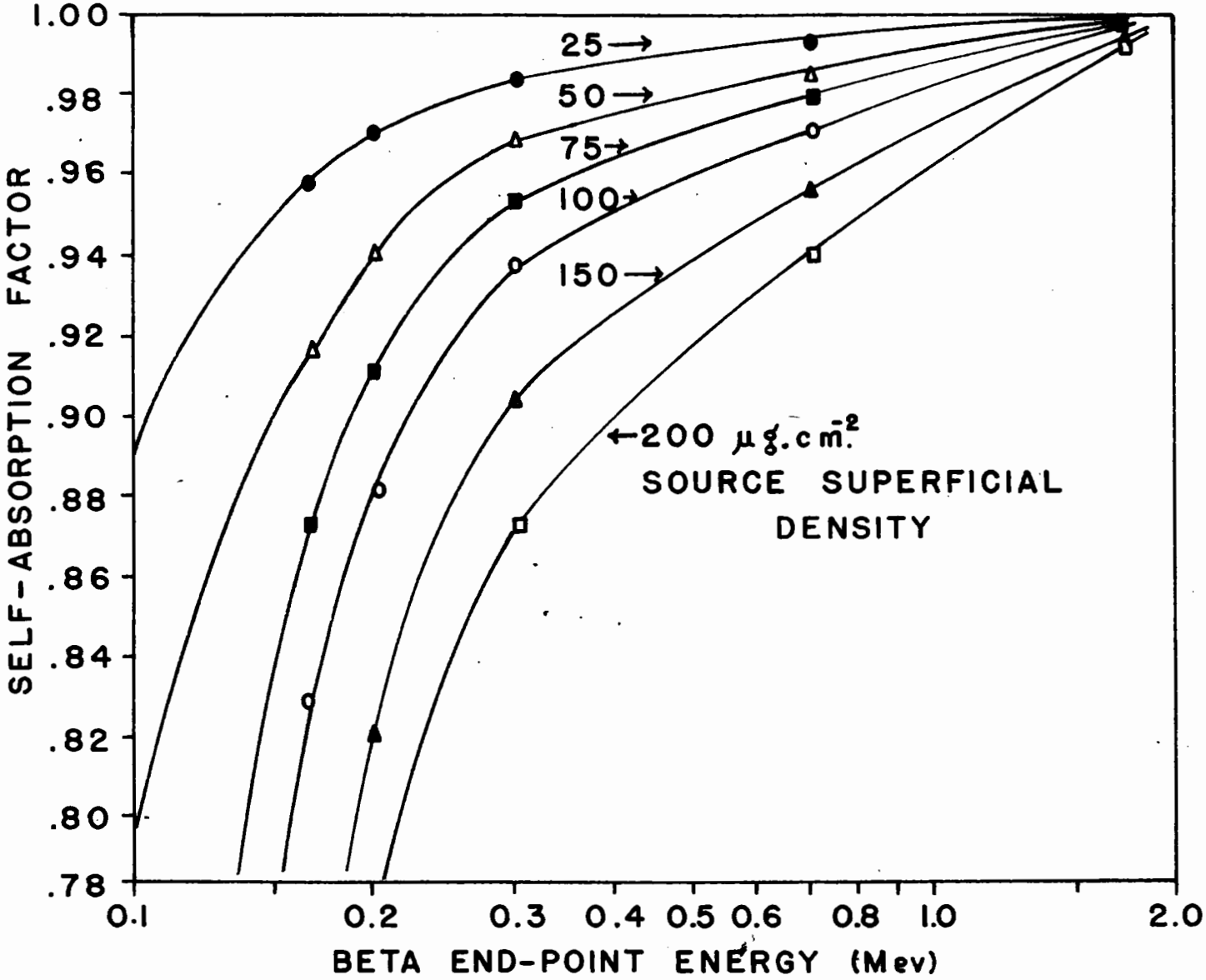
1.00
.98
.96
.94
.92
.90
.88
.86
.84
.82
.80
.78
SELF-ABSORPTION FACTOR
25→
50→
75→
100→
150→
←200 μg.cm⁻²
SOURCE SUPERFICIAL
DENSITY
0.1
0.2
0.3
0.4
0.5
0.6
0.8
1.0
2.0
BETA END-POINT ENERGY (Mev)

Figure 9

Self-Absorption Correction for a

4π-Proportional Counter.

Source Thickness as a Function of

β End-Point Energy.

Pate and Yaffe (52)

Fishman and Yaffe (59)

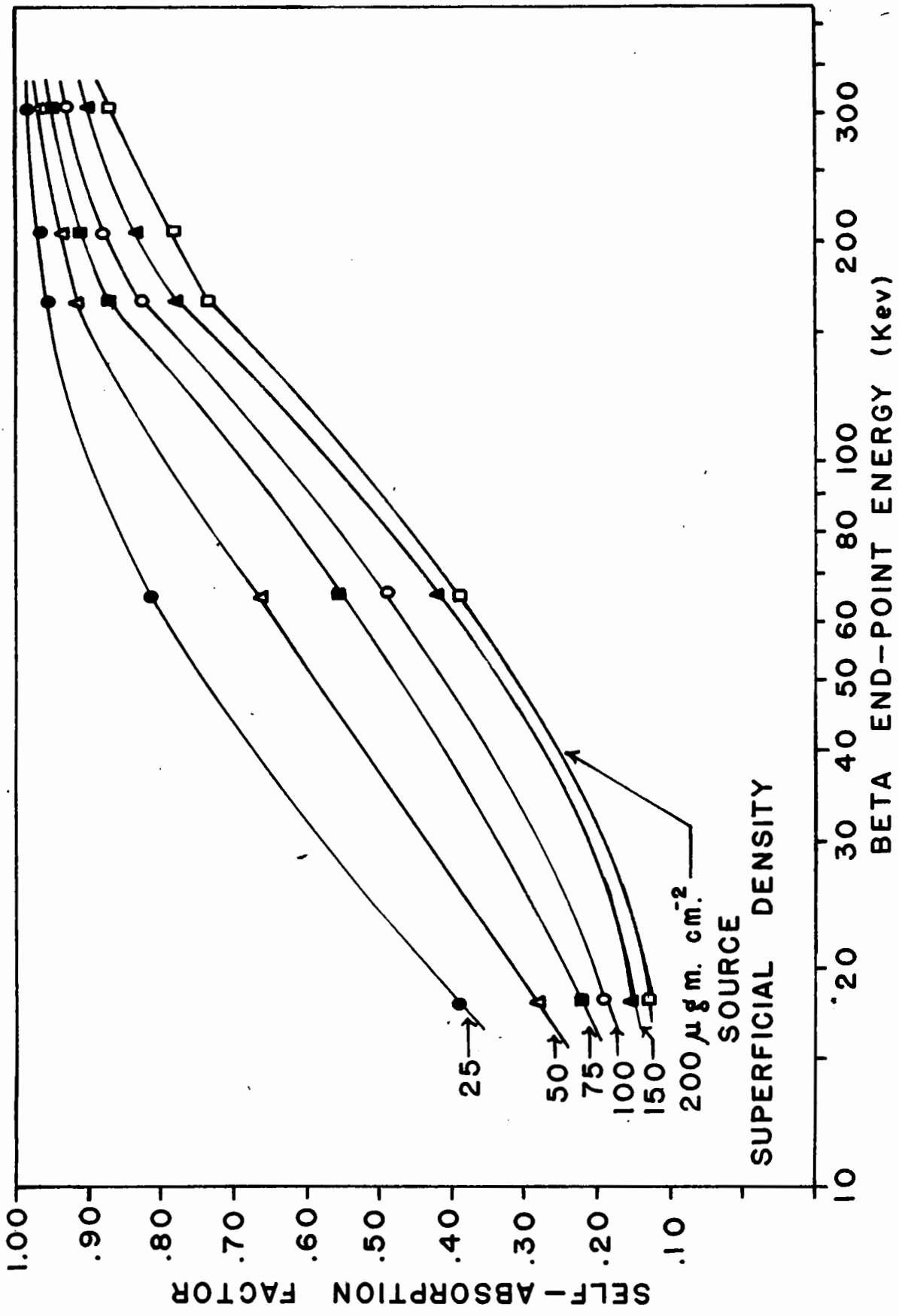
SELF-ABSORPTION FACTOR
1.00
.90
.80
.70
.60
.50
.40
.30
.20
.10
10
20
30
40
50
60
80
100
200
300
BETA END-POINT ENERGY (Kev)
SUPERFICIAL DENSITY
SOURCE
200 µgm. cm.-2
150
100
75
50
25

Thus if 10,000 counts are recorded in one minute, the expected standard deviation is $\sqrt{10,000} = 100$. The counting rate can then be written as 10,000 $\pm$ 100 counts per minute.

B. Scintillation Counting

(a) Equipment

The γ scintillation spectrometer used is shown in block diagram in Figure 10. The detector consisted of a sodium iodide-thallium activated crystal which was viewed by a Du Mont Type 6292 photomultiplier tube. A cathode follower coupled the output signal into a modified Atomic Energy of Canada Ltd. amplifier-discriminator (AEP 1448). The amplified pulses were fed into a single-channel differential pulse height analyzer.* The analyzer operated by accepting only those pulses with a narrow range of amplitudes called the channel width. The acceptance channel was made to scan the entire region of pulse amplitudes by rotating an analyzer bias potentiometer. The output from the pulse analyzer operated a Measurement Engineering Ltd. counting-rate meter (AEP 1902-A). The output from the counting-rate meter was plotted against the analyzer bias voltage by a Speedomax Chart-recording potentiometer. This was done indirectly and was made possible since both the analyzer bias voltage and the chart drives moved with respect to time.

---

* Atomic Energy of Canada Ltd. Automatic Scanning Kicksorter (AEP 2209).

Figure 10

Block Diagram of γ-Ray
Scintillation Spectrometer

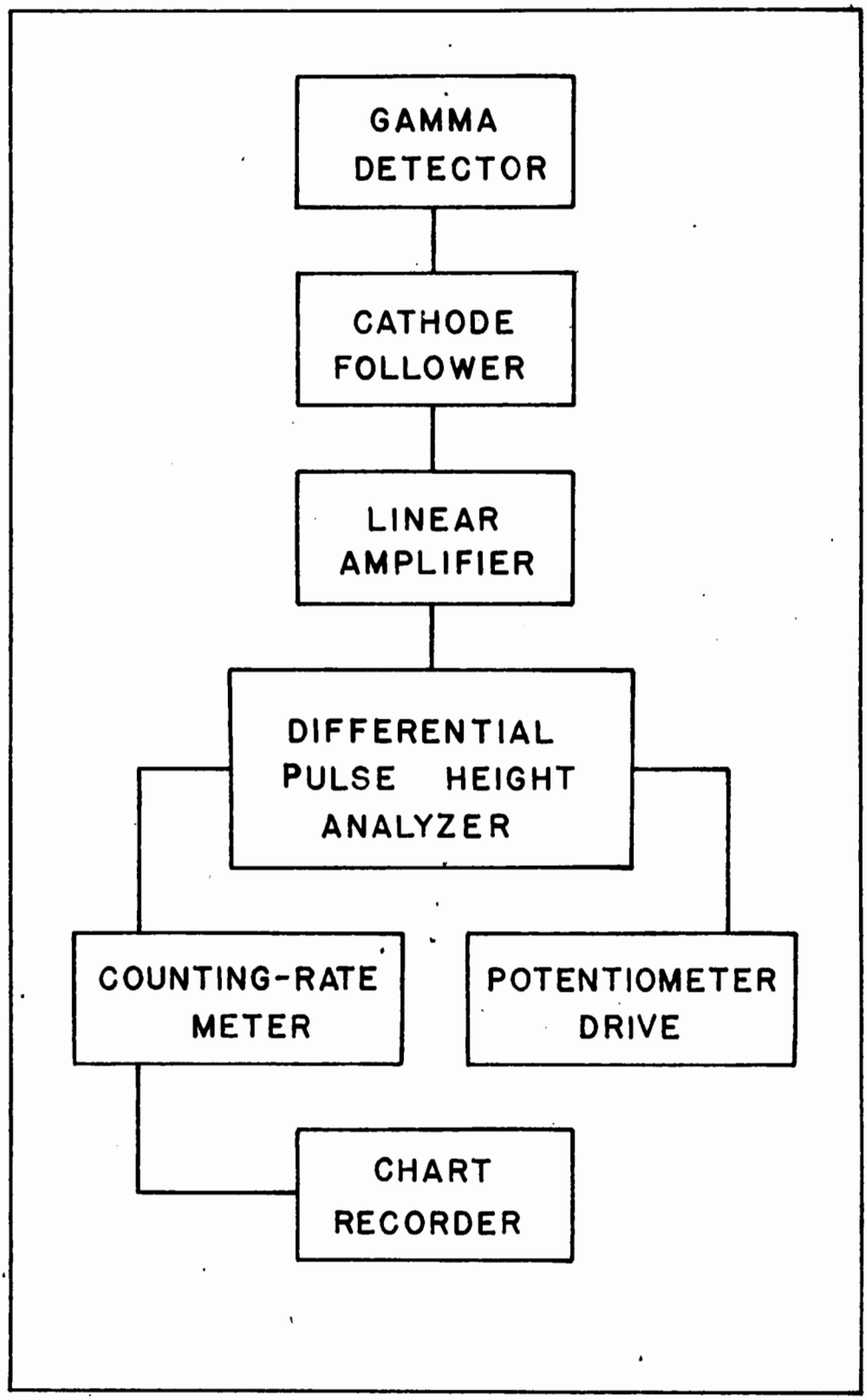
GAMMA DETECTOR
CATHODE FOLLOWER
LINEAR AMPLIFIER
DIFFERENTIAL PULSE HEIGHT ANALYZER
COUNTING-RATE METER
POTENTIOMETER DRIVE
CHART RECORDER

The peaked responses in the pulse height scan are known as photoelectric peaks and each peak occurs at a pulse height proportional to the incident γ energy. In general, the maximum photopeaks are measured and qualitative identification of the γ emitters is made possible by comparing the voltage of the photopeaks with a calibrated curve for the instrument. Quantitative estimates of the various γ-emitting nuclides can be obtained by measuring the areas under the respective photopeaks and comparing them with areas under the photopeaks obtained from standards of known disintegration rates. Since the shape of photopeaks approximates a Gaussian distribution, the area under each photopeak is proportional to its peak height. In this work peak positions were measured to determine γ energies. Peak heights were measured and plotted against time to obtain γ half-lives. The purpose of scintillation counting was to aid in the identification of fission product nuclides and establish radiochemical purity of separations.

(b) Spectrometer Characteristics

The scintillation spectrometer was operated at a channel width two per cent of full scale. The change in photopeak position with voltage applied to the photomultiplier tube was determined using sources of known γ energies. In Figure 11 γ energy is plotted against photopeak position (% scan) for different applied voltages. At lower voltages

Figure 11

High Voltage Characteristic Curves

for the Scintillation Spectrometer

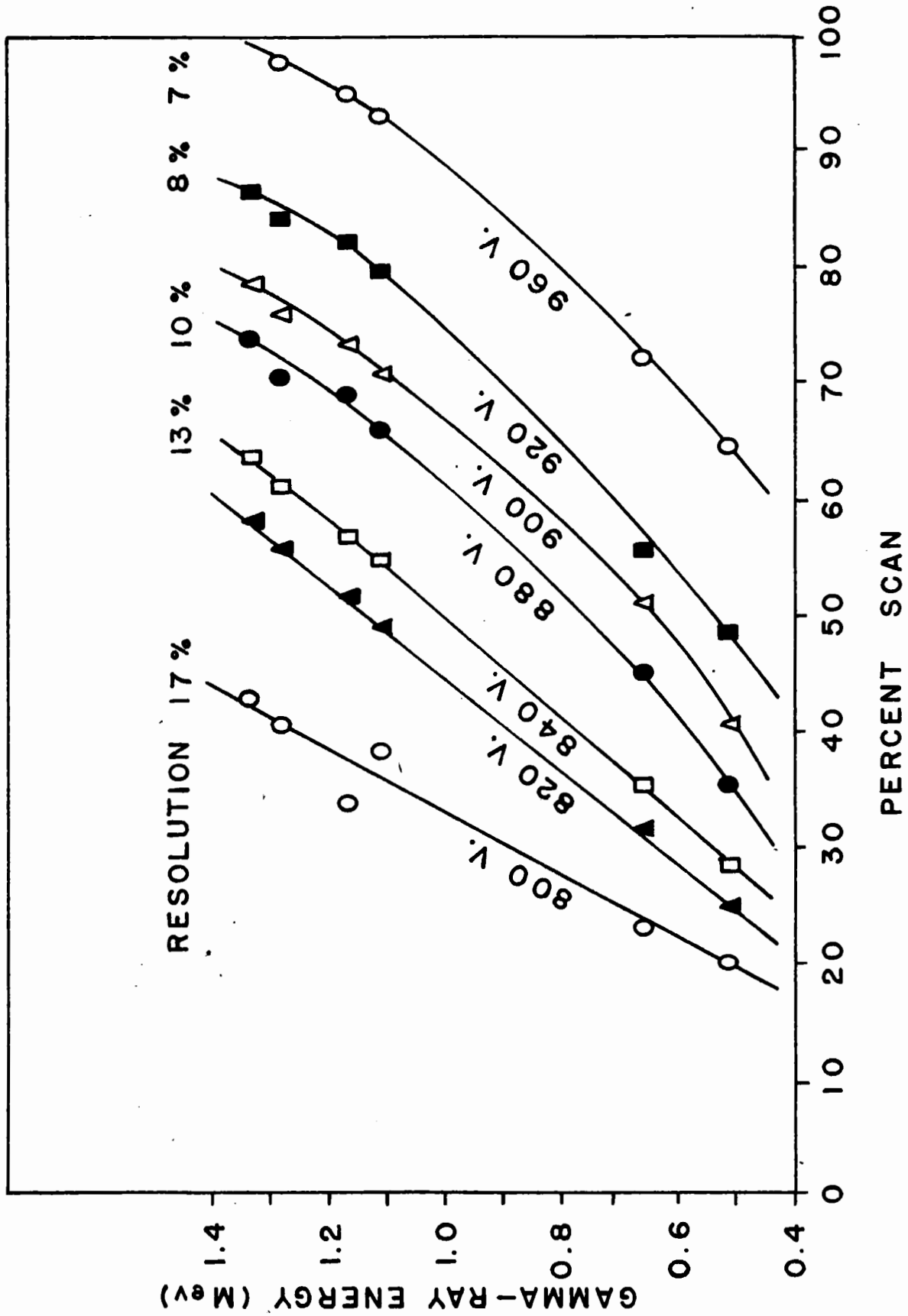
RESOLUTION 17%
13%
10%
8%
7%
800 V.
820 V.
840 V.
880 V.
900 V.
920 V.
960 V.
GAMMA-RAY ENERGY (Mev)
PERCENT SCAN
0.4
0.6
0.8
1.0
1.2
1.4
0
10
20
30
40
50
60
70
80
90
100

the photopeaks are very close together. Increasing the voltage causes the photopeak to spread out. In addition, higher voltages result in a nonlinear relationship between γ energy and observed photopeak position. The ability of the crystal and the pulse analyzer to resolve photopeaks is termed resolution. This factor can be determined experimentally from the following relationship.

$$\text{Resolution } (\%) = \frac{\text{width of peak at 1/2 of peak height x 100}}{\text{distance of peak from origin of scan}}$$

The per cent resolution is usually quoted for the Cs^{137} 661 Kev γ-ray. In Figure 11 the resolution varied from 17.0 % at 800 volts to 7.0 % at 960 volts. In choosing an operating voltage three conditions were desired.

(i) Good resolution.

(ii) A linear γ energy - % scan relationship.

(iii) Scan range extending to 1.5 Mev.

On the basis of these factors an operating voltage of 880 volts was chosen as a compromise. Figure 12 shows a complete energy calibration curve for the γ-ray scintillation spectrometer at 880 volts. From a measured peak position and this curve an unknown γ energy could be determined.

Figure 12

γ-Ray Scintillation Spectrometer

Energy Calibration Curve

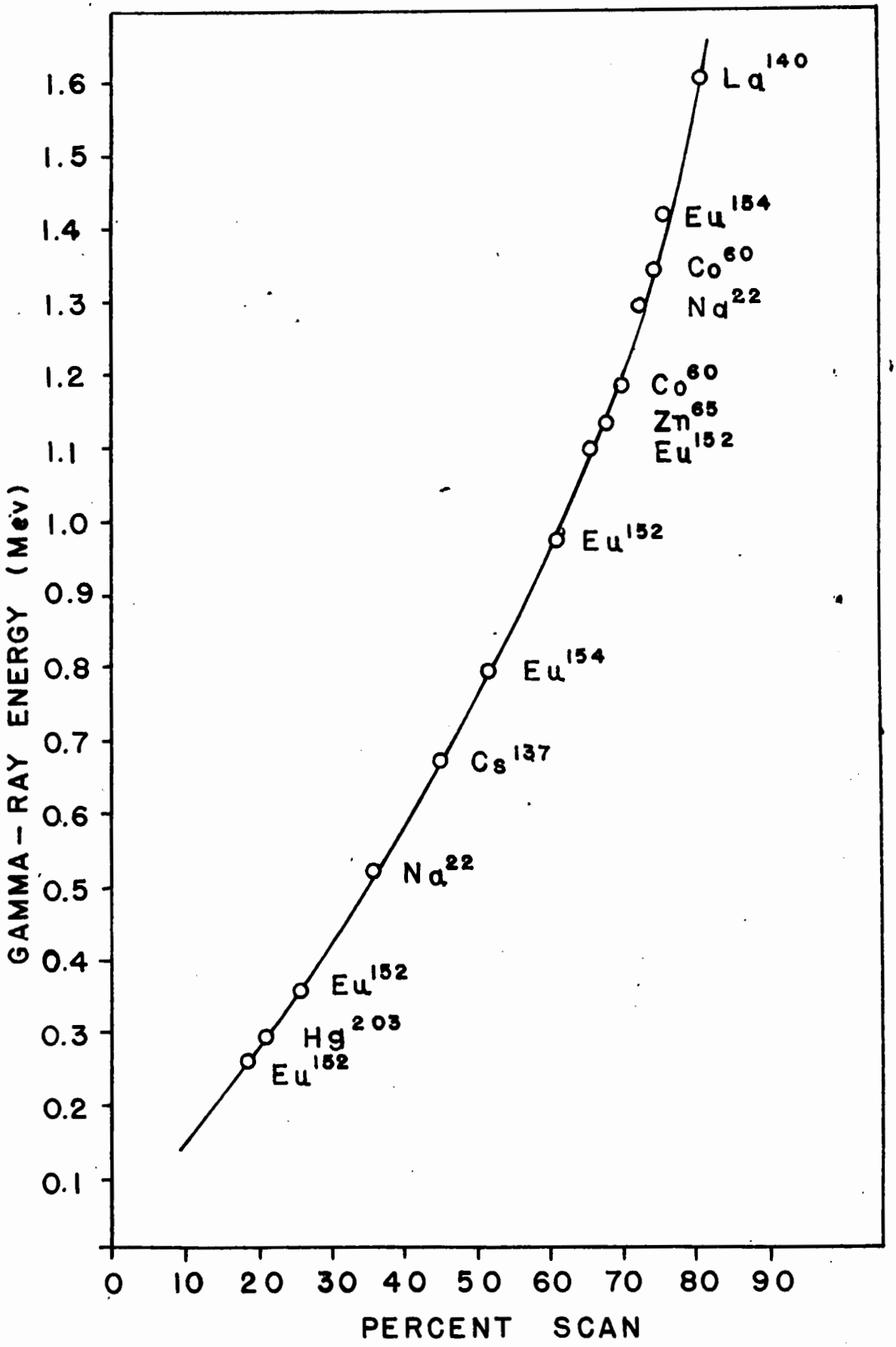
GAMMA-RAY ENERGY (Mev)
1.6
1.5
1.4
1.3
1.2
1.1
1.0
0.9
0.8
0.7
0.6
0.5
0.4
0.3
0.2
0.1
0
10
20
30
40
50
60
70
80
90
PERCENT SCAN
La140
Eu154
Co60
Na22
Co60
Zn65
Eu152
Eu152
Eu154
Cs137
Na22
Eu152
Hg203
Eu152

(c) Counting of Active γ Sources

The standard γ sources as well as the fission product activities were counted as 2 ml. aliquots of solution. The small screw-top glass vials which were used to hold the activities were placed at measured positions above the crystal detector. Since all counting rates were measured relative to γ standards, the only correction factor required was for variations in geometrical efficiency. By altering the source geometry, counting rates were kept below 20,000 counts per minute where resolution losses were found to be small. Scans of the fission product activities were interspersed with those of the γ standards.

5. Equations used

The following is an abbreviated derivation of the equations used in this work for the determination of absolute fission yields.

(a) Fission Yield

Under neutron irradiation the rate of depletion of uranium is given by

$$\frac{dU}{dt} = -U\, I\, \sigma_{abs} \qquad \ldots \quad (1)$$

Thus $U = U_o \exp(-I\, \sigma_{abs}\, T)$, $\qquad \ldots \quad (2)$

where U is the number of atoms of uranium present at any time T during an irradiation,

U_o is the number of atoms of uranium initially present,

I is the thermal-neutron flux, and

σ_{abs} is the thermal-neutron absorption cross section.

The rate at which fission occurs is

$$\left(\frac{dU}{dt}\right)_f = -U\ I\ \sigma_f \quad , \qquad \ldots . \quad (3)$$

where σ_f is the thermal-neutron fission cross section for uranium.

In terms of the uranium present initially

$$\left(\frac{dU}{dt}\right)_f = -U_o\ I\ \sigma_f\ \exp(-I\ \sigma_{abs}\ T) \quad . \qquad \ldots . \quad (4)$$

The net rate of formation of a fission product during an irradiation is

$$\frac{dN}{dt} = -\left(\frac{dU}{dt}\right)_f Y_f - \lambda N \ , \qquad \ldots . \quad (5)$$

where Y_f is the fission yield of the nuclide in question,

N is the number of atoms of the nuclide in question present at any time T, and

λ is the disintegration constant of the nuclide.

In terms of the uranium initially present equation (5) becomes

$$\frac{dN}{dt} = Y_f\ U_o\ I\ \sigma_f\ \exp(-I\ \sigma_{abs}\ T) - \lambda N \qquad \ldots . \quad (6)$$

Integrating and multiplying through by λ gives the disintegration rate for the fission product activity.

$$N\lambda = \frac{Y_f\ U_o\ I\ \sigma_f\ \left[\exp(-I\ \sigma_{abs}\ T) - \exp(-\lambda T)\right]}{\lambda - I\ \sigma_{abs}} \qquad \ldots . \quad (7)$$

Since $(I\ \sigma_{abs})$ is very small ($< 3 \times 10^{-7}$ in this work)

$\exp(-I\,\sigma_{abs}) = 1.$ and equation (7) simplifies to

$$N\lambda = Y_f\, U_o\, I\, \sigma_f\left[1- \exp(-\lambda T)\right]. \quad \ldots . \quad (8)$$

If we represent the fission rate by R,

then $R = U_o\, I\, \sigma_f$, $\quad \ldots . \quad (9)$

and $N\lambda = R\, Y \left[1- \exp(-\lambda T)\right]$. $\quad \ldots . \quad (10)$

Equations (8) or (10) are the basic equations used in the calculation of absolute fission yields. As the irradiation time becomes long compared to the half-life of the fission product activity, $N\lambda$ approaches a maximum limiting value $R\, Y_f$. Then

$$N\lambda = R\, Y_f = (N\lambda)_{max} \left[1-\exp(-\lambda T)\right]. \quad \ldots . \quad (11)$$

The limiting value $(N\lambda)_{max}$ is known as saturation activity. Under such conditions activities present during an irradiation can be compared one with another, since the number of atoms of an activity being formed per unit time equals the number of such atoms disintegrating per unit time, irrespective of its half-life.

For the decay chain

$$A \dashrightarrow B \dashrightarrow C$$

the yield of A will be given by equation (10). If A were the first member of the chain, this yield would represent the independent as well as the total yield for nuclide A. The yield of B will be given by

$$Y_B = Y_A + (Y_i)_B \quad \ldots . \quad (12)$$

where Y_A is the cumulative yield of A which includes the sum of the independent yields of any precursors of A plus the independent yield of A, and $(Y_i)_B$ is the independent yield of nuclide B. The disintegration rate of B formed independently during an irradiation of time T is

$$(N\lambda)_B^i = R\ (Y_i)_B\ [1-\exp(-\lambda T)]\ . \qquad \ldots\ (13)$$

However, B also grows from A during the irradiation. The disintegration rate of B formed from the decay of A during the irradiation is given by

$$(N\lambda)_B^A = R\ Y_A \left[1 + \frac{\lambda_B \exp(-\lambda_A T) - \lambda_A \exp(-\lambda_B T)}{\lambda_A - \lambda_B}\right] \ldots\ (14)$$

At a time t after the irradiation these amounts have decayed exponentially, so that

$$(N\lambda)_B^i \text{ at } t = (N\lambda)_B^i \exp(-\lambda_B t) \qquad \ldots\ (15)$$

and

$$(N\lambda)_B^A \text{ at } t = (N\lambda)_B^A \exp(-\lambda_B t)\ . \qquad \ldots\ (16)$$

From the end of the irradiation until the time t, B continues to grow from A.

$$(N\lambda)_B^{A'} \text{ at } t = \frac{R\ Y_A \lambda_B \left[1-\exp(-\lambda_A T)\right]\left[\exp(-\lambda_A t)-\exp(-\lambda_B t)\right]}{\lambda_B - \lambda_A} \qquad \ldots\ (17)$$

Therefore, the total disintegration rate of B after an irradiation time T and a decay time t is

$$(N\lambda)_B = (N\lambda)_B^i \exp(-\lambda_B t) + (N\lambda)_B^A \exp(-\lambda_B t) + (N\lambda)_B^{A'} . \qquad (18)$$

$$= R\,(Y_i)_B\left[1-\exp(-\lambda_B T)\right]\exp(-\lambda_B t)$$

$$+ R\,Y_A\left[1+\frac{\lambda_B\exp(-\lambda_A T)-\lambda_A\exp(-\lambda_B T)}{\lambda_A-\lambda_B}\right]\exp(-\lambda_B t)$$

$$+ \frac{R\,Y_A\,\lambda_B}{\lambda_B-\lambda_A}\left[1-\exp(-\lambda_A T)\right]\left[\exp(-\lambda_A t)-\exp(-\lambda_B t)\right] \quad . \quad . \quad (19)$$

When rearranged, equation (19) becomes

$$(N\lambda)_B = \frac{R\,Y_A}{\lambda_A-\lambda_B}\left\{\lambda_A\left[1-\exp(-\lambda_B T)\right]\exp(-\lambda_B t)-\lambda_B\left[1-\exp(-\lambda_A T)\right]\exp(-\lambda_A t)\right\}$$

$$+ R\left\{(Y_i)_B\left[1-\exp(-\lambda_B T)\right]\exp(-\lambda_B t)\right\} \quad . \quad . \quad (20)$$

The first part of equation (20) is the disintegration rate of the amount of B formed from A during and after an irradiation, and need only be considered when the independent yield of B is small.

In the present work the time between the end of the irradiation and the chemical separation was often very long compared to the half-lives of the precursors of B. Under these conditions A had decayed and equation (20) simplified to

$$(N\lambda)_B = R\left[Y_A + (Y_i)_B\right]\left[1-\exp(-\lambda_B T)\right]\exp(-\lambda_B t) \quad . \quad . \quad (21)$$

or

$$(N\lambda)_B = R\,Y_B\left[1-\exp(-\lambda_B T)\right]\exp(-\lambda_B t) \quad . \quad . \quad (22)$$

Similarly the disintegration rate of nuclide D would be given by

$$(N\lambda)_D = R\,Y_D\left[1-\exp(-\lambda_D T)\right]\exp(-\lambda_D t) \quad . \quad . \quad (23)$$

By dividing equation (22) by equation (23) and rearranging, the yield of B is obtained in terms of the two disintegration rates and the yield of A.

$$Y_B = \frac{Y_A\ (N\lambda)_B \left[1-\exp(-\lambda_A T)\right] \exp(-\lambda_A T)}{(N\lambda)_A \left[1-\exp(-\lambda_B T)\right] \exp(-\lambda_B T)} \quad . \ . \ . \ (24)$$

When a value for the fission yield of A has been obtained from an absolute measurement, the yields of other products may be determined relative to it. Such relative fission yield measurements do not require a knowledge of fission rates.

(b) General Growth and Decay Equations

The following is a summary of the general equations used for calculating radioactive growth and decay for various members of a decay chain. A complete derivation of these equations can be found in reference (61).

Let us consider decay chain

$$P \xrightarrow[\lambda_1]{} Q \xrightarrow[\lambda_2]{} R \xrightarrow[\lambda_3]{}$$

where P, Q and R represent the number of atoms of each member present at any time t, and λ_1, λ_2, and λ_3 are the decay constants for P, Q and R respectively.

Then $\frac{dP}{dt} = -\lambda_1 P$ . . . (25)

and $(P\lambda_1) = (P_o\lambda_1)\ \exp(-\lambda_1 t)$ . . . (26)

where P_o is the number of atoms of P originally present.

Also $\frac{dQ}{dt} = \lambda_1 P - \lambda_2 Q$ . . . (27)

and $(\lambda_2 Q) = (P_o\lambda_1)\ \frac{\lambda_2}{\lambda_2-\lambda_1}\left[\exp(-\lambda_1 t)-\exp(-\lambda_2 t)\right]$ . . (28)

The disintegration rate of the third member is given by

$$(R\lambda_3) = (P_o\lambda_1)\left[a\ \exp(-\lambda_1 t) + b\ \exp(-\lambda_2 t) + c\ \exp(-\lambda_3 t)\right] \quad . \ . \ (29)$$

(c) Neutron Attenuation

The neutron flux intensity at the surface of a sample being irradiated will differ from the flux intensity at any position inside the sample. It is therefore necessary to correct the flux value for any attenuation which occurs in the sample. The flux intensity at the surface I_o will be related to the intensity I inside the sample at a thickness d by

$$I = I_o \exp(-\frac{N}{A}\rho\sigma d) \quad . \quad . \quad . \quad (30)$$

where N is Avagadro's number,

ρ is the density of the sample,

σ is the total neutron cross section, and

A is the atomic weight of neutron absorbing material.

The neutron attenuation $\frac{I}{I_o}$ is usually calculated for half of the sample thickness in the case of a non-directional flux.

(d) Neutron Flux

At the end of an irradiation the disintegration rate of an active nuclide produced by a neutron capture reaction is given by

$$N\lambda = N_o \, I \, \sigma_c \left[1-\exp(-\lambda T)\right] \quad . \quad . \quad . \quad (31)$$

where N_o is the number of atoms of a nuclide present initially,

T is the duration of the irradiation,

I is the thermal-neutron flux, and

σ_c is the thermal-neutron capture cross section of the nuclide being irradiated.

As in equation (11), saturation activity is given by

$$(N\lambda)_{max} = \frac{N\lambda}{1-\exp(-\lambda T)} = N_o \, I \, \sigma_c \, . \qquad . \; . \; . \quad (32)$$

Thus a measured disintegration rate, corrected for decay and saturation bombardment, enables the neutron flux to be determined. It should be noted that the use of equations (31) and (11) to evaluate absolute fission yields depends on the ratio of two cross sections σ_f / σ_c.

ACTIVITIES ISOLATED AND RESULTS

1. Flux Determinations

After an irradiation, the cobalt monitor was dissolved, made up to a known volume, and counted directly. The maximum concentration of cobalt used was 1.63 mgm. per 10 ml. of solution. A source consisting of 20λ of this solution spread evenly over 1.0 $cm.^2$ area corresponds to a source superficial density of ~10 $\mu gm./cm.^2$ The β^- -energy for Co^{60} is given as 308 Kev (62). Therefore, the self-absorption correction to be applied to the counting rate is 0.994 and the source-mount absorption correction is 0.999. To determine the amount of Co^{60} activity lost by recoil on to the quartz vial, a γ-counting rate of an irradiated monitor and its quartz capsule were measured on the scintillation spectrometer. The cobalt wire was removed and the γ-counting rate of the vial alone was measured (see Figure 13). The amount of Co^{60} lost by recoil was found to be 0.31 %. A scan of the irradiated vial alone further indicated that no measurable activities were produced in the quartz material itself.

The amount of neutron attenuation in the cobalt wire had been determined experimentally * and the value agreed with that calculated by means of equation (30) on page 60.

$$\frac{I}{I_o} = \exp\left(\frac{-N\rho\sigma}{A}\right)$$

---

* We are grateful to Dr. R.E. Jervis, Chemistry Branch, Atomic Energy of Canada Ltd., Chalk River, Ontario, for making available to us the results of this determination.

Figure 13

Co^{60} γ Spectrum of an Irradiated Vial before and after the Removal of the Cobalt Flux Monitor.

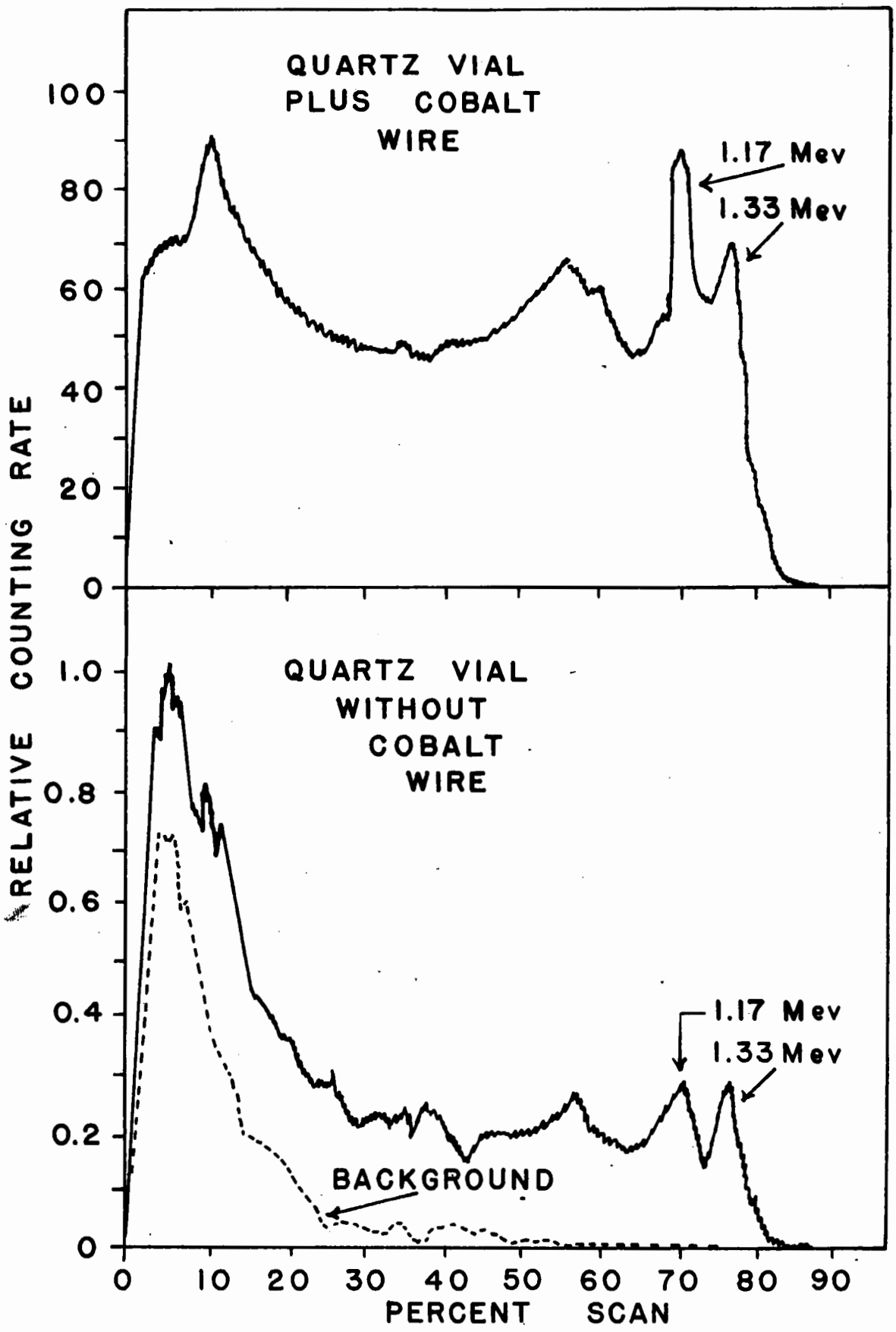
QUARTZ VIAL
PLUS COBALT
WIRE
1.17 Mev
1.33 Mev
100
80
60
40
20
0
QUARTZ VIAL
WITHOUT
COBALT
WIRE
1.17 Mev
1.33 Mev
BACKGROUND
1.0
0.8
0.6
0.4
0.2
0
RELATIVE COUNTING RATE
0 10 20 30 40 50 60 70 80 90
PERCENT SCAN

The attenuation factor was 0.979 for a wire of 0.0064 cm. radius. The cobalt capture cross section used was 36.3 barns (57,58).

For each irradiation the value of the thermal-neutron flux, as given in Table 2, was calculated from equation 31 on page 60.

$$\frac{dn}{dt} = I \sigma N\left[1-\exp(-\lambda T)\right] \exp(-\lambda t) \times \frac{1}{\text{attenuation}} .$$

The half-life of Co^{60} was taken at 5.24 years (63).

TABLE 2

THERMAL-NEUTRON FLUX VALUES

(In units of 10^{12} neutrons per $cm.^2$ per second)

Irradiation Number	A	B	C	D	E	E'	F
Flux	6.25	6.41	5.05	3.97	4.28	3.62	3.81

In irradiation E' one of the monitors was surrounded by cadmium foil and activated only by epi-cadmium neutrons. A disintegration rate per mgm. of cobalt for the unshielded monitor was 1.31×10^9 dis. per second, and for the shielded monitor was 2.31×10^7 dis. per second. Therefore, 1.76 % of the total Co^{60} produced was caused by epi-cadmium neutrons. The fast neutron flux was not calculated since a cobalt capture cross section was not known for the range of neutron energies present.

2. Fission-Rate Determinations

The rate at which the uranium sample underwent fission was calculated by means of equation (9) on page 56.

$$R = (U_o \; I \; \sigma_f) \times \text{attenuation}$$

The value of the fission cross section used was 524 barns (64). In calculating the neutron attenuation in the uranium it was necessary to consider the limits in which the uranium powder was spread out uniformly along the quartz tube or was heaped together at one end. For the heaviest sample used the attenuation factor ranged from between 0.975 and 0.989. The lightest sample used had an attenuation of from 0.986 to 0.997. The fission rate for each irradiation is given in Table 3.

TABLE 3

THERMAL-NEUTRON FISSION RATES OF U^{233}

(In units of 10^{10} fissions per second)

Irradiation Number	A	B	C	D_a	D_b	F
Rate	1.599	2.270	2.885	1.464	0.722	2.587

3. Fission Product Activities

(a) Bromine

The method of Glendenin et. al. (65) was used to separate bromine. An aliquot of the fission product stock solution was added to bromate and iodate carriers. Reduction with H_2S was used to ensure complete exchange between radiobromine and the carrier. Several cycles of water-carbon tetrachloride extractions were performed to isolate the

bromine. The use of $NH_2OH.HCl$ to reduce Br_2 to Br^- without reducing I_2 permitted removal of iodine activities. After purification, the bromine was reduced to bromide with a water solution of SO_2, and made up to a volume of 10 ml. Three 2.0 ml. aliquots of the bromide solution were removed, made slightly acidic and warmed to remove the SO_2. About 0.5 ml. of 0.1 M. $AgNO_3$ was added drop-wise to precipitate the bromide in each aliquot. The precipitates were allowed to digest before being filtered. A small quantity of warm water and alcohol was used to wash the precipitates. Before being weighed, each precipitate was dried for 20 minutes at 110° C. and desiccated for one hour. The chemical yield was calculated from the weight of AgBr obtained.

Exactly 100 λ aliquots of the bromide solution were mounted on prepared VYNS films. A drop of very dilute $AgNO_3$ solution was added to reduce oxidation and thus prevent the loss of halogen activity by volatilization. The decay of the bromine activity, as followed in a 4π-proportional counter, is shown in Figure 14. The observed half-life of the decay was 34.5 hours. Because of the low activity present no γ spectrum was obtained.

The two longest lived isotopes of bromine formed in fission are 36-hour Br^{82} and 2.3-hour Br^{83} (66). Since the bromine separation was carried out 40.6 hours after the end of the irradiation, there could be no 2.3-hour activity present.

Figure 14

β - Decay Curve of Br^{82}

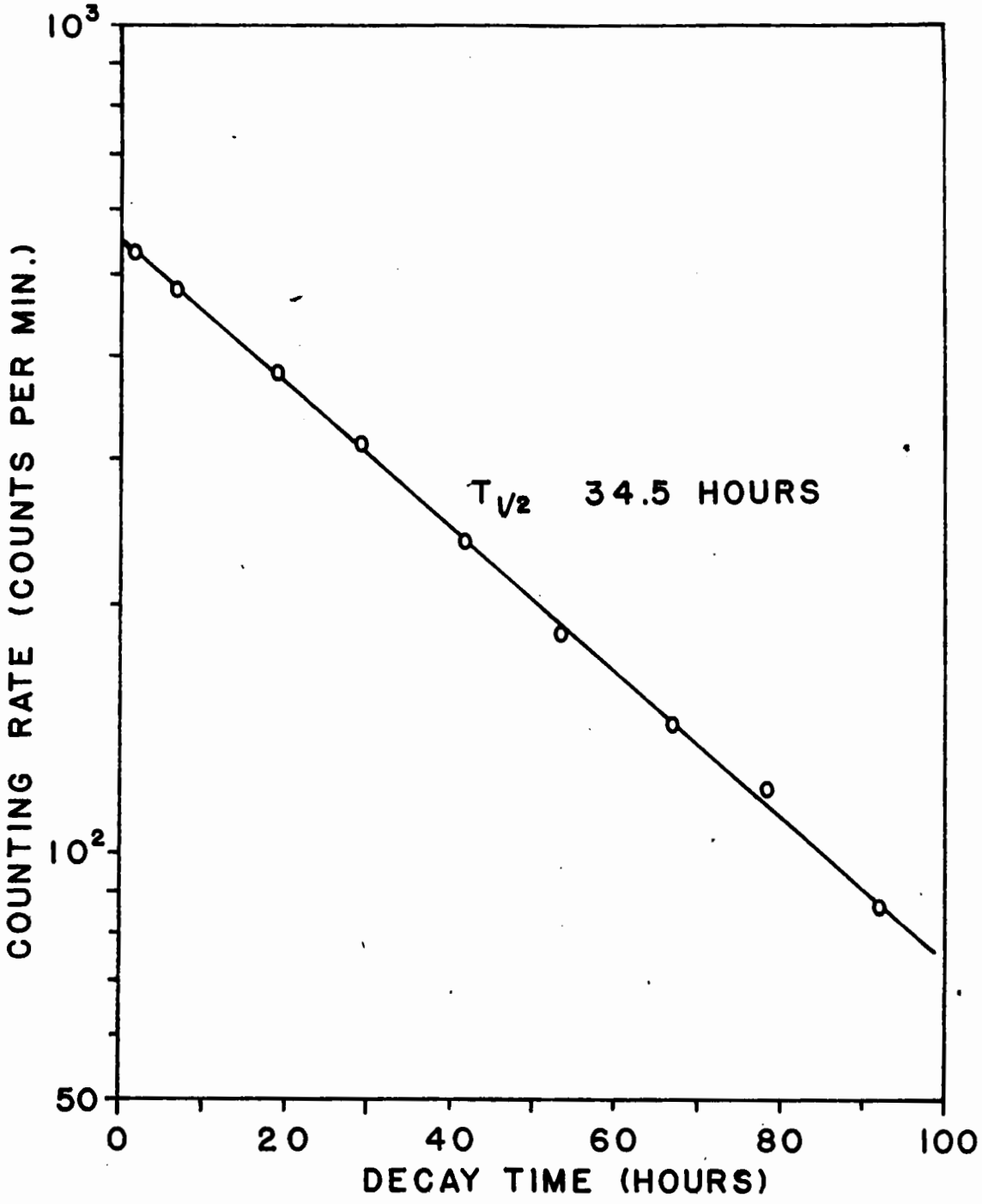
10^3
10^2
50
COUNTING RATE (COUNTS PER MIN.)
$T_{1/2}$ 34.5 HOURS
0
20
40
60
80
100
DECAY TIME (HOURS)

All precursors of Br^{83} are known to be short lived. The observed activity of 34.5 hours was therefore Br^{82}. Since Br^{82} is a shielded nuclide produced only by direct formation, its fission yield constitutes an independent yield measurement. The possibility of obtaining Br^{82} by the (nγ) reaction of Br^{81} present as an impurity does not exist. The uranium sample had originally been heated to 1000°C. which would have removed most of any bromine impurity originally present. None was detected in the spectrographic determination.

Reported studies on the decay scheme for Br^{82} show that the nuclide decays by the emission of 460 Kev β^- radiation with γ radiation in coincidence (67,68). It was only necessary to apply source-mount and self-absorption corrections to obtain a disintegration rate. All factors involved in the calculation of the Br^{82} fission yield are given in Table 4.

(b) Strontium

A slight modification to the method of Glendenin (69) was used for the separation of strontium activities. The procedure involved adding carriers of strontium and barium and precipitating both of these as nitrates with fuming nitric acid. Ferric hydroxide scavenging was used for additional purification. Barium was removed by a chromate precipitation in a buffered solution. Strontium was separated as the oxalate, dissolved in nitric acid and reprecipitated with

fuming nitric acid. The nitrate precipitate was washed with ethanol before being dissolved in water and made up to 10 ml. of solution.

TABLE 4

FISSION YIELD DATE FOR 36-HOUR Br^{82}

Irradiation B 1

Observed activity	553 counts per minute
Self-absorption factor	0.924
Source-mount Absorption factor	0.995
Aliquot factor	1250
Chemical yield	43.7 %
Time after irradiation	40.6 hours
Decay factor	0.4577
Time in reactor	24 hours
Saturation factor	0.3700
Activity at saturation	1.694×10^5 dis. per second
Fission rate	2.270×10^{10} fissions per second
Fission yield	$(7.46 \pm 0.17\%) \times 10^{-4}$ %

Chemical yields were determined by precipitating aliquots of the strontium solution as the oxalate under controlled conditions. The precipitates were weighed as $SrC_2O_4.H_2O$ after an alcohol-ether washing and vacuum desiccation.

Both 20 and 50λ aliquots were removed periodically from the strontium solution and their counting rates determined in the 4π -counter. Each strontium separation showed the presence of a 50.0 to 50.5-day activity and a long-lived component (see Figure 15). One separation which was performed shortly after the end of the irradiation exhibited a 9.7-hour activity in addition to the 50-day and the long-lived products (see Figure 16). Although large amounts of β activity were obtained in the strontium separations, no γ photopeaks were observed on the scintillation spectrometer except when the 9.7-hour activity was present. Figure 17 shows the observed 550, 740 and 1020 Kev γ peaks. A plot of γ-counting rate vs. time in Figure 18 indicates that the 740 and 1020 Kev peaks also decay with a 9.7-hour half-life. The initial growth and subsequent 9.7-hour decay of the 550 Kev peak displays the formation of a shorter-lived daughter activity from the 9.7-hour parent.

The observed 50-day β-activity was assigned as Sr^{89} which has a reported half-life of 50.4 days (70). It was assumed that the long-lived component was Sr^{90} which was known to be produced in fission (71). The most recently reported half-life of Sr^{90} is 27.7 years (72). Unquestionably, the 9.7-hour activity is that of Sr^{91} with a half-life of 9.7 hours (70). The decay chains involving these nuclides are:

Figure 15

Decay of Sr^{89} in the Presence of Long-lived Sr^{90}

o Experimental Points

Δ Longer-lived Activity Subtracted

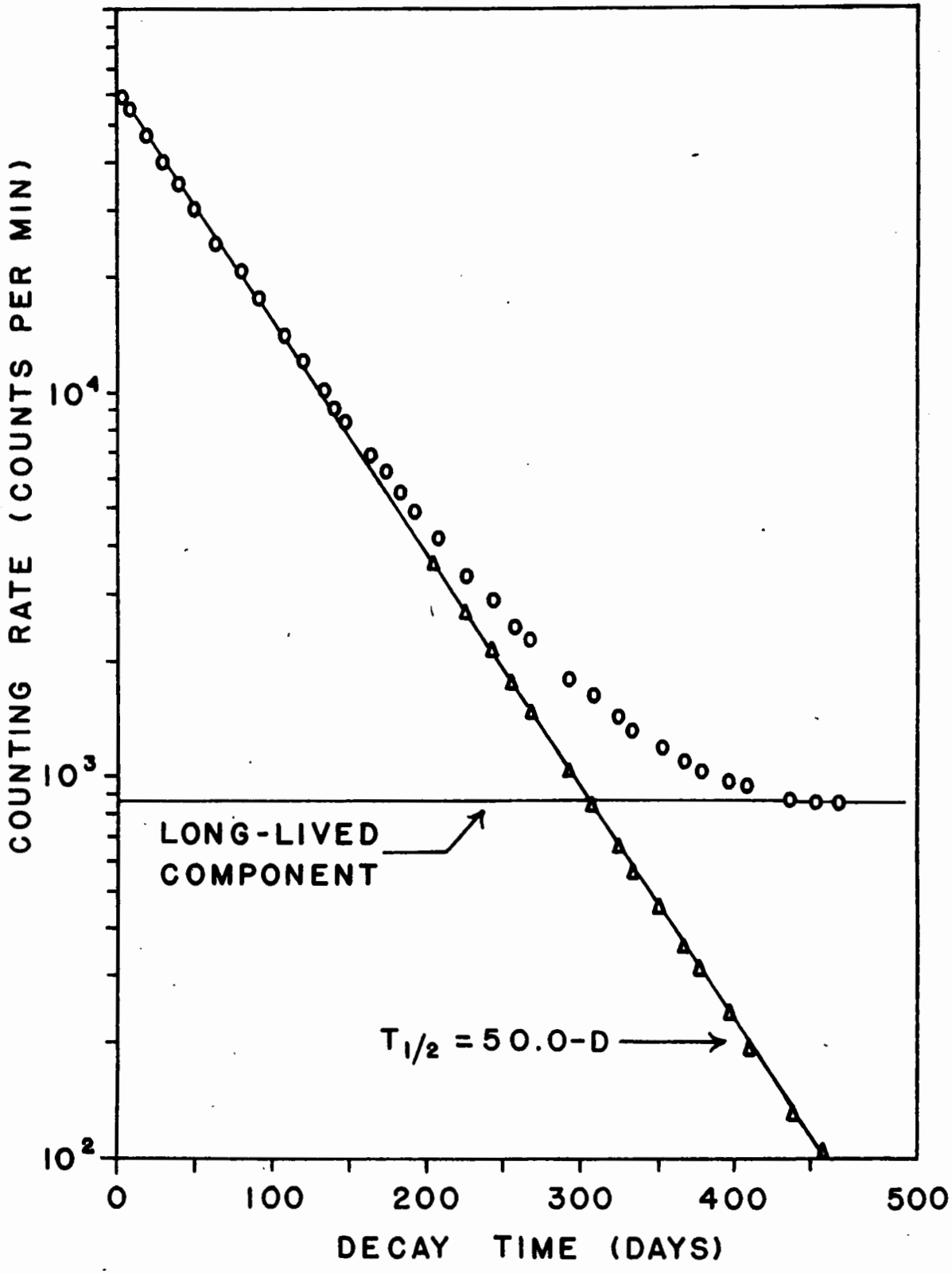
COUNTING RATE (COUNTS PER MIN)
10^4
10^3
10^2
LONG-LIVED
COMPONENT
$T_{1/2}$ = 50.0-D
0
100
200
300
400
500
DECAY TIME (DAYS)

Figure 16

Decay Curve of Sr^{91}

O Experimental Points

Δ Longer-lived Activity Subtracted

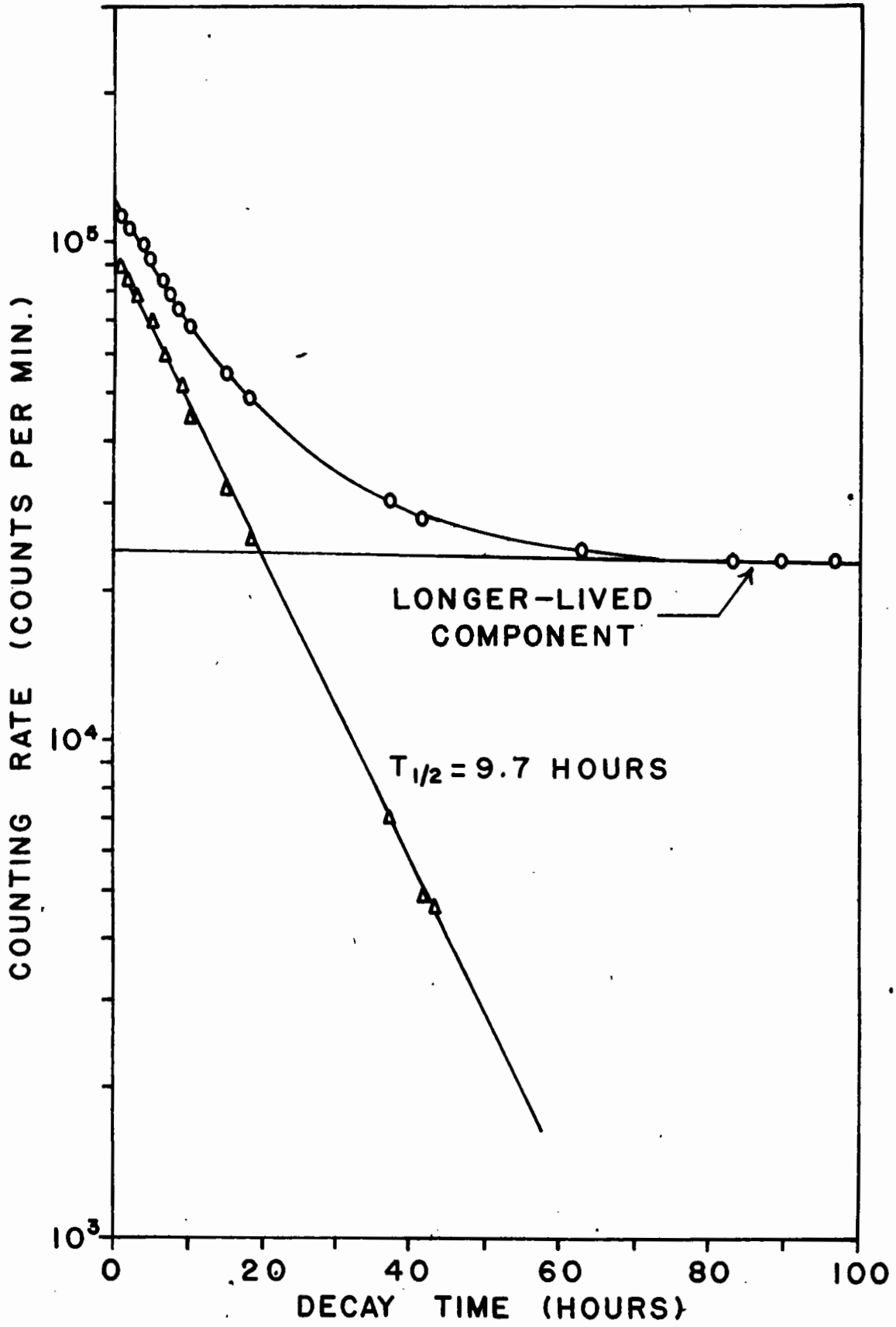
COUNTING RATE (COUNTS PER MIN.)
10^5
10^4
10^3
LONGER-LIVED
COMPONENT
$T_{1/2}$ = 9.7 HOURS
0
20
40
60
80
100
DECAY TIME (HOURS)

Figure 17

γ Spectrum of Sr^{91}-Y^{91} as Measured on a Scintillation Spectrometer

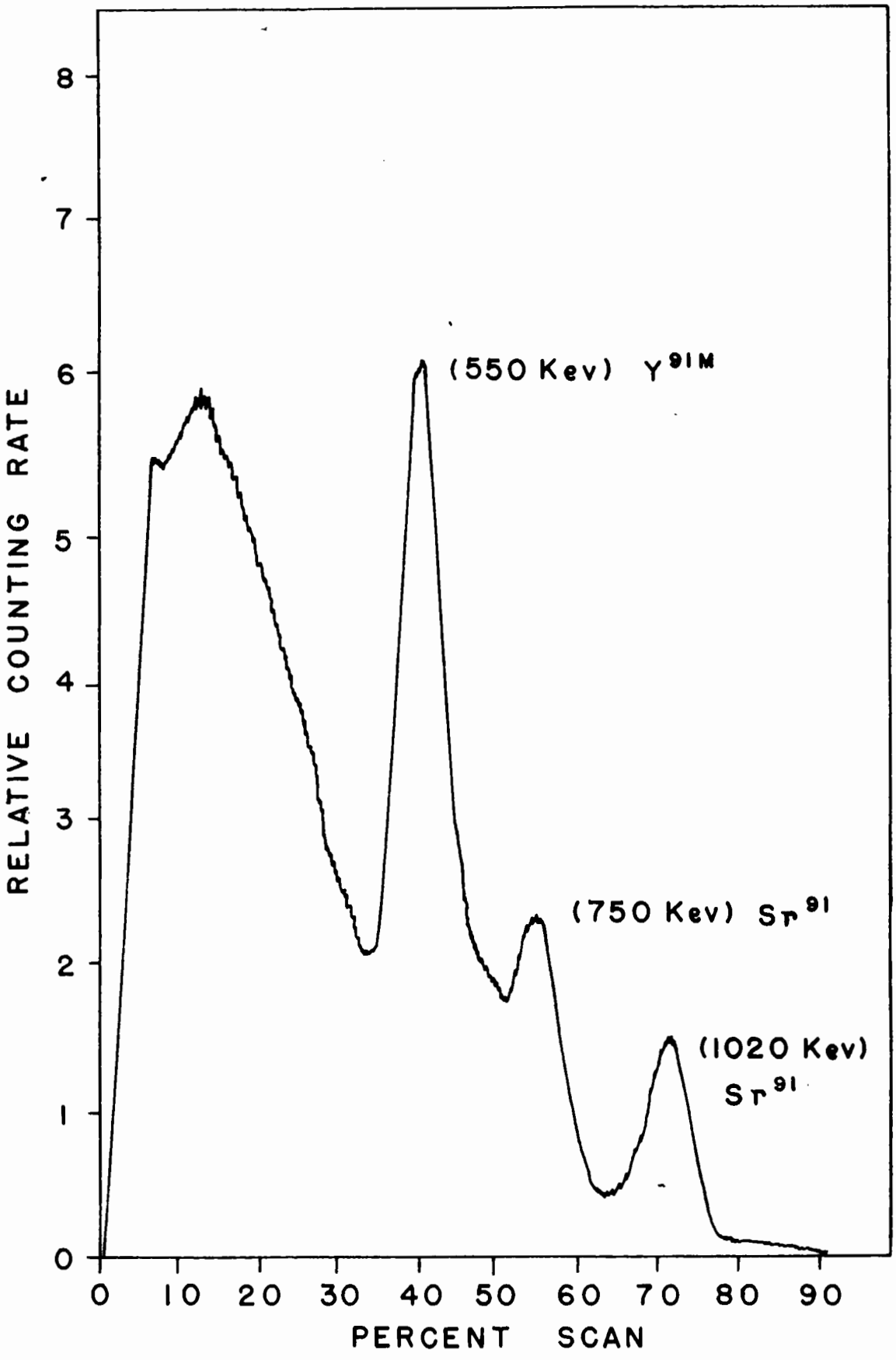
RELATIVE COUNTING RATE
0
1
2
3
4
5
6
7
8
0
10
20
30
40
50
60
70
80
90
PERCENT SCAN
(550 Kev) Y91M
(750 Kev) Sr91
(1020 Kev) Sr91

Figure 18

Decay of the γ Photopeaks Observed

On the Scintillation Spectrometer.

740 and 1020 Kev = Sr^{91}

550 Kev = Y^{91}

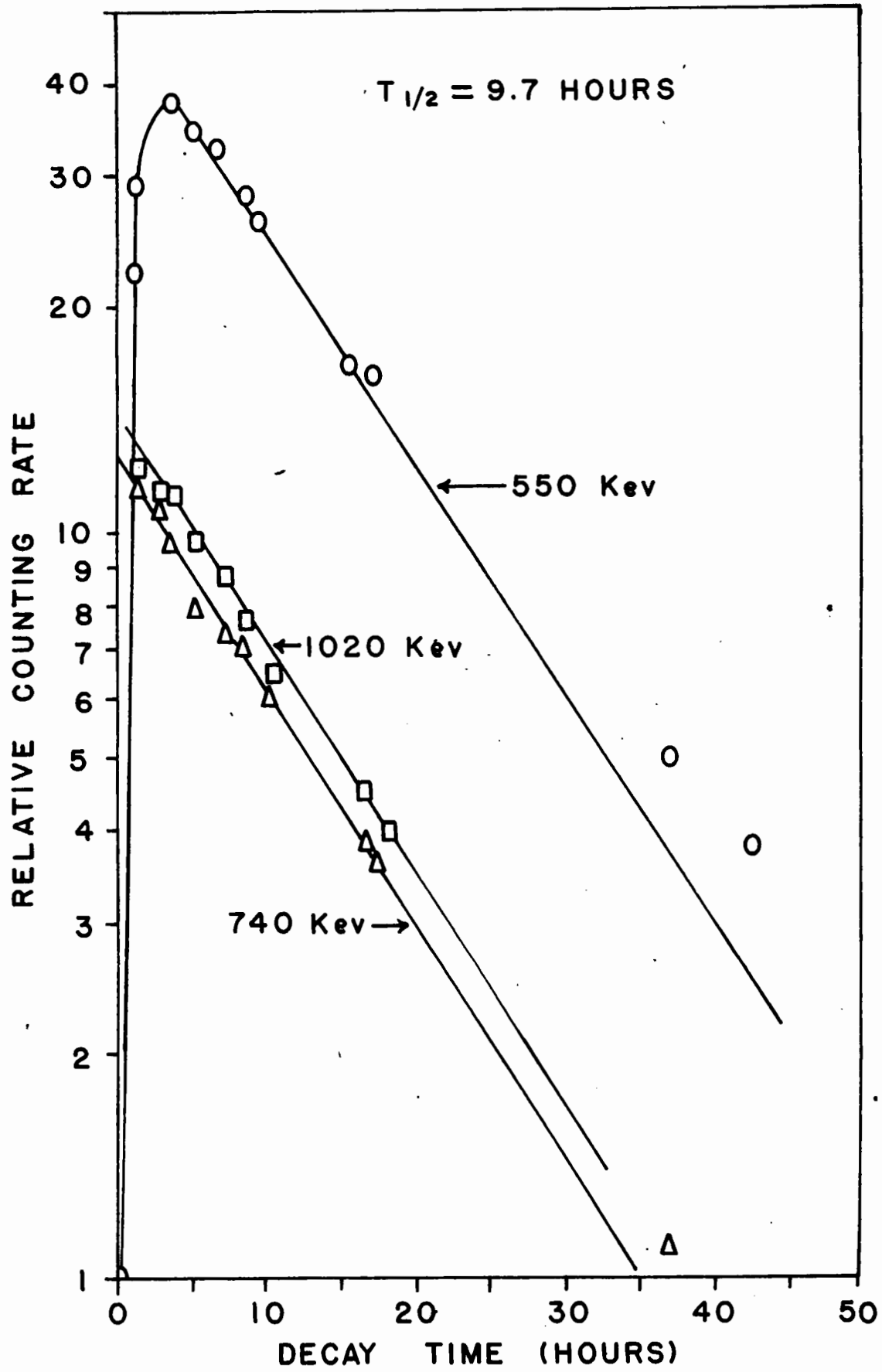
$T_{1/2}$ = 9.7 HOURS
550 Kev
1020 Kev
740 Kev
RELATIVE COUNTING RATE
DECAY TIME (HOURS)
40
30
20
10
9
8
7
6
5
4
3
2
1
0
10
20
30
40
50

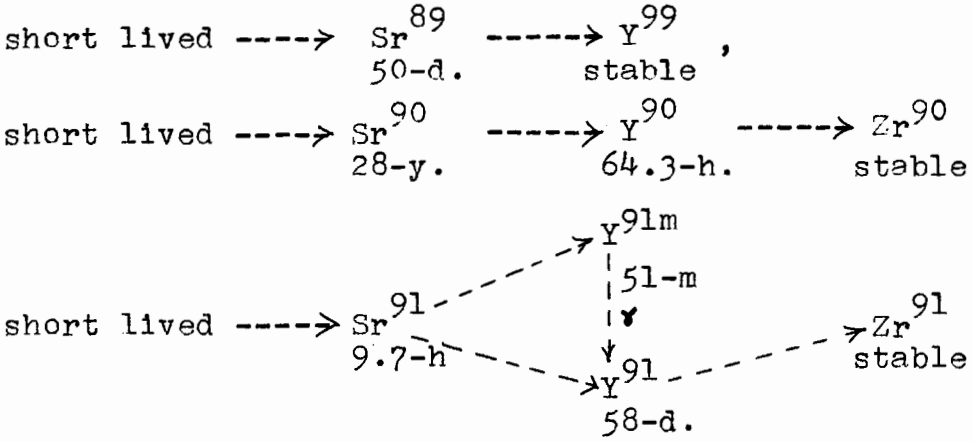

Sr^{89} decays by the emission of 1.462 Mev β^- (73), and Sr^{90} emits a 0.541 Mev β^- to form Y^{90} (74) which is also a β^- emitter. Consequently, the presence of Sr^{89} and $Sr^{90} + Y^{90}$ would not be expected to give any γ spectrum. On the other hand, Sr^{91} decays by the emission of 2.7 (25 %), 1.4 (25 %), and 0.8 (50 %) Mev β^- particles together with 0.748 and 1.025 Mev γ-rays (70,75). In addition, about 60 % of the Sr^{91} disintegrations lead to a 51-minute isomer Y^{91m}, and 40 % to 58-day Y^{91}. The yttrium is not present at the end of the strontium separation but grows in as the Sr^{91} decays. The Y^{91m} is shorter lived than the parent Sr^{91} so would grow in, reach a maximum value (transient equilibrium), and decay with a half-life characteristic of the parent. The γ energy of the isomeric transition Y^{91m} to Y^{91} is 0.550 Mev.

It was possible to resolve the gross decay curve of Sr^{89}, Sr^{90} and Y^{90} into its components by following the decay until Sr^{89} was undetectable. It was assumed that the remaining activity was due to Sr^{90} and Y^{90} in equilibrium.

This seems justified since no other long-lived strontium isotopes are formed in fission. In addition, no contamination from other elements appeared possible since shorter-lived activities of such elements were not detected. When in equilibrium, the disintegration rates of Sr^{90} and Y^{90} are equal. Therefore, one half of the observed residual counting rate, after applying absorption corrections, could be attributed to the Sr^{90} present. On this basis the fission yield of Sr^{90} was calculated. As a further check on the yield, a separated strontium sample was allowed to decay and the yttrium which formed was separated and counted. From the amount of Y^{90} obtained it was possible to calculate the amount of Sr^{90} present. A fission yield of Sr^{90} calculated on this basis agreed with that in which Sr^{90} was counted directly.

The counting rate of 50-d Sr^{89} was determined by subtracting the amount of the long-lived activity observed.

It is not possible to obtain the amount of Sr^{91} activity by direct analysis of the gross decay curve, due to the formation of Y^{91}. However, from the following considerations it is possible to determine the amount of Sr^{89} and Sr^{91} present. At the end of the strontium separation there is no yttrium, therefore the total observed activity (N_T^o) is

$$N_T^o = Sr^{89o} + Sr^{91o} + Sr^{90} .$$

At a time later when the Sr^{91} has completely decayed to form Y^{91}, the total observed counting rate (N'_T) is

$$N'_T = Sr^{89o} \exp(-\lambda_1 t) + \frac{\lambda_3}{\lambda_3 - \lambda_2} Sr^{91o} \exp(-\lambda_3 t) + (Sr^{90} + Y^{90})'$$

where $\lambda_1 = \lambda$ for Sr^{89}, $\lambda_2 = \lambda$ for Sr^{91} and $\lambda_3 = \lambda$ for Y^{91} and t = time from the end of separation until the time when N'_T is measured. Since N^o_T, N'_T, $(Sr^{90} + Y^{90})'$ can be measured, it is possible to solve for Sr^{89o} and Sr^{91o}. Since the decay of Sr^{91} involves delayed-γ emission, i.e., γ emission from the Y^{91m} state, it is necessary to know the efficiency of the counting unit for the detection of Y^{91m} disintegrations. The important factors involved are:

(i) the γ-detection efficiency,

(ii) the amount of internal conversion, and

(iii) the efficiency for detection of internal conversion electrons.

The decay chains involved in the determination of the Sr^{91} disintegration rate are

$$Sr^{91} \xrightarrow{.60} Y^{91m} \longrightarrow Y^{91} \longrightarrow Zr$$
$$9.7\text{-h.} \qquad 51\text{-m.} \qquad 58\text{-d.} \qquad \text{stable}$$

$$Sr^{91} \xrightarrow{.40} Y^{91} \longrightarrow Zr$$
$$9.7\text{-h.} \qquad 58\text{-d.} \qquad \text{stable}$$

By means of growth and decay equations and starting with pure Sr^{91}, the relative counting rates for Sr^{91}, Y^{91} and Y^{91m} were calculated for various decay times. The calculated rates were then compared to the observed relative counting rates at the same decay times. The observed relative counting rates were obtained by dividing the observed counting rate at time t by the counting rate

obtained by extrapolating the initial portion of the strontium decay curve to the time at which the separation had ended. This extrapolation procedure is justified if counting had begun soon after the separation, before Y^{91m} reached equilibrium with Sr^{91}. The calculated and observed values are given in Table 5.

TABLE 5

DECAY DATA FOR THE MASS 91 CHAIN

Decay time (hours)	Relative activity Sr^{91} + Y^{91}	Y^{91m}	Observed
0	1.00	0	1.00
1	0.931	0.321	0.928
2	0.868	0.441	0.867
3	0.808	0.474	0.804
4	0.753	0.469	0.752
5	0.701	0.449	0.701
10	0.493	0.322	0.484

The observed relative counting rate agrees with that calculated for Sr^{91} plus Y^{91}, indicating that the efficiency for counting Y^{91m} in the 4π -proportional counter is very low.

All data relating to the fission yields of strontium isotopes investigated are given in Tables 6, 7 and 8.

TABLE 6

FISSION YIELD DATA FOR 50.4-DAY Sr^{89}

Irradiation number	A 1	A 2
Observed activity	61880 c/m	47410 c/m
Self-absorption factor	0.988	0.988
Source-mount Absorption factor	1.000	1.000
Aliquot factor	5000	5000
Chemical yield	77.2 %	76.3 %
Time after irradiation	17.35 days	29.10 days
Decay factor	0.790	0.673
Time in reactor	24 hours	24 hours
Saturation factor	0.0135	0.0135
Activity at saturation	6.279×10^8 d/s	6.010×10^8 d/s
Average activity At saturation	6.227×10^8 d/s	

All fission yields calculated for irradiation A were determined relative to Sr^{89} by means of equation 24 page 59. The saturation activity of the nuclide in question was compared to that of Sr^{89} for the same irradiation. After taking into account the errors involved in measurements, a "weighted" average saturation activity for Sr^{89} was calculated. The value for the fission yield of Sr^{89}, which will be discussed later, was taken as 5.56 %.

TABLE 6 (CONTINUED)

FISSION YIELD DATA FOR 50.4-DAY Sr^{89}

Irradiation number	B 1	C 1
Observed activity	19916 c/m	58500 c/m
Self-absorption factor	0.998	0.997
Source-mount Absorption factor	1.000	1.000
Aliquot factor	12500	12500
Chemical yield	29.4 %	58.2 %
Time after irradiation	9.90 days	3.75 days
Decay factor	0.874	0.950
Time in reactor	24 hours	24 hours
Saturation factor	0.0135	0.0135
Activity at saturation	1.199×10^9 d/s	1.637×10^9 d/s
Fission rate	2.270×10^{10} f/s	2.885×10^{10} f/s
Fission yield	(5.28 ± 0.14) %	(5.67 ± 0.07) %

TABLE 6 (CONTINUED)

FISSION YIELD DATA FOR 50.4-DAY Sr^{89}

Irradiation number	D_a 1	D_a 2
Observed activity	18680 c/m	3570 c/m
Self-absorption factor	0.997	0.998
Source-mount Absorption factor	1.000	1.000
Aliquot factor	12500	12500
Chemical yield	58 %	33.0 %
Time after irradiation	15.44 days	95.44 days
Decay factor	0.811	0.273
Time in reactor	18.5 hours	18.5 hours
Saturation factor	0.0105	0.0105
Activity at saturation	7.936×10^8 d/s	7.904×10^8 d/s
Fission rate	1.464×10^{10} f/s	1.464×10^{10} f/s
Fission yield	(5.42 ± 0.18) %	(5.40 ± 0.08) %

TABLE 6 (CONTINUED)

FISSION YIELD DATA FOR 50.4-DAY Sr^{89}

Irradiation number	D_b 1	D_b 2
Observed activity	11960 c/m	20200 c/m
Self-absorption factor	0.997	0.997
Source-mount Absorption factor	1.000	1.000
Aliquot factor	5000	1666
Chemical yield	63.4 %	63.1 %
Time after irradiation	73.25 days	115.41 days
Decay factor	0.370	0.208
Time in reactor	18.5 hours	18.5 hours
Saturation factor	0.0105	0.0105
Activity at saturation	4.079×10^8 d/s	4.091×10^8 d/s
Fission rate	7.225×10^9 f/s	7.225×10^9 f/s
Fission yield	(5.65 ± 0.06) %	(5.66 ± 0.06) %

TABLE 6 (CONTINUED)

FISSION YIELD DATA FOR 50.4-DAY Sr^{89}

Irradiation number	E	F
Observed activity	1503 c/m	23370 c/m
Self-absorption factor	0.997	0.997
Source-mount Absorption factor	1.000	1.000
Aliquot factor	2500	25000
Chemical yield	52.2 %	52.1 %
Time after irradiation	27.0 days	1.5 days
Decay factor	0.693	0.980
Time in reactor	23.83 hours	24.17 hours
Saturation factor	0.0134	0.0136
Activity at saturation	1.295×10^{7} d/s	1.406×10^{9} d/s
Fission rate	fast fission	2.587×10^{10} f/s
Fission yield	-----	(5.43 ± 0.08) %

TABLE 7

FISSION YIELD DATA FOR 27.7-YEAR Sr^{90}

Irradiation A 1

Observed activity	400 counts per minute
Self-absorption factor	0.93
Source-mount Absorption factor	0.997
Aliquot factor	5000
Chemical yield	77.2 %
Time after irradiation	17.35
Decay factor	1.00
Time in reactor	24 hours
Saturation factor	6.781×10^{-5}
Activity at saturation	6.8674×10^{8} dis. per second
Relative fission yield	(6.16 ± 0.12) %

TABLE 7 (CONT'D.)

FISSION YIELD DATA FOR 27.7-YEAR Sr^{90}

(Determined by counting 64.3-hour Y^{90})

Irradiation number	D_b 2	D_a2
Observed activity	510 c/m	362 c/m
Self-absorption factor	0.996	0.982
Source-mount Absorption factor	1.000	1.000
Aliquot factor	1333	2500
Chemical yield	49.2 %	33.0 %
Time after irradiation	115.41 days	106 days
Decay factor	0.9922	0.9928
Time in reactor	18.5 hours	18.5 hours
Saturation factor	5.2×10^{-5}	5.2×10^{-5}
Activity at saturation	4.481×10^{8} d/s	9.025×10^{8} d/s
Fission rate	7.225×10^{9} f/s	1.464×10^{10} f/s
Fission yield	(6.20 ± 0.09) %	(6.16 ± 0.07) %

TABLE 8

FISSION YIELD DATA FOR 9.7-HOUR SR^{91}

Irradiation F 1

Observed activity	96630 counts per minute
Self-absorption factor	0.987
Source-mount Absorption factor	1.000
Aliquot factor	2500
Chemical yield	52.1 %
Time after irradiation	36.0 hours
Decay factor	0.07638
Time in reactor	24.16 hours
Saturation factor	0.8220
Activity at saturation	1.2464×10^{9} dis. per second
Fission rate	2.587×10^{10} fissions per second
Fission yield	(4.82 ± 0.25) %

The uranium sample in irradiation E was surrounded with cadmium foil. The observed strontium activity must then have been produced by a fast fission process. A comparison of the strontium activity in a shielded and an unshielded sample would give a measure of the fast fission factor. In irradiation C the strontium saturation activity was 3.151×10^{8} disintegrations per second per mgm. of sample. The measured flux value was 5.05×10^{12} neutrons per $cm.^{2}$ per second. The strontium saturation activity for irradiation E was 6.65×10^{6} disintegrations per second per mgm. of sample for a corresponding neutron flux. The percentage of strontium activity produced by fast neutrons to that produced by fast plus slow neutrons was 2.10 %. On page 65 it was shown that 1.76 % of the cobalt monitor activity was produced by the presence of fast neutrons. The difference between these two values is presumably due to the differences in fast and slow neutron cross sections. It was not necessary to apply a fast fission correction to the fission yield results since both the monitor and the fissile material were similarly influenced.

The possibility exists that Sr^{89} may be produced by radiative capture of natural strontium (82.6 % Sr^{88}) present as an impurity,

$$Sr^{88}(n\gamma)Sr^{89}.$$

Spectrographic analysis of the uranium sample indicated that

the amount of strontium present was less than 0.02 % of the uranium 233 content. For the heaviest sample irradiated there were 1.32×10^{19} atoms of U^{233}, so there could be no more than 2.2×10^{15} atoms of Sr^{88} present. By using equation (31) page 60, it is possible to calculate the amount of Sr^{89} formed. Taking the neutron capture cross section for Sr^{88} as 0.005 barns, about 34 disintegrations per minute is obtained. This activity can be considered negligible.

(c) Yttrium

The method used for the separation of yttrium was that given by Ballou (76). Since the chemical properties of yttrium are similar to those of the rare earth elements, it was necessary to add carriers of cerium, lanthanum, praseodymium as well as yttrium. The rare earths and yttrium were separated from other fission product activities by the precipitation of their fluorides. After the fluorides were dissolved in an HNO_3-H_3BO_3 mixture, cerium was oxidized with chloric acid and precipitated as the iodate. The rare earth activities were separated from yttrium by the precipitation of potassium-rare earth carbonates. Yttrium was recovered from the remaining solution by an oxalate precipitation.

In the sepration of yttrium from a strontium-yttrium mixture, fluoride and hydroxide precipitations were carried out in the presence of strontium hold-back carrier. The separated yttrium was dissolved in dilute acid and made up to a volume of 10 ml.

Chemical yields were determined by precipitating and weighing the hydrated yttrium oxalate which had been dried by vacuum desiccation.

Periodically, 20 λ aliquots of the yttrium activity were mounted on VYNS films and counted in the 4π -proportional counter. Half-lives of 65 hours (Figure 19) and 59 days (Figure 20) were obtained. The 65-hour activity was that separated from strontium which had previously been separated and allowed to decay. This daughter activity was obviously that of Y^{90} which has a reported half-life of 64.8 hours (77) and decays with a β energy of 2.26 Mev (78). The 59-day activity was assigned as Y^{91}. The half-life of Y^{91} is given as 58.3 days (77) and the β end-point energy is 0.36 Mev (79). A 2.0 ml. aliquot of the yttrium solution was analyzed on the scintillation spectrometer and showed no γ-photopeaks.

The decay chains for the activities detected are

$$\text{short lived} \xrightarrow{} \underset{28\text{-y}}{Sr^{90}} \xrightarrow{} \underset{65\text{-h.}}{Y^{90}} \xrightarrow{} \underset{\text{stable}}{Zr^{90}}$$

$$\text{short lived} \xrightarrow{} \underset{58\text{-d.}}{Y^{91}} \xrightarrow{} \underset{\text{stable}}{Zr^{91}} .$$

The Y^{90} detected was formed only from the decay of Sr^{90}. For this reason the data for the fission yields based on Y^{90} measurements have been included in Table 7 for the fission yield of Sr^{90}. The activity of Y^{91} was determined long after

Figure 19

Decay Curve of Y^{90}

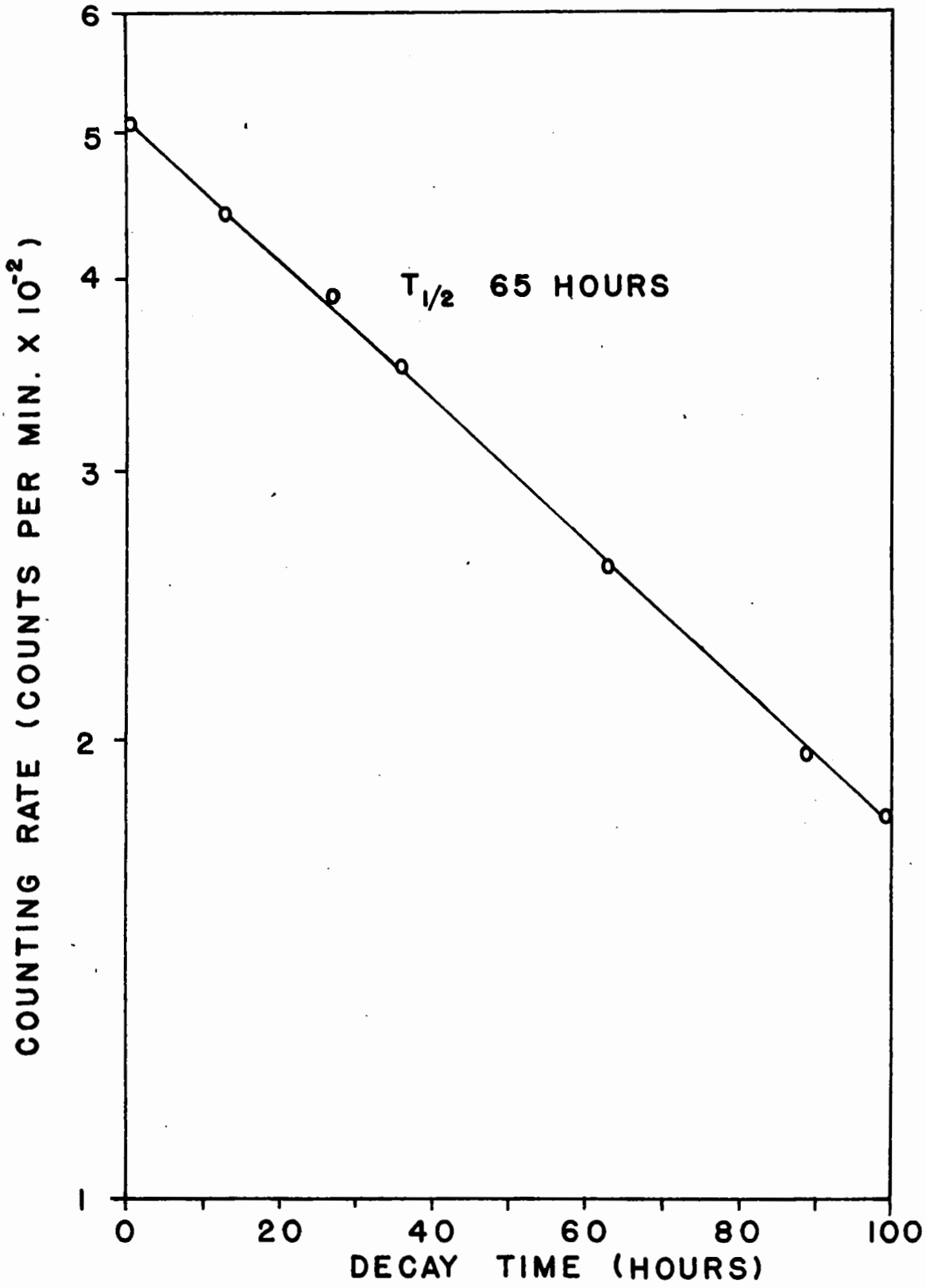
6
5
4
3
2
1
COUNTING RATE (COUNTS PER MIN. X 10^{-2})
$T_{1/2}$ 65 HOURS
0
20
40
60
80
100
DECAY TIME (HOURS)

Figure 20

Decay Curve of Y^{91}

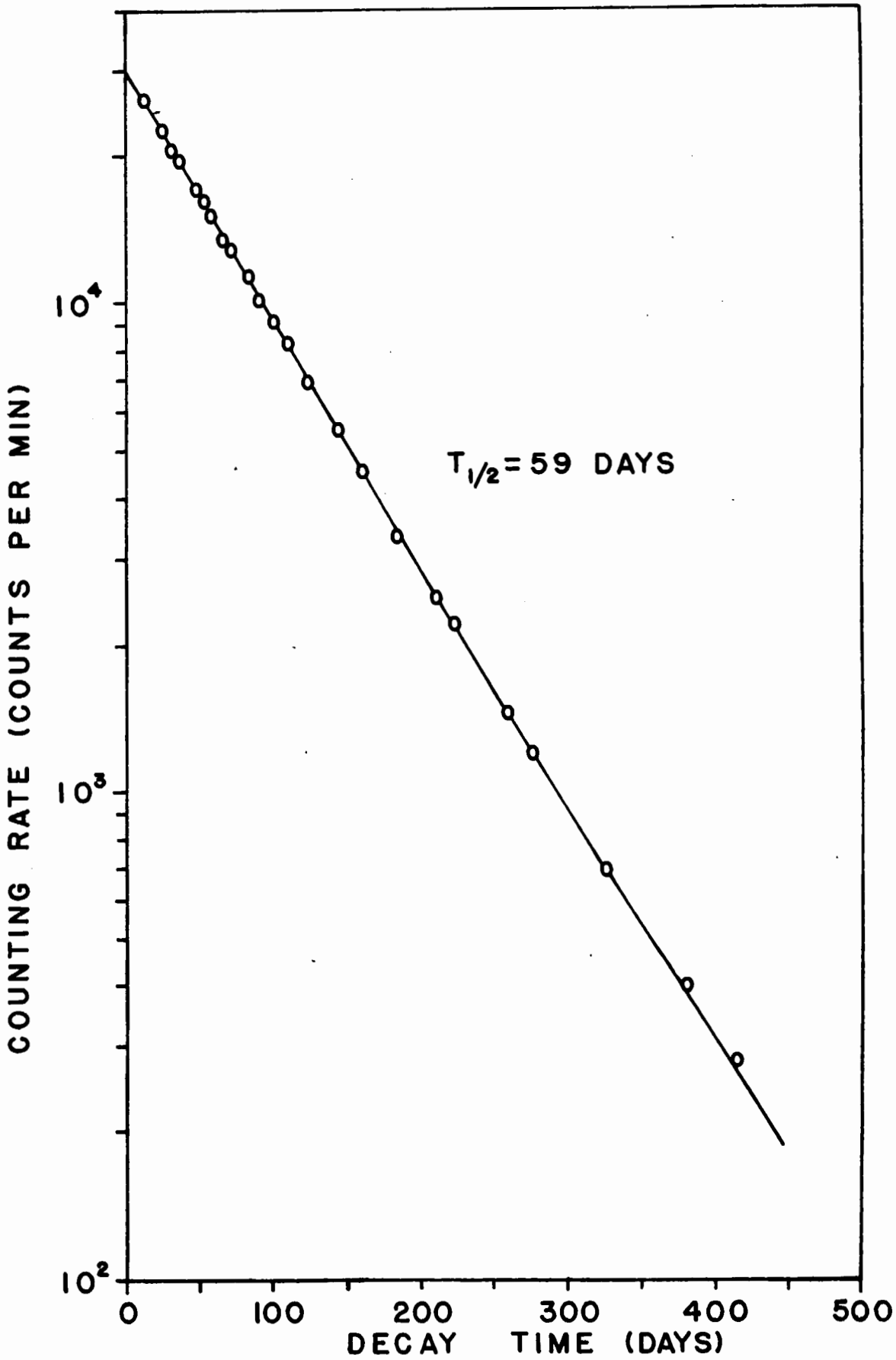
COUNTING RATE (COUNTS PER MIN)
10^4
10^3
10^2
$T_{1/2}$ = 59 DAYS
0
100
200
300
400
500
DECAY TIME (DAYS)

the end of the irradiation so that all known precursors had decayed. The data for the yield of Y^{91} is presented in Table 9.

TABLE 9

FISSION YIELD DATA FOR 58.3-DAY Y^{91}

Irradiation number	B 1	C 1
Observed activity	4973 c/m	7360 c/m
Self-absorption factor	0.996	0.996
Source-mount Absorption factor	1.000	1.000
Aliquot factor	6250	4166
Chemical yield	36.6 %	21.5 %
Time after irradiation	158 days	137.64 days
Decay factor	0.1514	0.1931
Time in reactor	24 hours	24 hours
Saturation factor	0.01188	0.01188
Activity at saturation	7.897×10^8 d/s	1.0394×10^9 d/s
Fission rate	2.2695×10^{10} f/s	2.8848×10^{10} f/s
Fission yield	(3.48 ± 0.18) %	(3.60 ± 0.11) %

No natural yttrium was detected in a spectrographic analysis of the original uranium sample.

(d) Zirconium

The method used for the separation of radio-zirconium was essentially a combination of a procedure given by Hume (80)

and one given by Moore (81). Exactly 20 mgm. of zirconium carrier was added to an aliquot of the fission product stock solution. This solution was made 2 M in HNO_3 and 0.5 M in hydroxylamine hydrochloride. The solution was extracted for 10 to 15 minutes with an equal volume of 0.5 M 2-thenoyl-trifluoroacetone (TTA) in xylene. After the phases had separated, the organic layer was removed and washed for three minutes with an equal volume of 1 M HNO_3. The zirconium was then removed from the organic phase by a three minute extraction with an equal volume of 0.25 M HNO_3 - 0.25 M HF. About 50 mgm. of Ba^{++} carrier was added to the separated aqueous phase followed by the addition of 1 ml. of HF. The $BaZrF_6$ was removed by centrifugation, washed and dissolved in a dilute boric acid-nitric acid solution. Borate and fluoride ions were removed by passing the solution through a column containing Dowex-1 anion exchange resin. The zirconium was precipitated from the effluent with ammonia, washed with water, dissolved in dilute acid and then made up to a volume of 10 ml.

Chemical yields were determined by precipitating aliquots of the zirconium solution with a 6 % cupferron solution and igniting to ZrO_2.

The counting of 50 and 100 λ portions of the zirconium activity in the 4π-proportional counter indicated an initial growth and subsequent decay with a 65-day half-life as shown

in Figure 21. A 740 Kev γ-photopeak was observed on the scintillation spectrometer (Figure 22). The γ-counting rate also increased at first and then decayed with a half-life of about 65 days (Figure 23). The observed activity was attributed to 65-day Zr^{95} (83) and its decay products. The decay chain for this nuclide is

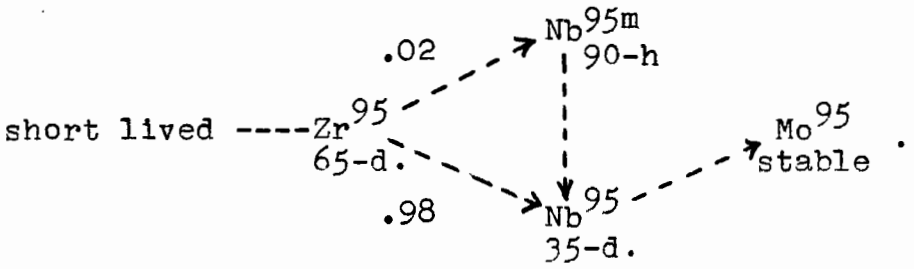

In the decay of Zr^{95}, γ rays of energy 754 and 722 Kev are emitted. In addition, γ rays may be expected from 90-hour Nb^{95m} (236 Kev) and 35-day Nb^{95} (770 Kev). No Nb^{95m} was observed in the γ spectrum. The initial observed γ peak at 740 Kev was a combination of 754 and 722 Kev energies. The growth of this peak was due to the formation of the 770 Kev γ-emitter Nb^{95}.

The counting rate for Zr^{95} was obtained by counting sources immediately after the separation and by making a short extrapolation back to the end of separation where no niobium activity was present. A correct counting rate for Zr^{95} could not be obtained in the presence of niobium activities due to incomplete knowledge of the decay schemes involved and the detection efficiency of radiations emitted. The fission yield data for Zr^{95} are given in Table 10.

Figure 21

β Decay Curve of Zr^{95}

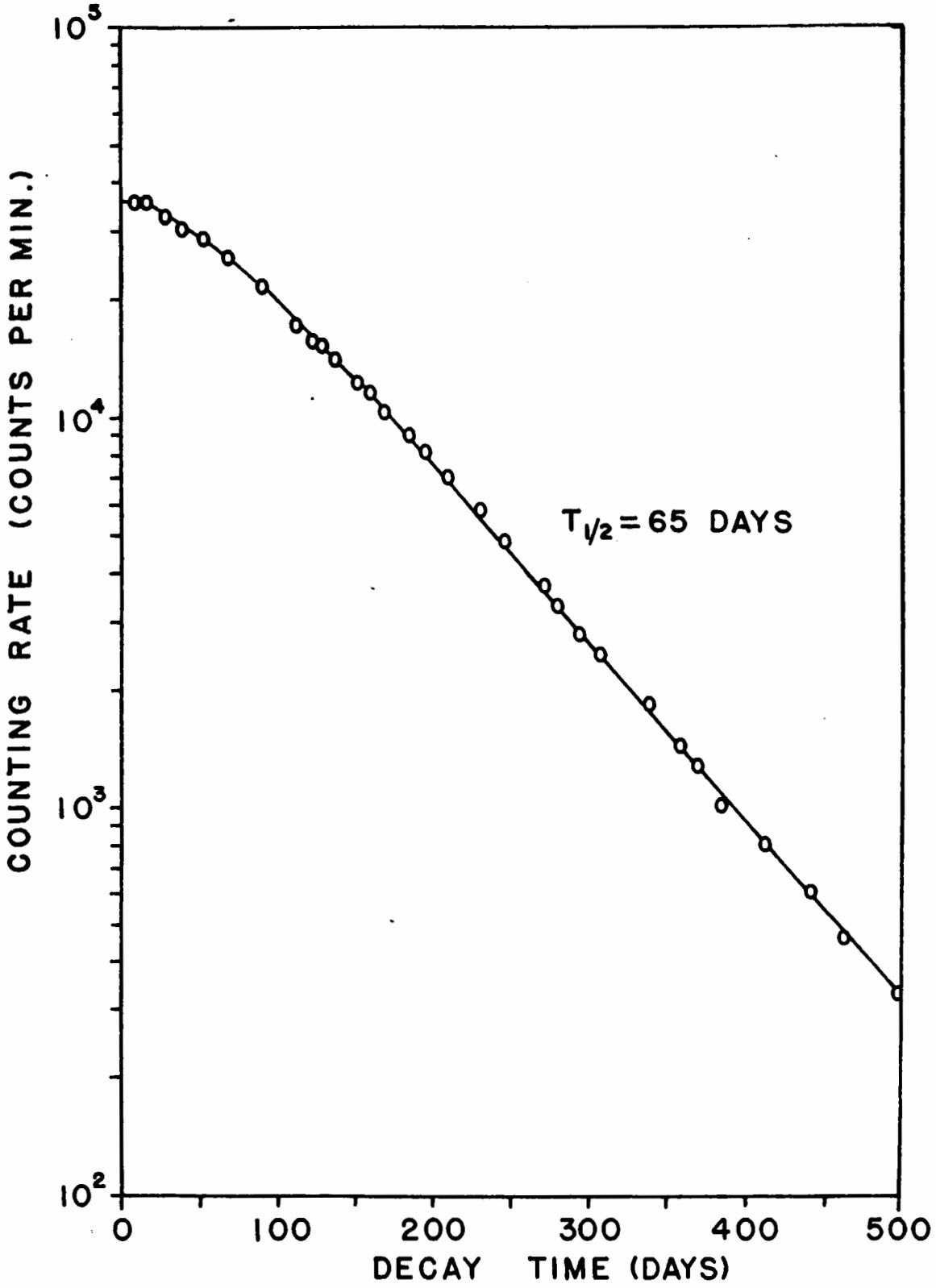
COUNTING RATE (COUNTS PER MIN.)
10^5
10^4
10^3
10^2
$T_{1/2}$ = 65 DAYS
0
100
200
300
400
500
DECAY TIME (DAYS)

Figure 22

γ Spectrum of Zr^{95} as Measured on a Scintillation Spectrometer

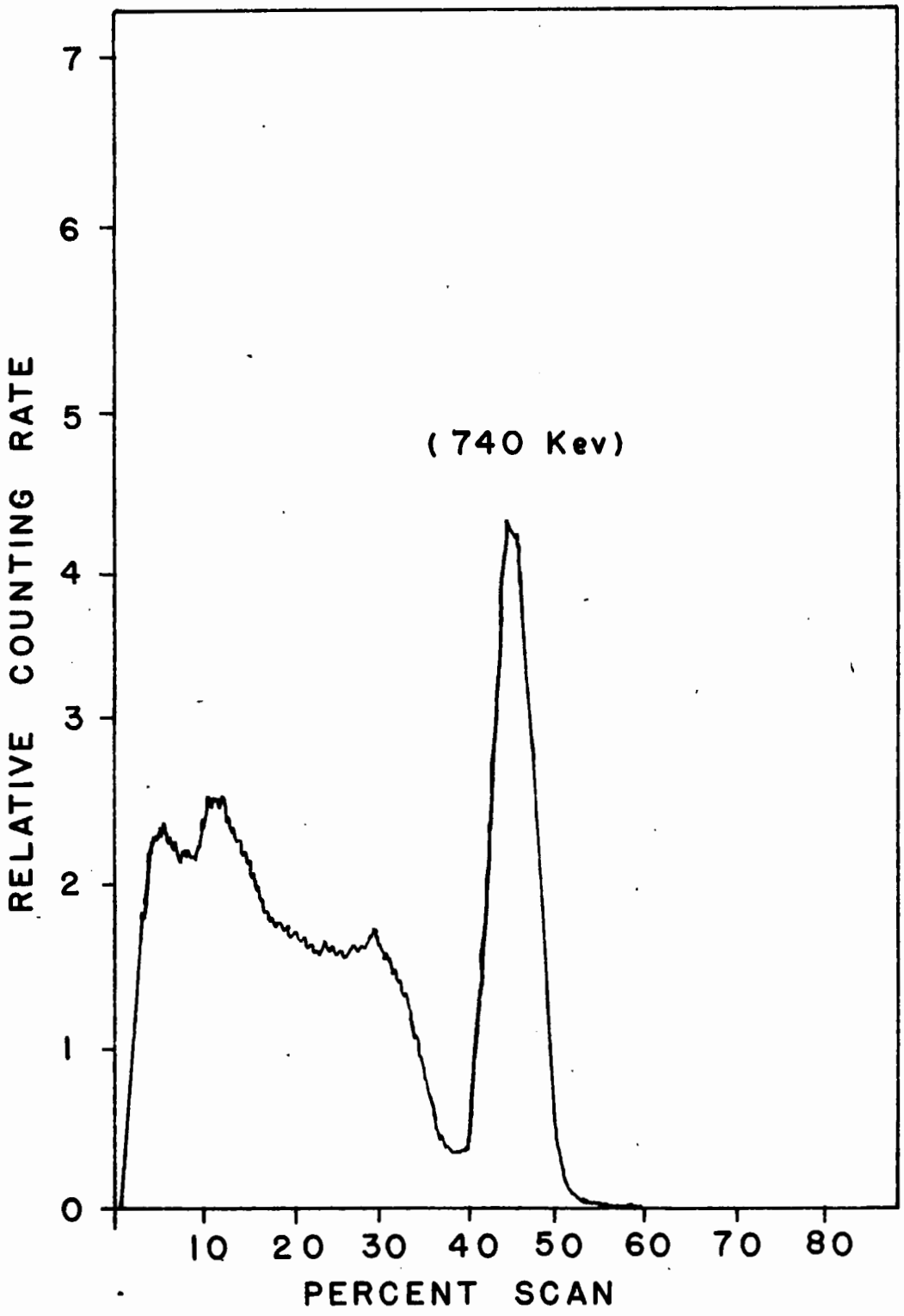
RELATIVE COUNTING RATE
0
1
2
3
4
5
6
7
(740 Kev)
10
20
30
40
50
60
70
80
PERCENT SCAN

Figure 23

Growth and Decay Curve for the 740 Kev γ Photopeak Observed for Zr^{95} -Nb^{95}

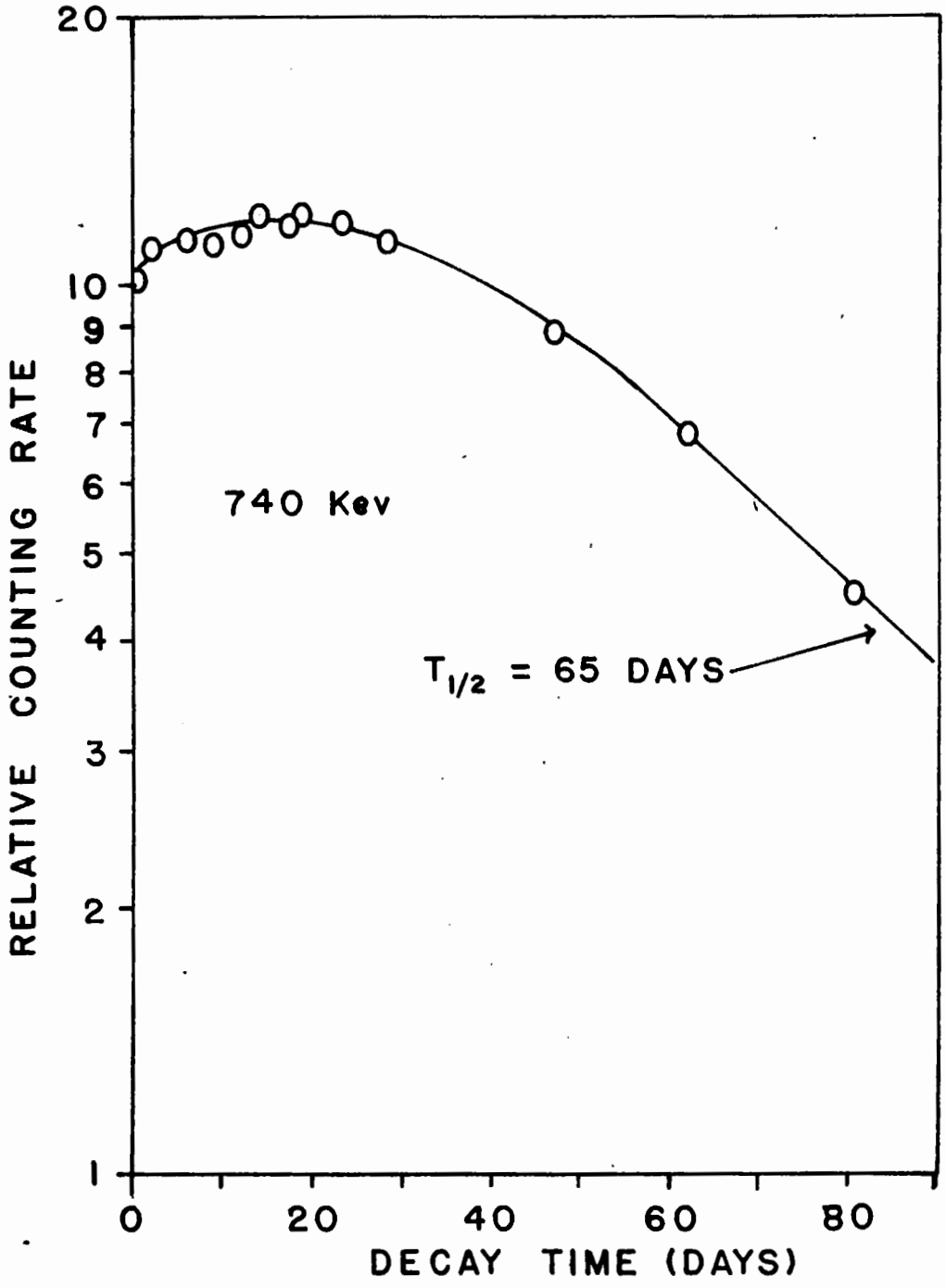
20
10
9
8
7
6
5
4
3
2
1
RELATIVE COUNTING RATE
740 Kev
$T_{1/2}$ = 65 DAYS
0
20
40
60
80
DECAY TIME (DAYS)

Spectrographic analysis of the sample irradiated indicated that the amount of zirconium present as an impurity was less than 0.02 % of the U^{233} content. The amount of Zr^{95} formed by the reaction

$$Zr^{94}(n\gamma)Zr^{95}$$

was calculated by means of equation (31) on page 60. The abundance of Zr^{94} is 17.4 % and its thermal-neutron cross section is 0.1 barns. The maximum amount of Zr^{94} which might be present is 4.5×10^{14} atoms and this would produce an

TABLE 10

FISSION YIELD DATA FOR 65-DAY ZIRCONIUM 95

Irradiation number	A 1	B 1
Observed activity	35000 c/m	35400
Self-absorption factor	0.760	0.973
Source-mount Absorption factor	1.000	1.000
Aliquot factor	2500	3610
Chemical yield	38.8 %	21 %
Time after irradiation	13.1 days	28.63 days
Decay factor	0.870	0.737
Time in reactor	24 hours	24 hours
Saturation factor	0.0106	0.0106
Activity at saturation	5.365×10^8 d/s	1.309×10^8 d/s
Fission rate	relative yield	2.270×10^{10} f/s
Fission yield	(4.82 ± 0.50) %	(5.77 ± 1.44) %

activity of about one count per minute.

(e) Niobium

The separation of niobium from other fission products was based on the specific precipitation of Nb_2O_5 from an oxalate solution with chloric acid (84). Niobium carrier was added to an aliquot of the fission product stock solution. After several cycles of precipitations, the niobium was dissolved in a minimum of oxalic acid and made up to a volume of either 10 or 25 ml.

Chemical yields were determined by precipitating and weighing Nb_2O_5. The precipitate was washed with a dilute ammonium chloride solution and then with ethanol before being dried at 110°C. for 30 minutes.

Prepared 20, 50 and 100 λ sources of the niobium activity were counted in the 4π -proportional counter. All sources which had been separated at least 33 days after the end of the irradiation decayed with a half-life of 35 days (Figure 24). A 2.0 ml. sample of the niobium when analyzed on the scintillation spectrometer indicated the presence of a nuclide emitting a 770 Kev γ ray with a half-life of about 35 days (Figures 25 and 26). These decay characteristics are those of 35-day Nb^{95} (83) which is one of the daughter activities of Zr^{95} previously discussed.

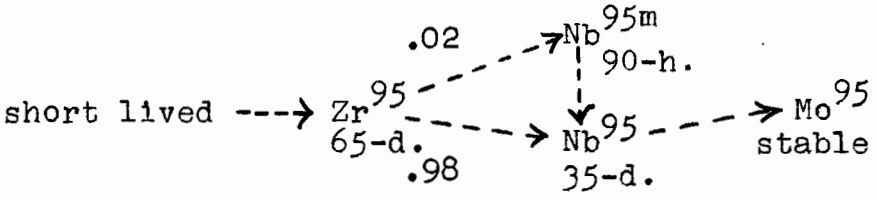

Figure 24

β Decay Curve of 35-Day Nb^{95}

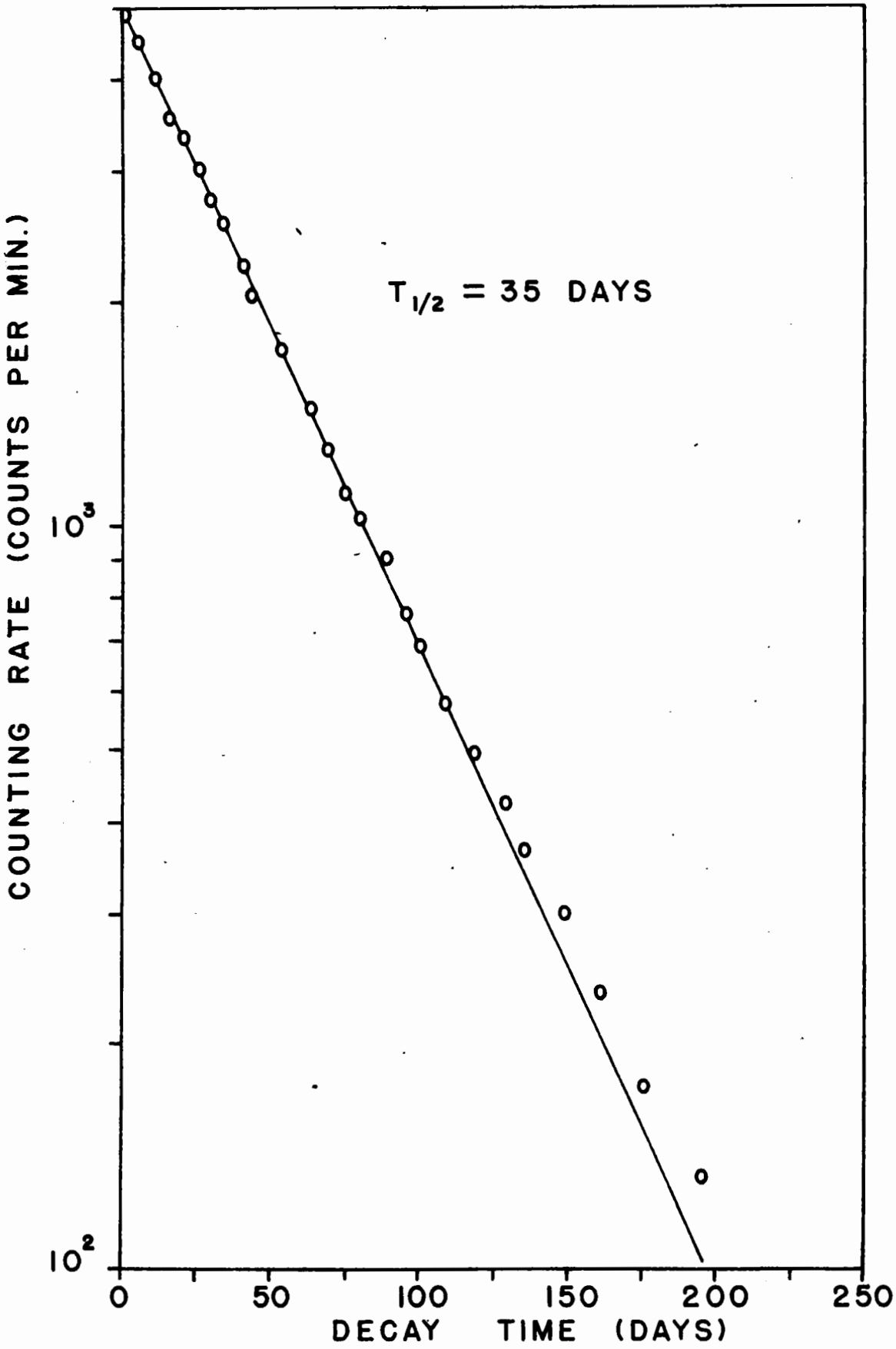
$T_{1/2}$ = 35 DAYS
COUNTING RATE (COUNTS PER MIN.)
10^3
10^2
0
50
100
150
200
250
DECAY TIME (DAYS)

Figure 25

γ Spectrum of Nb^{95}

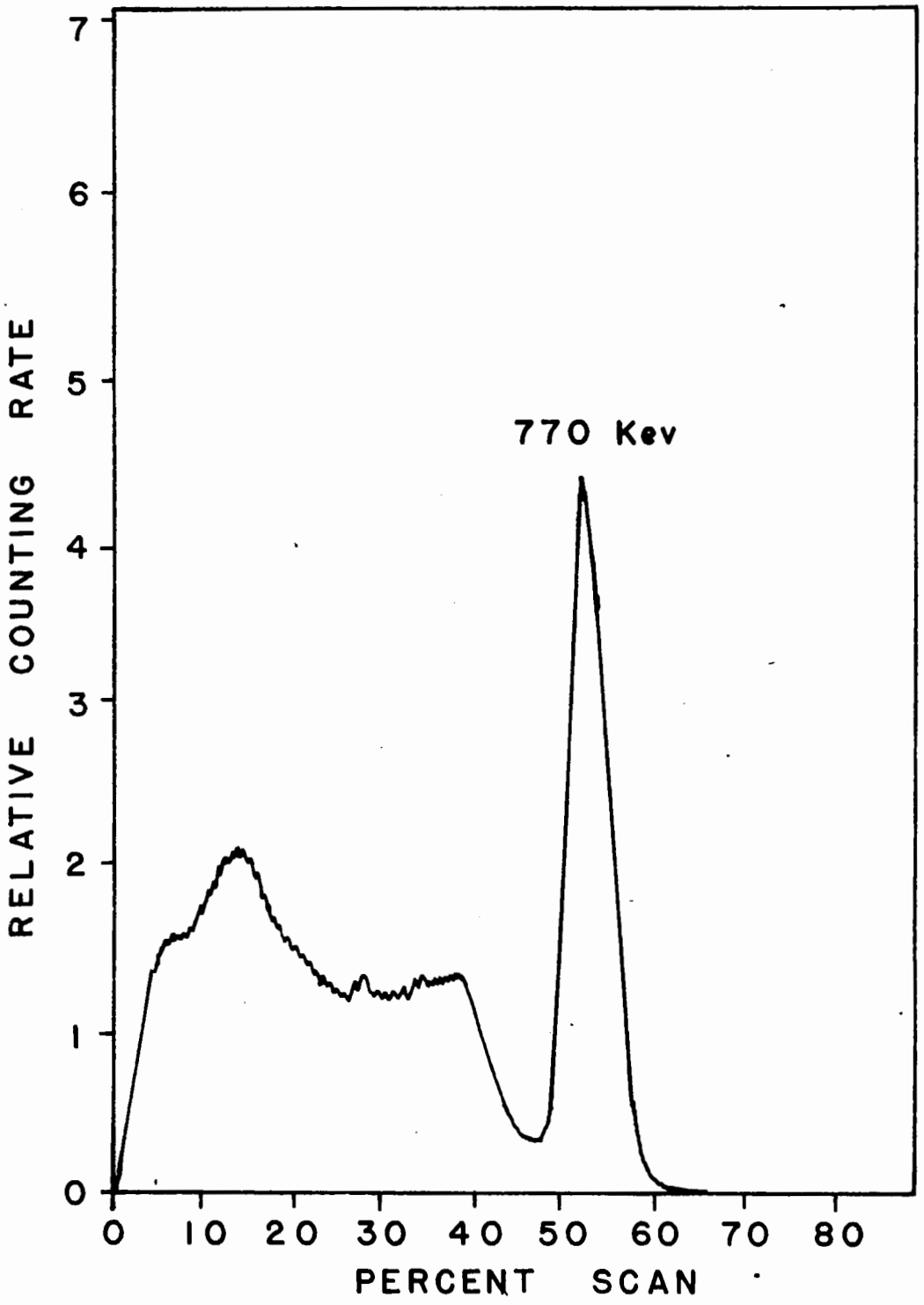
770 Kev
RELATIVE COUNTING RATE
PERCENT SCAN
0
1
2
3
4
5
6
7
0
10
20
30
40
50
60
70
80

Figure 26

Decay Curve of Nb^{95} -770 Kev γ Peak

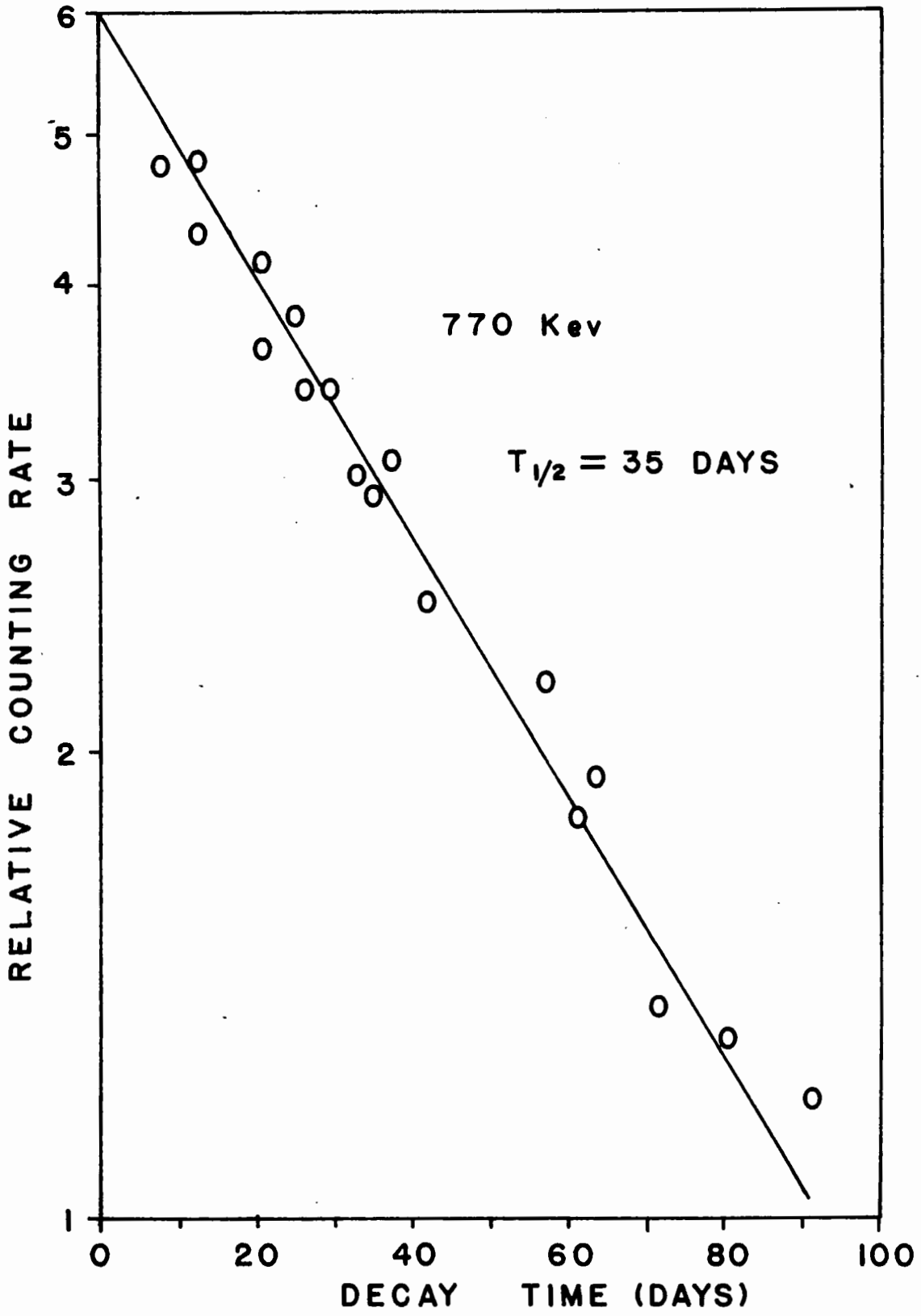
6
5
4
3
2
1
RELATIVE COUNTING RATE
770 Kev
$T_{1/2}$ = 35 DAYS
0
20
40
60
80
100
DECAY TIME (DAYS)

The absence of any detectable 90-hour Nb^{95m} indicates that the amount of this isomer formed from the decay of Zr^{95} must be small as is indicated above by the decay scheme.

An attempt was made to measure Nb^{95m} by separating niobium 4.2 days after an irradiation. However, the samples were found to be contaminated with tellurium activity so that no yield of Nb^{95m} could be accurately obtained.

The calculation of a disintegration rate for Nb^{95} involves applying rather large self-absorption corrections. To keep the niobium in solution it was necessary to add an excess of oxalic acid which increased the source superficial density. The total source thickness was determined by weighing an aliquot of the sample which had been evaporated on to a known area.

The data for the fission yield of Nb^{95} are given in Table 11.

TABLE 11

FISSION YIELD DATA FOR 35-DAY Nb^{95}

Irradiation number	F 1	F 2
Observed activity	12300 c/m	26800 c/m
Self-absorption factor	0.680	0.780
Source-mount Absorption factor	0.990	0.990
Aliquot factor	15625	6250
Chemical yield	91 %	96.8 %
Time after irradiation	87.1 days	114.25 days
Decay factor	0.2079	0.12414
Time in reactor	24.17 hours	24.17 hours
Saturation factor	0.01971	0.01971
Activity at saturation	1.281×10^9 d/s	1.561×10^9 d/s
Fission rate	2.587×10^{10} f/s	2.587×10^{10} f/s
Fission yield	(4.94 ± 0.29) %	(6.03 ± 0.99) %

(f) Ruthenium

Carriers of ruthenium (Ru^{+3}), iodide and bromide were added to an aliquot of the fission product stock solution. Following an oxidation with sodium bismuthate and perchloric acid, ruthenium was separated from the other fission products by distilling the volatile RuO_4 into a NaOH solution (87). Ruthenium oxide was precipitated several times in the presence of NaOH by reduction with ethanol. The oxide was dissolved in 6 M HCl and after the final separation, ruthenium was made up to a volume of 10 ml.

Chemical yields were determined by adding magnesium metal to precipitate ruthenium as the metal. Excess magnesium was dissolved in concentrated HCl. The ruthenium metal was filtered, washed and dried at 110°C. for 20 minutes. From the weight of Ru obtained the percent of carrier recovered was calculated.

The decay of ruthenium was measured by counting 50 and 100 λ sources in the 4π -proportional counter. A drop of dilute LiOH was added to the active sources on VYNS films to aid in drying. A 40-day activity and a longer-lived component ($\sim$ one year) were observed. The decay is plotted in Figure 27. A γ spectrum was obtained (Figure 28) which shows the presence of a 500 Kev γ ray. The half-life of the γ decay was also 40 days (Figure 29). It was then apparent that the observed 40-day activity was Ru^{103}. This nuclide decays to a metastable state (Rh^{103m}) by the emission of a 220 Kev β-

Figure 27

β Decay Curve of 40-Day Ru^{103} and 1-Year Ru^{106}

O Experimental Points

Δ 1-Year Activity Subtracted

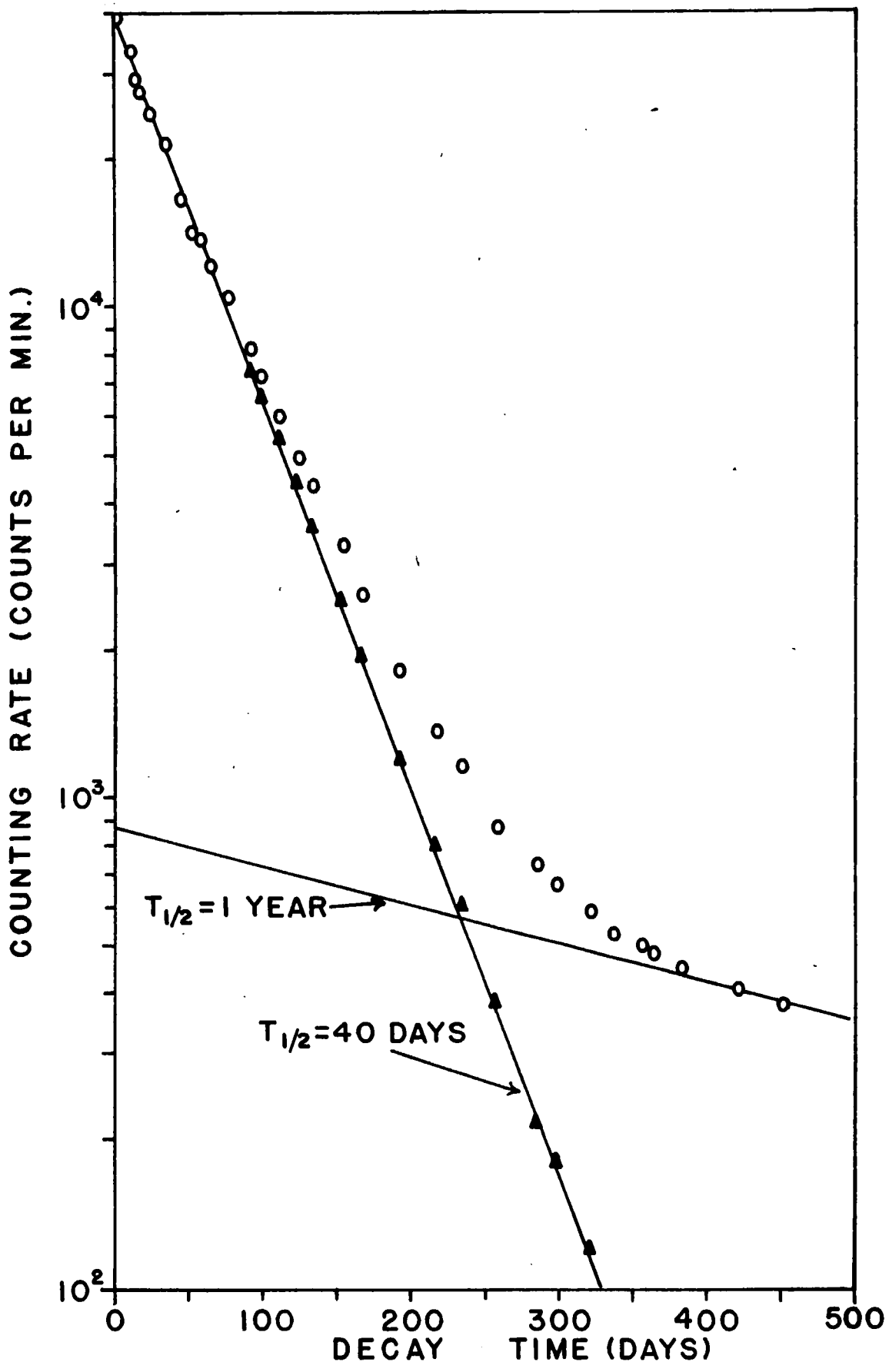
COUNTING RATE (COUNTS PER MIN.)
10^4
10^3
10^2
$T_{1/2}$=1 YEAR
$T_{1/2}$=40 DAYS
0
100
200
300
400
500
DECAY TIME (DAYS)

Figure 28

γ Spectrum of Ru^{103}

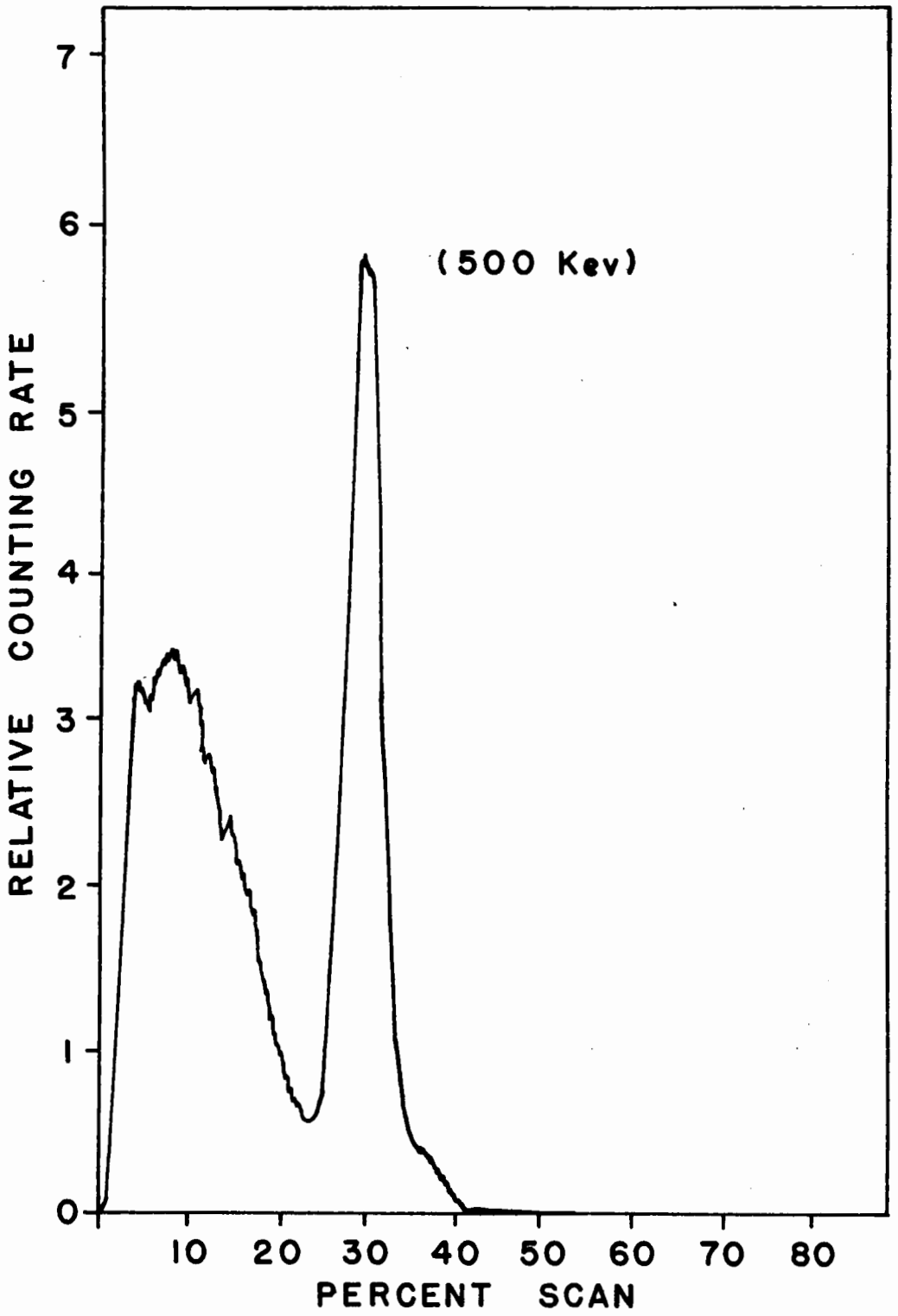
(500 Kev)
RELATIVE COUNTING RATE
0
1
2
3
4
5
6
7
10
20
30
40
50
60
70
80
PERCENT SCAN

Figure 29

Decay Curve of Ru^{103}-500 Kev γ Peak

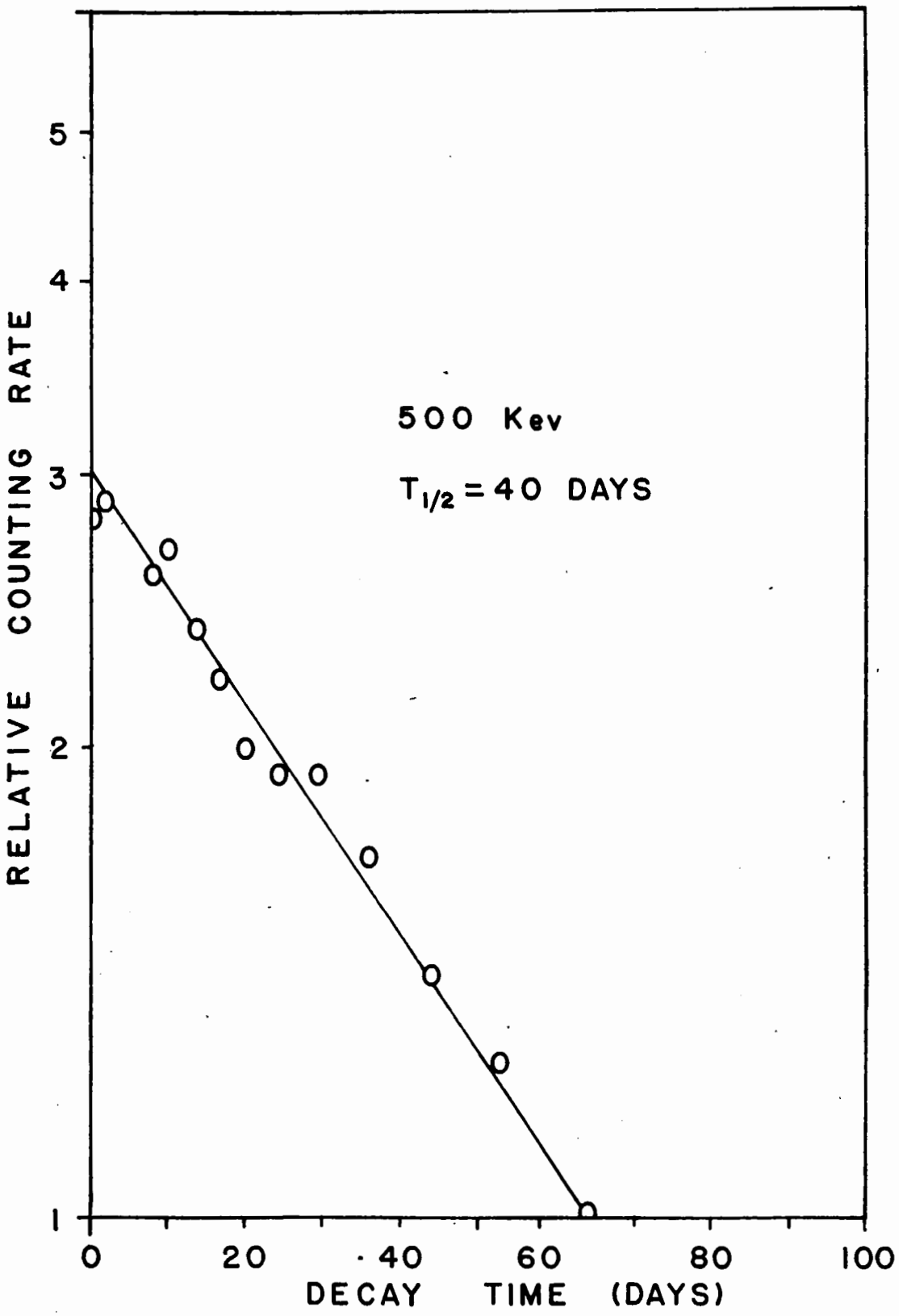
RELATIVE COUNTING RATE
5
4
3
2
1
500 Kev
$T_{1/2}$ = 40 DAYS
0
20
40
60
80
100
DECAY TIME (DAYS)

particle in coincidence with a 495 Kev γ ray (88). The Rh^{103m} nuclide de-excites with a half-life of 57 minutes through the emission of a 55 Kev γ ray. The decay chain for mass 103 is

short lived ---> Ru^{103} (40-d.) ----> Rh^{103m} (57-m.) .
γ ↓
Rh^{103} stable

The residual activity with a half-life of about one year was assigned to Ru^{106}, a known fission product with a half-life of 1.02 years (89) and a β^- end-point energy of 39.2 Kev (90). The decay chain involving Ru^{106} is

$$Ru^{106}\ (1.0\text{-y.}) \longrightarrow Rh^{106}\ (30\text{-s.}) \longrightarrow Pd^{106}\ \text{stable} \quad .$$

The measurement of a disintegration rate for both Ru^{103} and Ru^{106} is difficult due to the low energy of the radiation and the presence of short-lived daughter activities,

For Ru^{103} it was necessary to consider the effects of the delayed-γ emitter Rh^{103m}. The total internal conversion coefficient (α_T) for the 40.2 Kev γ ray is about 484 (91). From this value can be calculated N_{e^-}, the number of conversion electrons emitted.

$$N_{e^-} = \frac{\alpha_T}{1 + \alpha_T} = 0.998$$

Therefore, 99.8 % of Rh^{103m} disintegrations involve conversion electron emission. The energies of these electrons

can be estimated from the following relationship

$$E_{e^-} = E_{\gamma} - E_{b.e.} ,$$

where E_{e^-} is the energy of an emitted conversion electron,

E_{γ} is the unconverted γ energy, and

$E_{b.e.}$ is the binding energy of an electron in its atomic orbit.

Values of $E_{b.e.}$ for ruthenium can be obtained from X-ray absorption energy measurements. The values for the K and L electrons are approximately 22.1 and 3.0 Kev respectively (86). The energies of the converted electrons would then be from 18 to 39 Kev. By using the source-mount and self-absorption data described earlier, it is found that these electrons are almost completely absorbed. It must be remembered that the absorption data were measured for the end-point energy of a β spectrum. Since conversion electrons are monoenergetic, a slight difference in absorption would be expected. An upper limit of 5 % was set for the detection of Rh^{103m} disintegrations. Perhaps a better method for determining the disintegration rate of Ru^{103} would be to completely absorb the conversion electrons by laminating the source with thin films of known superficial density. An absorption correction could then be accurately applied to the β emitter.

The observed one-year activity represents an equilibrium counting rate for Ru^{106} and Rh^{106}. Absorption losses are to be expected for the Ru^{106} radiation but not for Rh^{106} since the latter has maximum β^- energies of 3.5 (82 %) and 2.3 (18 %) Mev. (92).

Fission yield data are presented for Ru^{103} and Ru^{106} in Tables 12 and 13 respectively.

TABLE 12

FISSION YIELD DATA FOR 40-DAY Ru^{103}

Irradiation B 1

Observed activity	38630 counts per minute
Self-absorption factor	0.857
Source-mount Absorption factor	0.985
Aliquot factor	1250
Chemical yield	18 %
Time after irradiation	22.53 days
Decay factor	0.6768
Time in reactor	24 hours
Saturation factor	0.01718
Activity at saturation	4.5809×10^{8} dis. per second
Fission rate	2.2695×10^{10} fissions per second
Fission yield	(2.02 ± 0.08) %

TABLE 13

FISSION YIELD DATA FOR 1.02-YEAR Ru^{106}

Irradiation B 1

Observed activity	865 counts per minute
Self-absorption factor	0.95
Source-mount	
Absorption factor	1.000
Aliquot factor	1250
Chemical yield	18 %
Time after irradiation	22.53 days
Decay factor	0.9583
Time in reactor	24 hours
Saturation factor	0.00188
Activity at saturation	5.8813×10^7 dis. per second
Fission rate	2.2695×10^{10} fissions per second
Fission yield	(0.259 ± 0.03) %

No natural ruthenium or rhodium was detected in the original uranium sample.

(g) Rhodium

The separation of rhodium was based on its extraction into pyridine from a strongly alkaline solution (93), Carriers of rhodium (Rh^{+3}) and tellurium (Te^{+4}) were used. Rhodium was recovered from the pyridine phase by a sulphide precipitation. The precipitate was dissolved and ruthenium carrier was added. Ruthenium activities were removed by fuming with perchloric acid. The rhodium sulphide precipitation was repeated and the precipitate, after being washed, was dissolved in a minimum of aqua regia and diluted to 10 ml.

Chemical yields were determined by reducing aliquots of rhodium solution with magnesium metal. The precipitate formed was filtered, washed, dried at 110°C. for 30 minutes and weighed as rhodium metal.

Sources consisting of 20 λ portions of the separated rhodium, when counted in the 4π-proportional counter, were observed to give a 36-hour decay curve (Figure 30). The presence of a 320 Kev photopeak in the γ spectrum for this activity (Figure 31) established its identity as Rh^{105}. The fission product decay chain for this nuclide is

short lived ----> Ru^{105} (4.5-h.) ----> Rh^{105m} (γ ↓ 35-s.) Rh^{105} (36.5-h.) ----> Pd^{105} stable

Rh^{105} decays by the emission of β - particles of maximum energies 210 (4 %) and 570 (96 %) Kev. A 320 Kev γ ray is emitted in coincidence with the β radiation (94).

The fission yield data for Rh^{105} are given in Table 14.

TABLE 14

FISSION YIELD DATA FOR 36.5-HOUR Rh^{105}

Irradiation F 1

Observed activity	1550 counts per minute
Self-absorption factor	0.920
Source-mount Absorption factor	1.000
Aliquot factor	8333
Chemical yield	26 %
Time after irradiation	144.6 hours
Decay factor	0.0643
Time in reactor	24.16 hours
Saturation factor	0.368
Activity at saturation	3.770×10^{7} dis. per second
Fission rate	2.587×10^{10} fissions per second
Fission yield	(0.146 ± 0.037) %

Figure 30

Decay Curve of Rh^{105}

O Experimental Points

Δ Background Subtracted

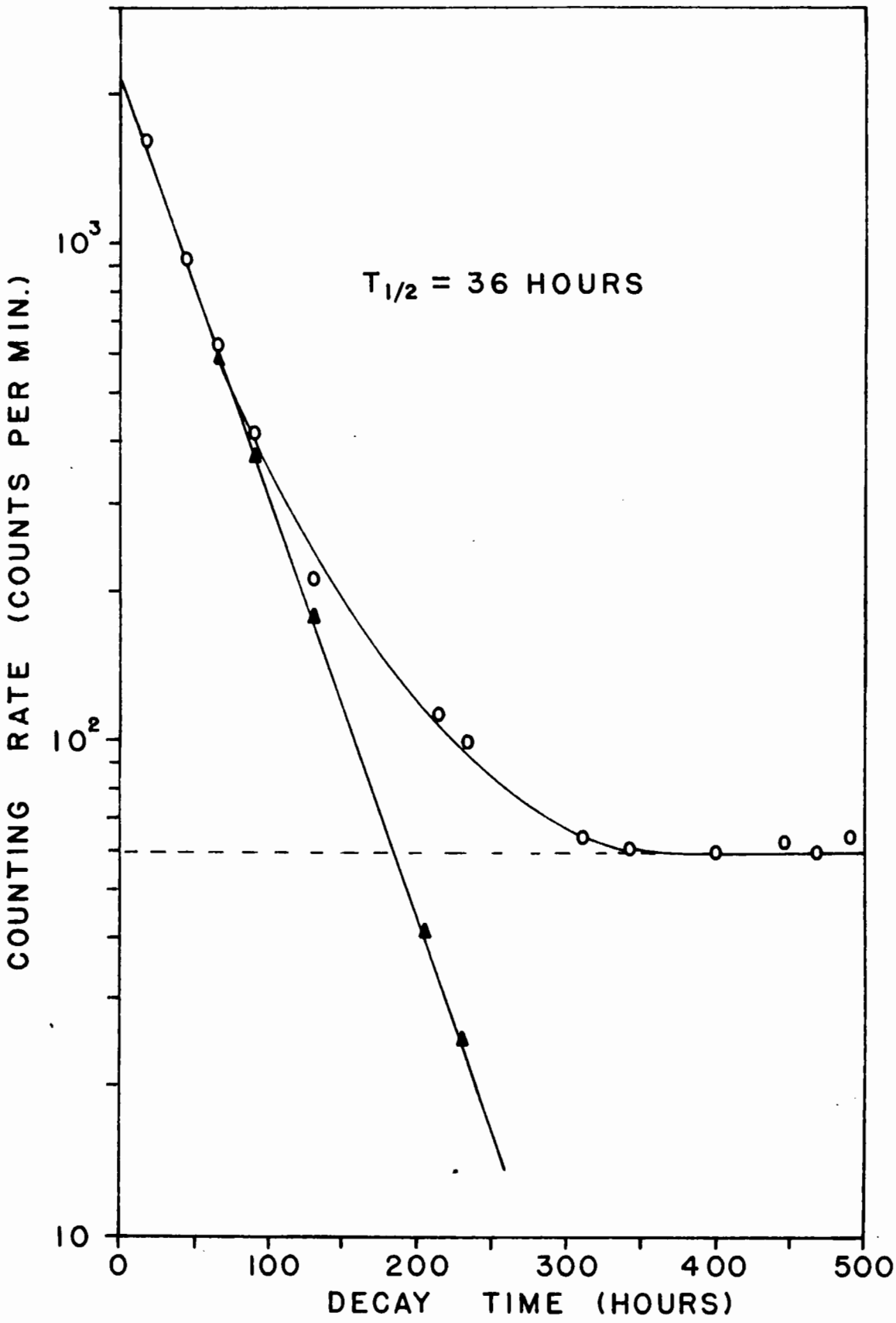
$T_{1/2}$ = 36 HOURS
COUNTING RATE (COUNTS PER MIN.)
10^3
10^2
10
0
100
200
300
400
500
DECAY TIME (HOURS)

Figure 31

γ Spectrum of Rh^{105}

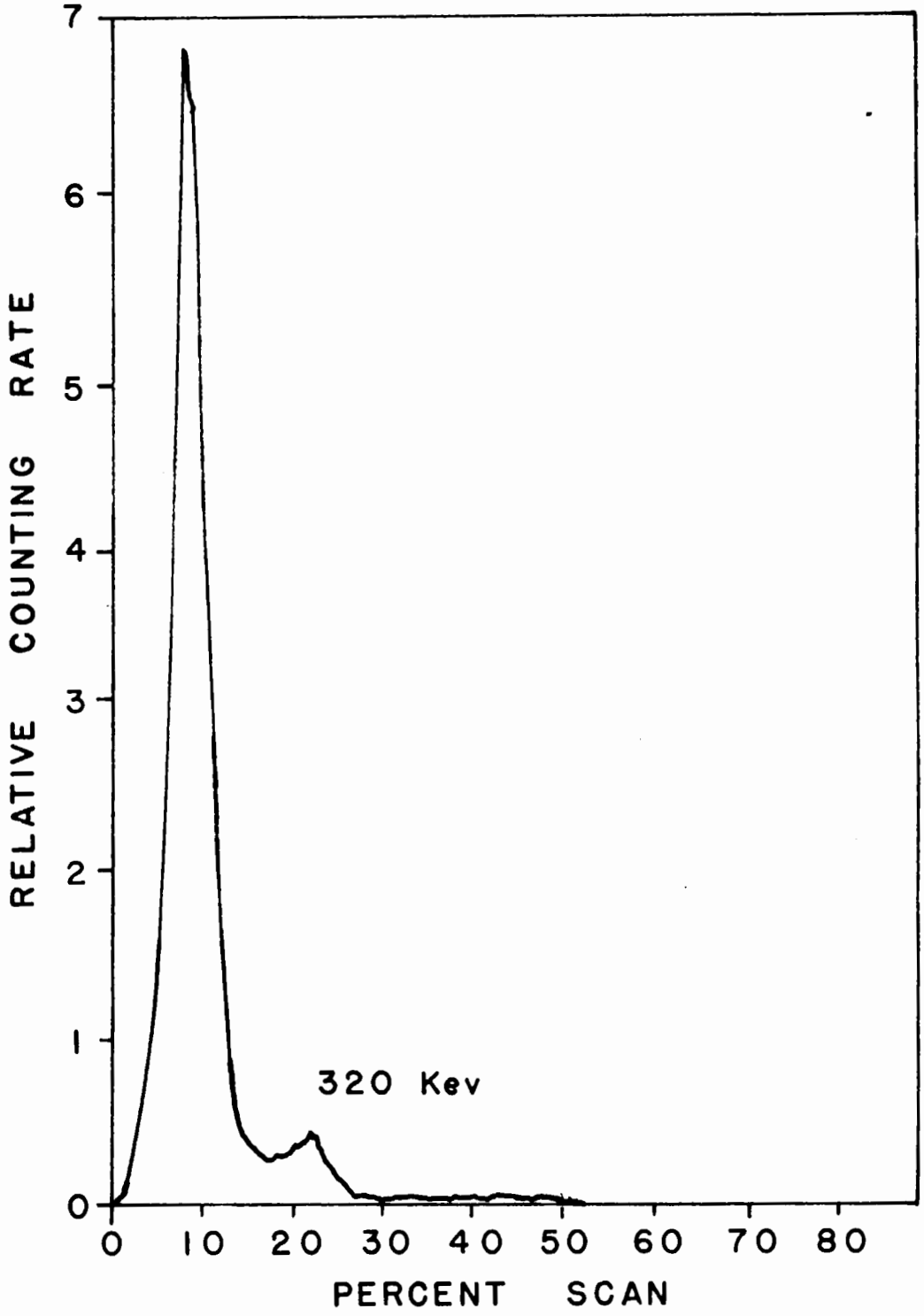
RELATIVE COUNTING RATE
7
6
5
4
3
2
1
0
320 Kev
0
10
20
30
40
50
60
70
80
PERCENT SCAN

(h) Silver

Silver was separated from other fission products by adding silver carrier and precipitating AgCl from a HNO_3 solution with HCl. Additional decontamination was achieved as suggested ~~by~~ Glendenin (95) by alternative $Fe(OH)_3$ scavengings and Ag_2S precipitations from an ammonical solution. The final AgCl precipitate was dissolved in a minimum of ammonia solution and diluted to 10 ml.

Chemical yields were determined on aliquots of the silver solution by adding 5 drops of 2 M HCl and then 1 ml. of 6 M HNO_3. The mixture was heated to boiling, filtered, washed with water and ethanol, and finally dried at 110°C. for 15 minutes. The precipitate was weighed as AgCl.

The decay of 20, 50 and 100 λ sources of silver were followed in the 4π-proportional counter. The observed 3.2-hour activity (Figure 32) and the 7.6-day activity (Figure 33) were taken to be Ag^{112} and Ag^{111} respectively. A very low-intensity 620 Kev γ photopeak was observed on the scintillation spectrometer which appeared to be associated with the 2.3-hour β activity. The decay chains for the observed silver activities are

$$\text{short-lived} \longrightarrow \underset{7.6\text{-d.}}{Ag^{111}} \longrightarrow \underset{\text{stable}}{Cd^{111}}$$

$$\text{short-lived} \longrightarrow \underset{21\text{-h.}}{Pd^{112}} \longrightarrow \underset{3.2\text{-h.}}{Ag^{112}} \longrightarrow \underset{\text{stable}}{Cd^{112}} .$$

The reported half-life for Ag^{111} is 7.6 days (96). This nuclide decays by the emission of β particles of energies

Figure 32

Decay Curve of 3.2-Hour Ag^{112}

O Experimental Points

Δ Longer-Lived Components Subtracted

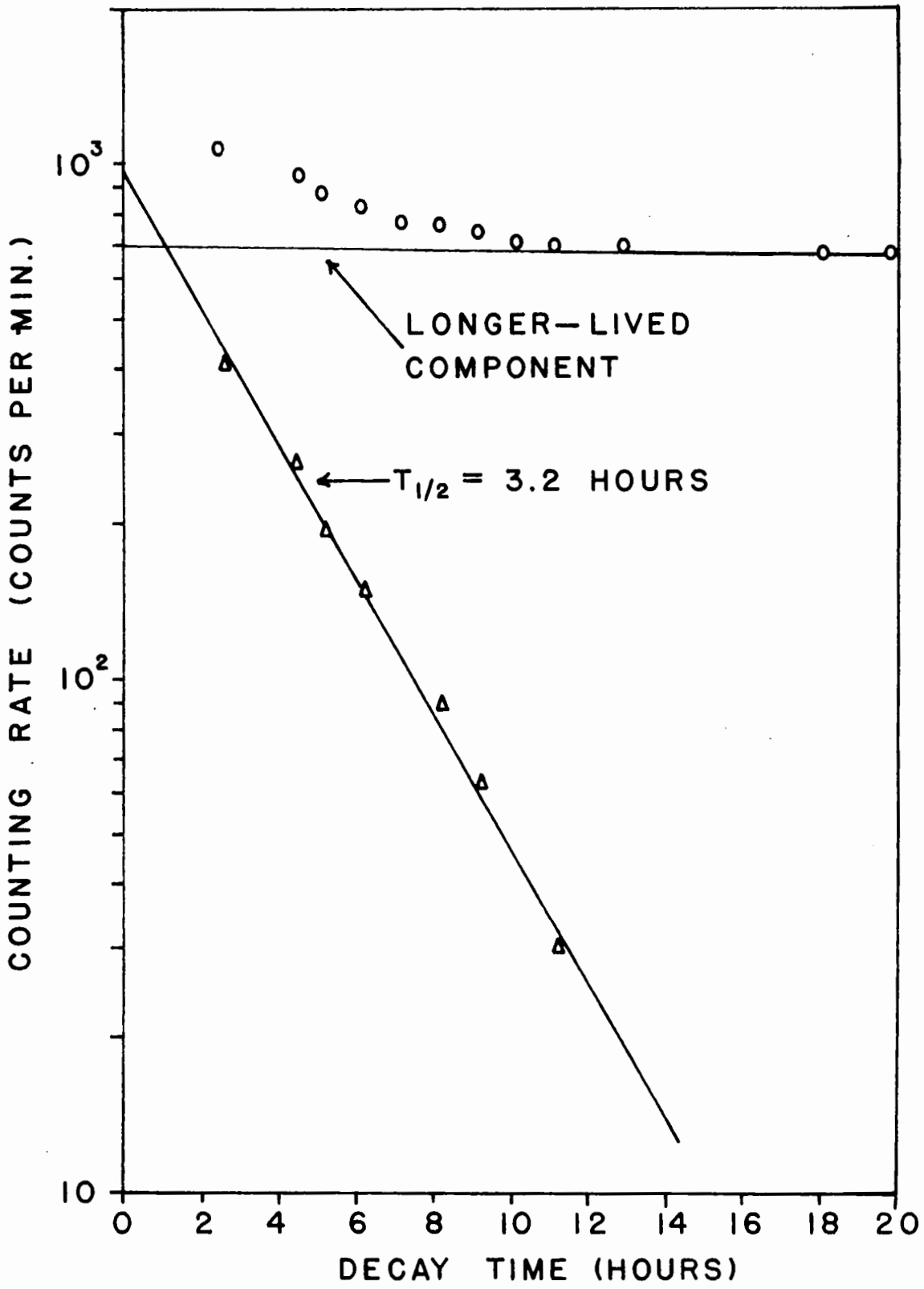
COUNTING RATE (COUNTS PER MIN.)
10^3
10^2
10
LONGER—LIVED
COMPONENT
$T_{1/2}$ = 3.2 HOURS
0
2
4
6
8
10
12
14
16
18
20
DECAY TIME (HOURS)

Figure 33

Decay Curve of 7.6-Day Ag^{111}

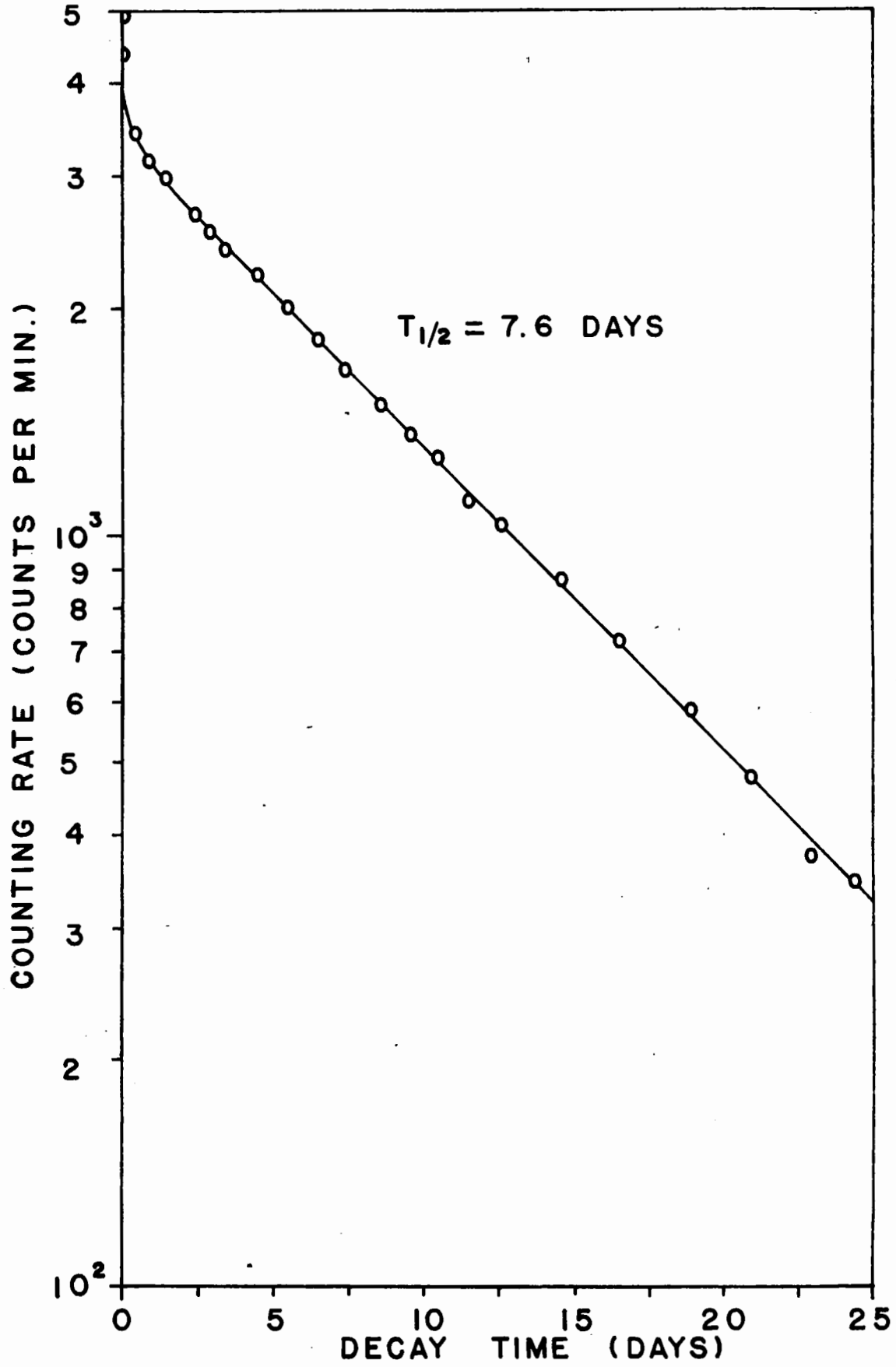
5
4
3
2
10^3
9
8
7
6
5
4
3
2
10^2
COUNTING RATE (COUNTS PER MIN.)
$T_{1/2}$ = 7.6 DAYS
0
5
10
15
20
25
DECAY TIME (DAYS)

1.04 (91 %), 0.80 (1 %) and 0.70 (8 %) Kev (97). Ag^{112} has a half-life of 3.2 hours (98) and decays by the emission of a series of energetic β particles (99); 4.1 (25 %), 3.5 (40 %), 2.7 (20 %) and 1.0 (15 %) Mev. In the decay of Ag^{112} a 620 Kev γ ray is emitted in coincidence with β emission. The length of time from the end of the irradiation to the silver separation was such that all independently formed Ag^{112} represents that formed from the decay of the parent Pd^{112}. Because of this, the Ag^{112} data have been presented in Table 17 with the fission yield data for Pd^{112}. The fission yield calculated for Ag^{111} is given in Table 15.

TABLE 15

FISSION YIELD DATA FOR 7.6-DAY Ag^{111}

Irradiation number	B 1	D 1
Observed activity	2200 c/m	3380 c/m
Self-absorption factor	0.994	0.972
Source-mount Absorption factor	1.000	1.000
Aliquot factor	2500	1250
Chemical yield	29.4 %	58.3 %
Time after irradiation	1.91 day	2.5 days
Decay factor	0.8401	0.7962
Time in reactor	24 hours	18.5 hours
Saturation factor	0.08717	0.0578
Activity at saturation	4.28×10^6 d/s	2.701×10^6 d/s
Fission rate	2.270×10^{10} f/s	1.464×10^{10} f/s
Fission yield	(0.0188 $\pm$0.0003) %	(0.0185$\pm$0.0007) %

(i) Palladium

The separation of palladium from other fission products was accomplished by the precipitation of palladium dimethylglyoxime from an acid solution. Scavenging with $Fe(OH)_3$ and AgI was performed for additional purification. Palladium was finally precipitated with demethylglyoxime, dissolved in hot concentrated nitric acid and made up to a volume of 10 ml.

Chemical yields were determined by precipitating and weighing palladium dimethylglyoxime.

The decay curves for palladium, as measured on the 4π - proportional counter, are resolved in Figure 34. Since the longest-lived palladium isotope expected in fission has been reported as 21-hour Pd^{112} (100), it then appears as if an incomplete separation of palladium has been obtained. Silver and zirconium might be expected to contaminate palladium in the separation procedure used (101). If so, the observed 65-day activity may be due to Zr^{95}. The other resolved half-lives are probably mixtures of nuclides. It was found that by analyzing the initial portion of the gross decay curve, a 21-hour activity could be resolved (Figure 35). This activity was taken as Pd^{112} and a fission yield was calculated (Table 16). The decay chain for the suspected palladium nuclide is

$$\underset{\text{21-h.}}{Pd^{112}} \longrightarrow \underset{\text{3.2-h.}}{Ag^{112}} \longrightarrow \underset{\text{stable}}{Cd^{112}} \quad .$$

The γ peaks observed on the scintillation spectrometer were not sufficiently resolved to permit an identification of nuclides present. It was then questionable that the observed

Figure 34

Decay Curve of a Palladium Separation

O Experimental Points

Δ 65-Day Activity Subtracted

□ 9-Day Activity Subtracted

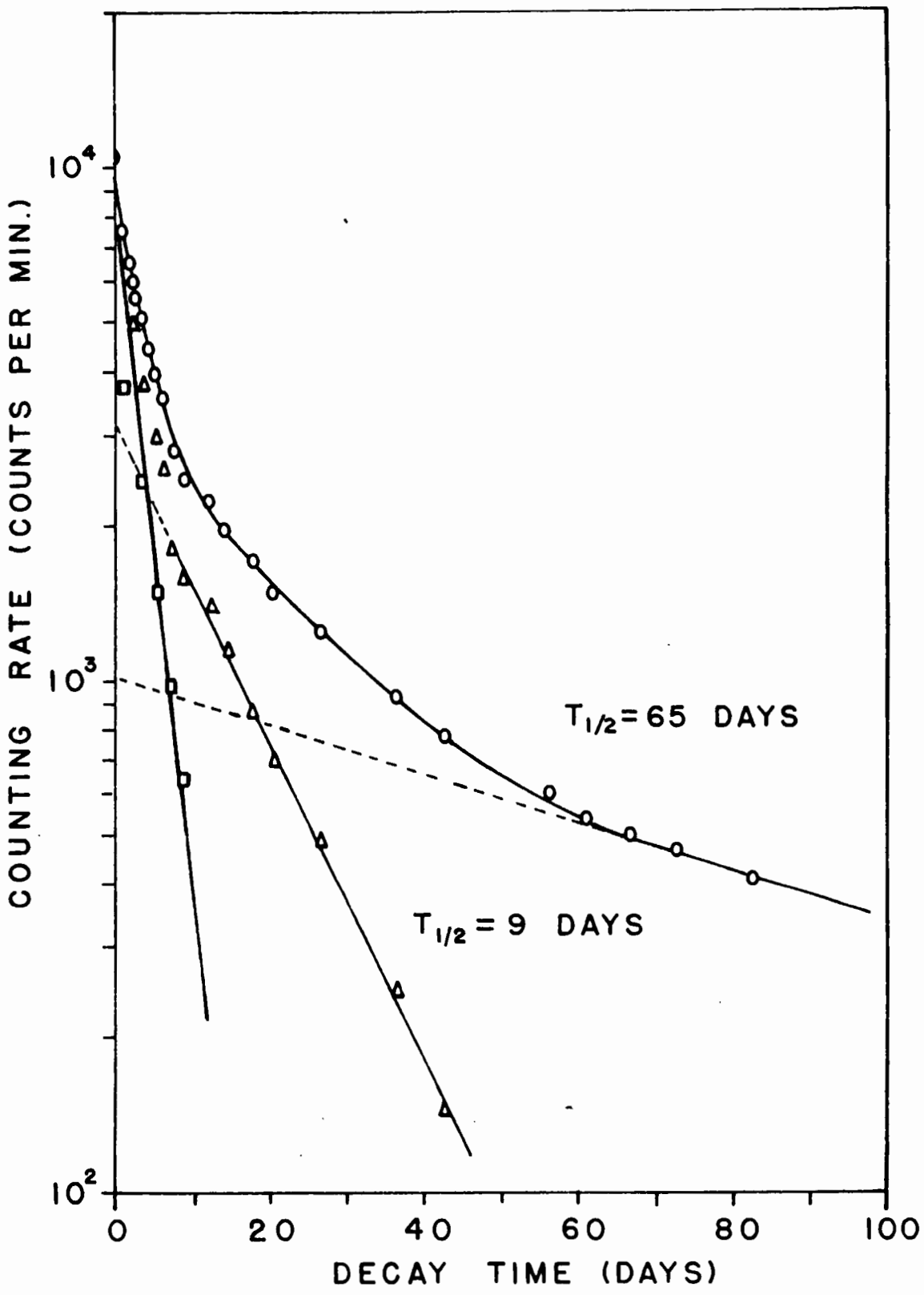
COUNTING RATE (COUNTS PER MIN.)
10^4
10^3
10^2
$T_{1/2}$=65 DAYS
$T_{1/2}$ = 9 DAYS
0
20
40
60
80
100
DECAY TIME (DAYS)

Figure 35

Decay Curve of a Palladium Separation

O Experimental Points

Δ Longer-Lived Components Subtracted

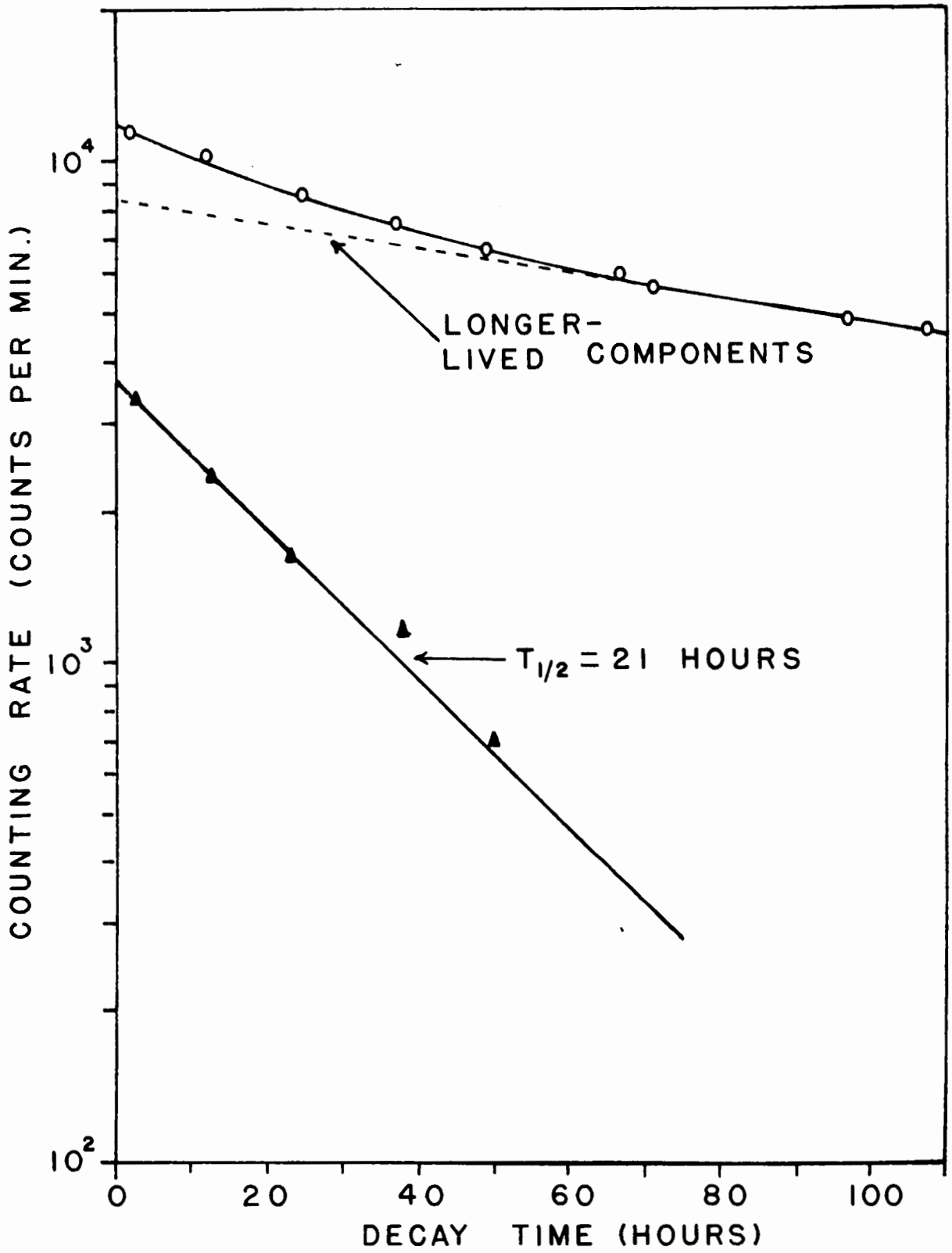
COUNTING RATE (COUNTS PER MIN.)
10^4
10^3
10^2
LONGER-
LIVED COMPONENTS
$T_{1/2}$ = 21 HOURS
0
20
40
60
80
100
DECAY TIME (HOURS)

TABLE 16

FISSION YIELD DATA FOR 21-HOUR Pd^{112}

Irradiation number	B 1	F 1
Observed activity	3640 c/m	945 c/m
Self-absorption factor	0.860	0.942
Source-mount Absorption factor	0.990	0.990
Aliquot factor	1250	4166
Chemical yield	50.0 %	49.8 %
Time after irradiation	69.5 hours	76.2 hours
Decay factor	0.10091	0.08089
Time in reactor	24 hours	24 hours
Saturation factor	0.5471	0.5495
Activity at saturation	2.776×10^6 d/s	3.180×10^6 d/s
Fission rate	2.270×10^{10} f/s	2.587×10^{10} f/s
Fission yield	(0.0122 ± 0.0001) %	(0.0123 ± 0.0001) %

TABLE 17

FISSION YIELD DATA FOR 21-HOUR Pd^{112}

(Determined from the Daughter 3.2-Hour Ag^{112})

Irradiation number	B 1	D 1
Observed activity	3050 c/m	3490 c/m
Self-absorption factor	0.999	0.996
Source-mount Absorption factor	1,000	1,000
Aliquot factor	2500	1250
Chemical yield	29.4 %	58.3 %
Time after irradiation	44.8 hours	58.7 hours
Decay factor	0.2690	0.1700
Time in reactor	24 hours	18.5 hours
Saturation factor	0.5471	0.4260
Activity at saturation	2.938×10^6 d/s	1.729×10^6 d/s
Fission rate	2.270×10^{10} f/s	1.464×10^{10} f/s
Fission yield	(0.0129 $\pm$ 0.0001) %	(0.0118 $\pm$ 0.0005) %

21-hour decay line was due only to Pd^{112}. If the 65-day activity represents Zr^{95}, then 17-hour Zr^{97} might also be present and add to the counting rate of Pd^{112}. As a further check on the Pd^{112} yield, the daughter activity Ag^{112} was counted and from its measurements the yield for Pd^{112} was indirectly determined (Table 17). The value obtained for the yield of Pd^{112} by both methods agreed favorably.

(j) Antimony

The method of Boldridge and Hume (102) was used to separate antimony from other fission products. Antimony (Sb^{+3}) carrier was added and oxidized to the pentavalent state with bromine water to ensure complete chemical exchange. Metallic antimony was precipitated by adding an excess of chromous chloride. After dissolving the antimony in aqua regia, water was added and a sulphide precipitation was performed. The sulphide was dissolved in a minimum of HCl and the solution was boiled before being diluted to a volume of 10 ml.

Chemical recovery was determined by precipitating metallic antimony with chromous chloride. The metal was filtered, washed and dried at 110°C. for 30 minutes before being weighed.

The decay of antimony activities, as measured by the 4π-proportional counter, are shown in Figure 36. Half-lives of 3.79 days and 75 days were observed. An intense 245 Kev γ photopeak was observed on the scintillation spectrometer (Figure 37) which also decayed with a 3.6-day half-life (Figure 38). Two less defined γ peakes were observed at

Figure 36

Decay Curves of 3.8-Day Sb^{127} and an

Unidentified 75-Day Component

O Experimental Points

▲ 75-Day Activity Subtracted

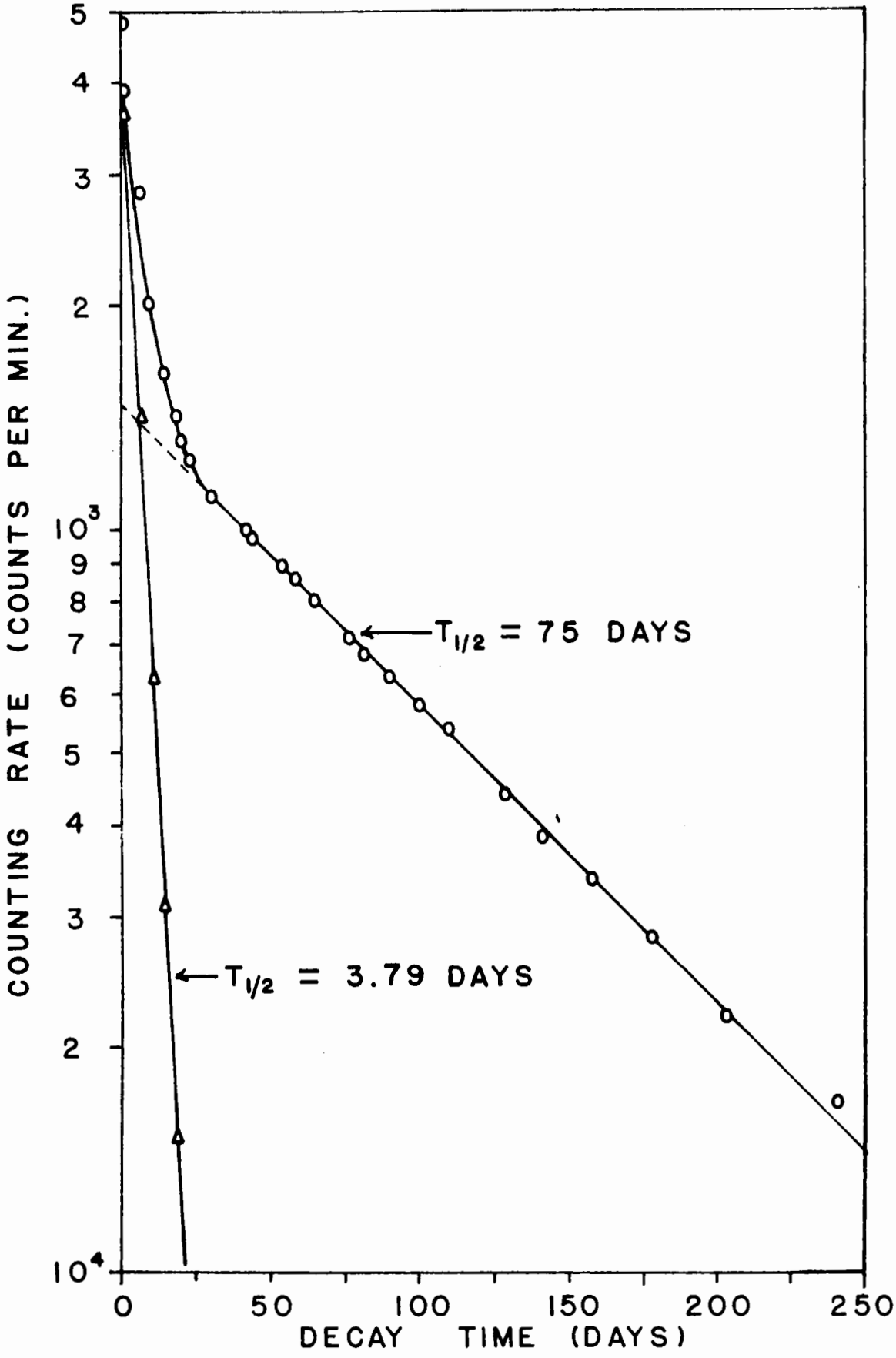
COUNTING RATE (COUNTS PER MIN.)
5
4
3
2
10^3
9
8
7
6
5
4
3
2
10^4
$T_{1/2}$ = 75 DAYS
$T_{1/2}$ = 3.79 DAYS
0
50
100
150
200
250
DECAY TIME (DAYS)

Figure 37

Spectrum of an Antimony Separation

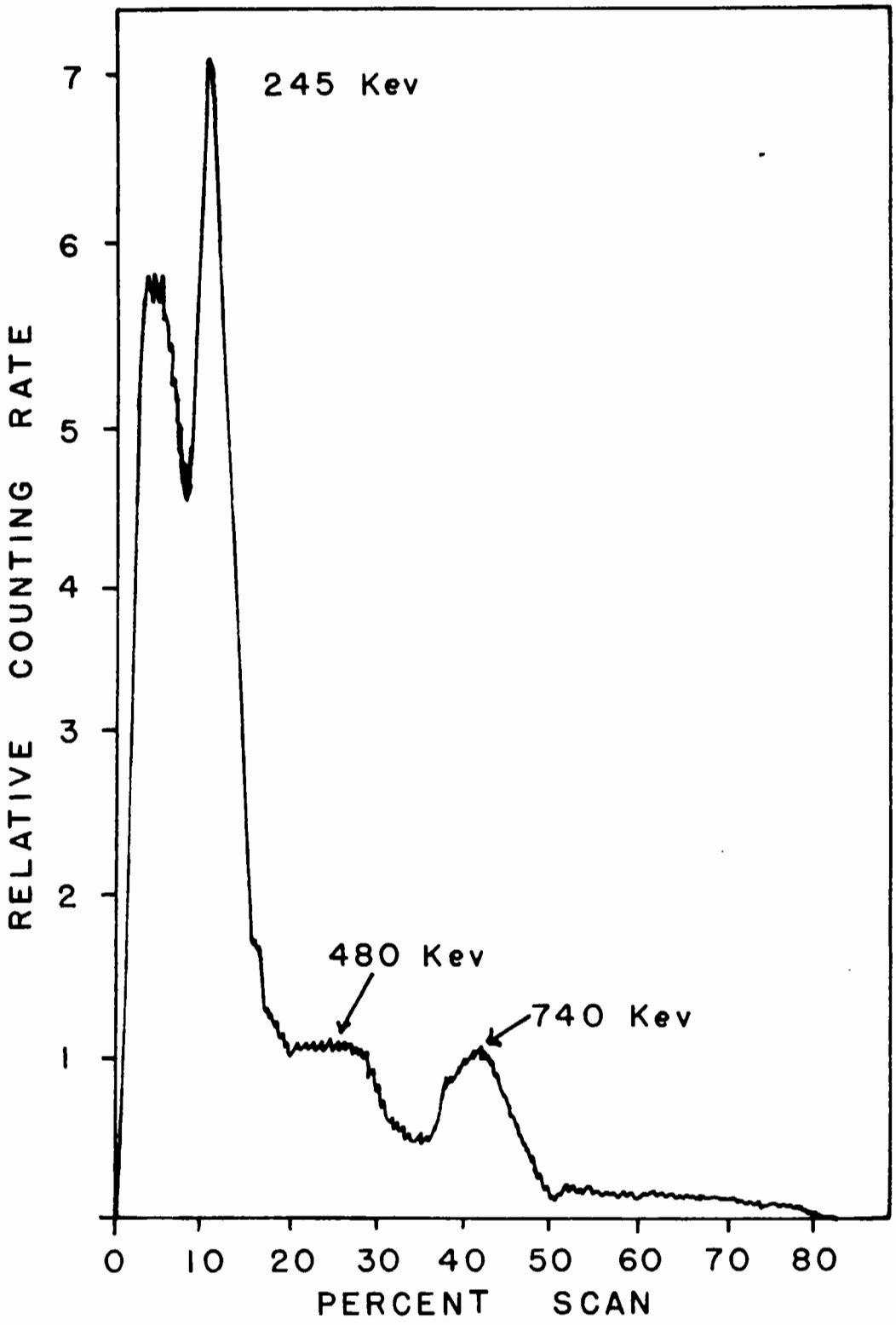
245 Kev
480 Kev
740 Kev
RELATIVE COUNTING RATE
PERCENT SCAN
0
10
20
30
40
50
60
70
80
1
2
3
4
5
6
7

Figure 38

γ Decay Curves for an Antimony Separation

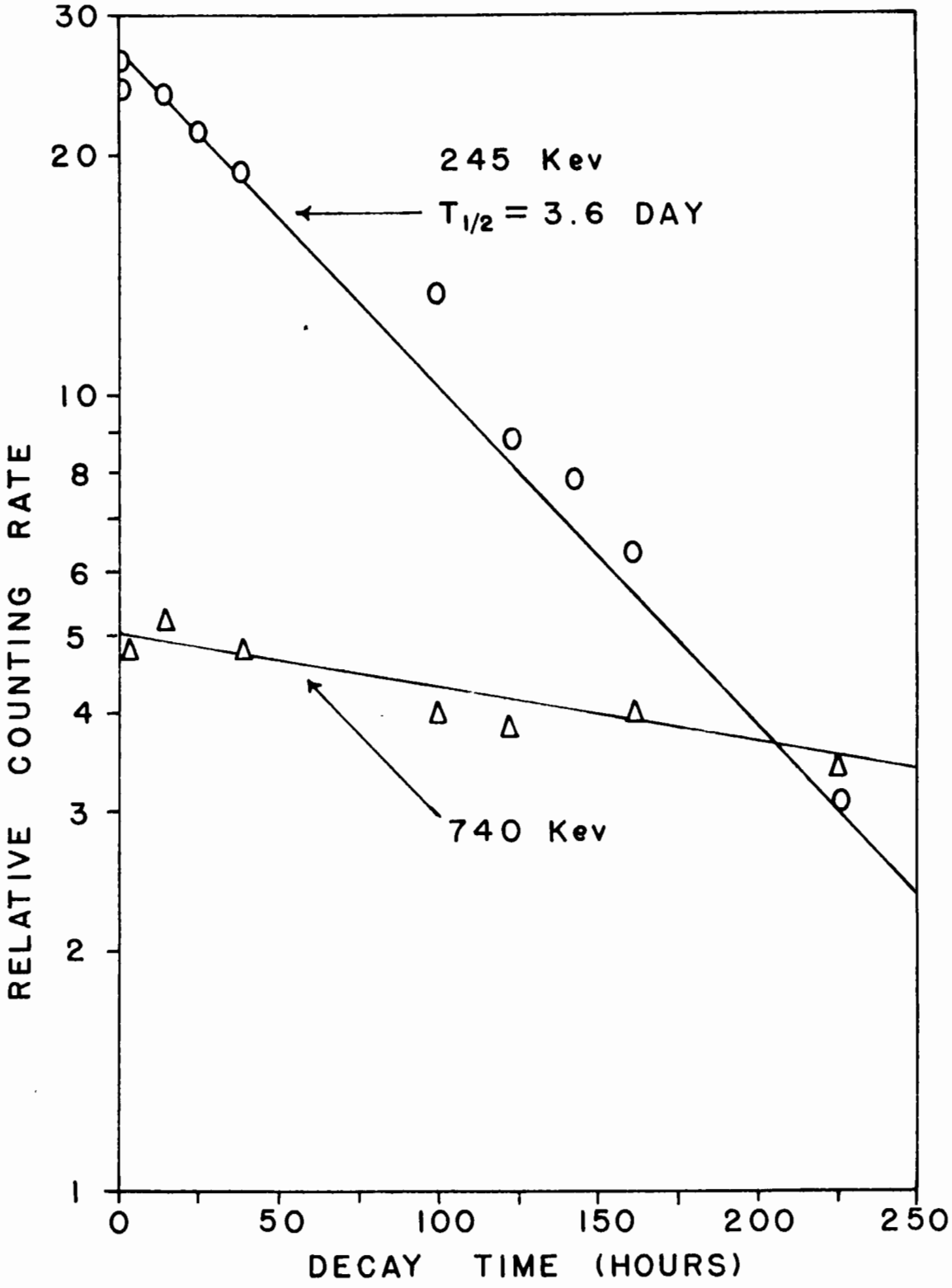
30
20
10
8
6
5
4
3
2
1
RELATIVE COUNTING RATE
245 Kev
$T_{1/2}$ = 3.6 DAY
740 Kev
0
50
100
150
200
250
DECAY TIME (HOURS)

740 and 480 Kev. These peaks appeared to be associated with the 75-day activity. The shorter-lived activity was assigned to Sb^{127}. Half-lives reported recently for this nuclide are 88 hours (103) and 93 hours (104). The value used in this work was the observed 91 hours. The energies of the β particles emitted in the decay of Sb^{127} were given as 860 (50 %), 1110 (20%) and 1570 (30%) (104). The main γ transitions which were in coincidence with the β emission were reported as 248, 772, and 463 Kev (103). Although the observed γ peaks at 480 and 740 Kev appeared to correspond to the reported 463 and 772 Kev energies of Sb^{127}, the measured half-life was different. No observed 75-day antimony activity has yet been reported in fission. The longest-lived isotope detected was that of 2.0-year Sb^{125} (105). Both Sb^{124} and Sb^{126} are expected to be formed in fission. However, the first is a shielded nuclide and its yield is probably low. The second has been reported as a fission product (106), but no reliable half-life has been measured for this nuclide. The only antimony nuclide positively identified in this work is that of mass number 127. The decay chain for this nuclide is

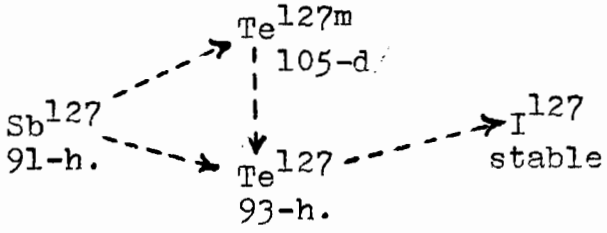

The yield for Sb^{127} is given in Table 18. A fission yield was calculated for the observed longer-lived antimony activity. A half-life of 75 days was used and the data are given in Table 19.

TABLE 18

FISSION YIELD DATA FOR 91-HOUR Sb^{127}

Irradiation number	B 1	D 1
Observed activity	4160	8300
Self-absorption factor	0.990	0.990
Source-mount absorption Absorption factor	1.000	1.000
Aliquot factor	1525	1905
Chemical yield	6 %	5 %
Time after irradiation	14.82 days	3.23 days
Decay factor	0.0706	0.5612
Time in reactor	24 hours	18.5 hours
Saturation factor	0.1638	0.1263
Activity at saturation	1.524×10^{8} d/s	7.511×10^{7}
Fission rate	2.270×10^{10} f/s	1.464×10^{10} f/s
Fission yield	(0.67 ± 0.13) %	(0.51 ± 0.12) %

TABLE 19

FISSION YIELD DATA FOR 75-DAY Sb ?

Irradiation number	B 1
Observed activity	1500 c/m
Self-absorption factor	1.00
Source-mount Absorption factor	1.00
Aliquot factor	2500
Chemical yield	6.9 %
Time after irradiation	14.82 days
Decay factor	0.872
Time in reactor	24 hours
Saturation factor	0.0092
Activity at saturation	1.121×10^{8} d/s
Fission rate	2.270×10^{10} f/s
Fission yield	(0.53 ± 0.14) %

(k) Tellurium

A direct separation of radiochemically pure tellurium was obtained by using a method reported by Glendenin (107). Tellurium (Te^{+4}) carrier was added and precipitated as the metal with SO_2 in an acid solution. Selenium contamination was removed by an HBr volatilization. The removal of ruthenium was assured by $Fe(OH)_3$ scavenging. Tellurium was finally recovered by precipitating the metal and dissolving it in a minimum of nitric acid. The solution was then made up to a volume of 10 ml.

Chemical yields were determined by precipitating tellurium as the metal.

The decay of tellurium was measured by counting 50 and 100 λ sources in the 4π-proportional counter. The final slope of the gross decay curve (Figure 39) indicated the presence of a 105-day activity. By subtracting the 105-day component from the curve a 37-day activity appeared (Figure 39). A subtraction of both the 105-day and 37-day activities from the initial portion of the decay curve produced a 3.2-day activity (Figure 40). A freshly separated tellurium sample analyzed on the scintillation spectrometer at first showed only a 220 Kev γ photopeak. Then, 670 and 780 Kev γ peaks grew in and later decayed. In equilibrium, all three peaks decayed with a half-life of 3.2 days (Figures 41 and 42).

The tellurium activities detected were 105-day Te^{127m} (108), 37-day Te^{129m}, (109), and 77-hour Te^{132} (110).

Figure 39

Decay Curves of 37-Day Te^{129m} and 105-Day Te^{127m}

O Experimental Points

▲ 105-Day Activity Subtracted

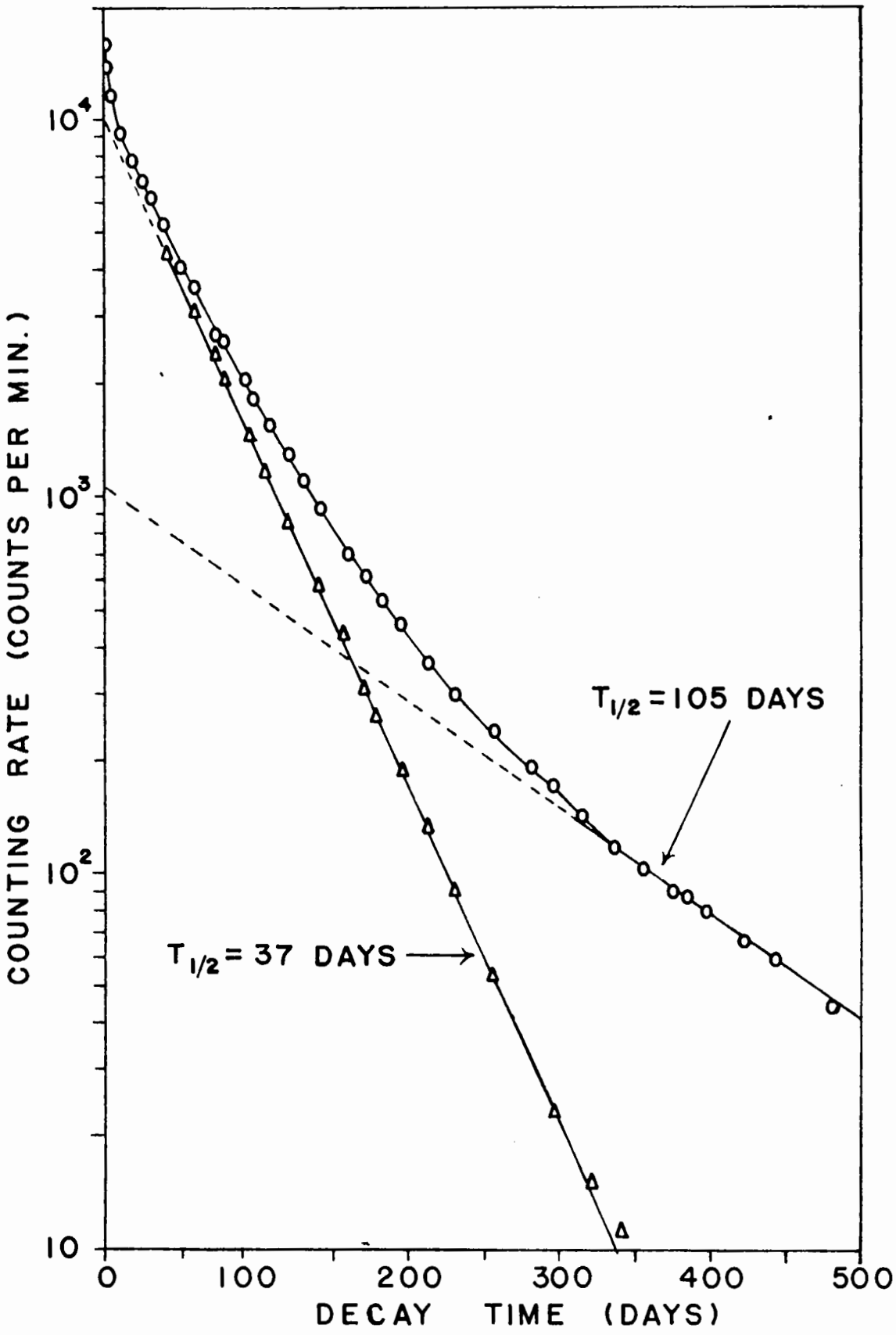
COUNTING RATE (COUNTS PER MIN.)
10^4
10^3
10^2
10
$T_{1/2}$ = 105 DAYS
$T_{1/2}$ = 37 DAYS
0
100
200
300
400
500
DECAY TIME (DAYS)

Figure 40

Decay Curve for 3.2-Day Te^{132}

o Experimental Points

▲ Longer-Lived Components Subtracted

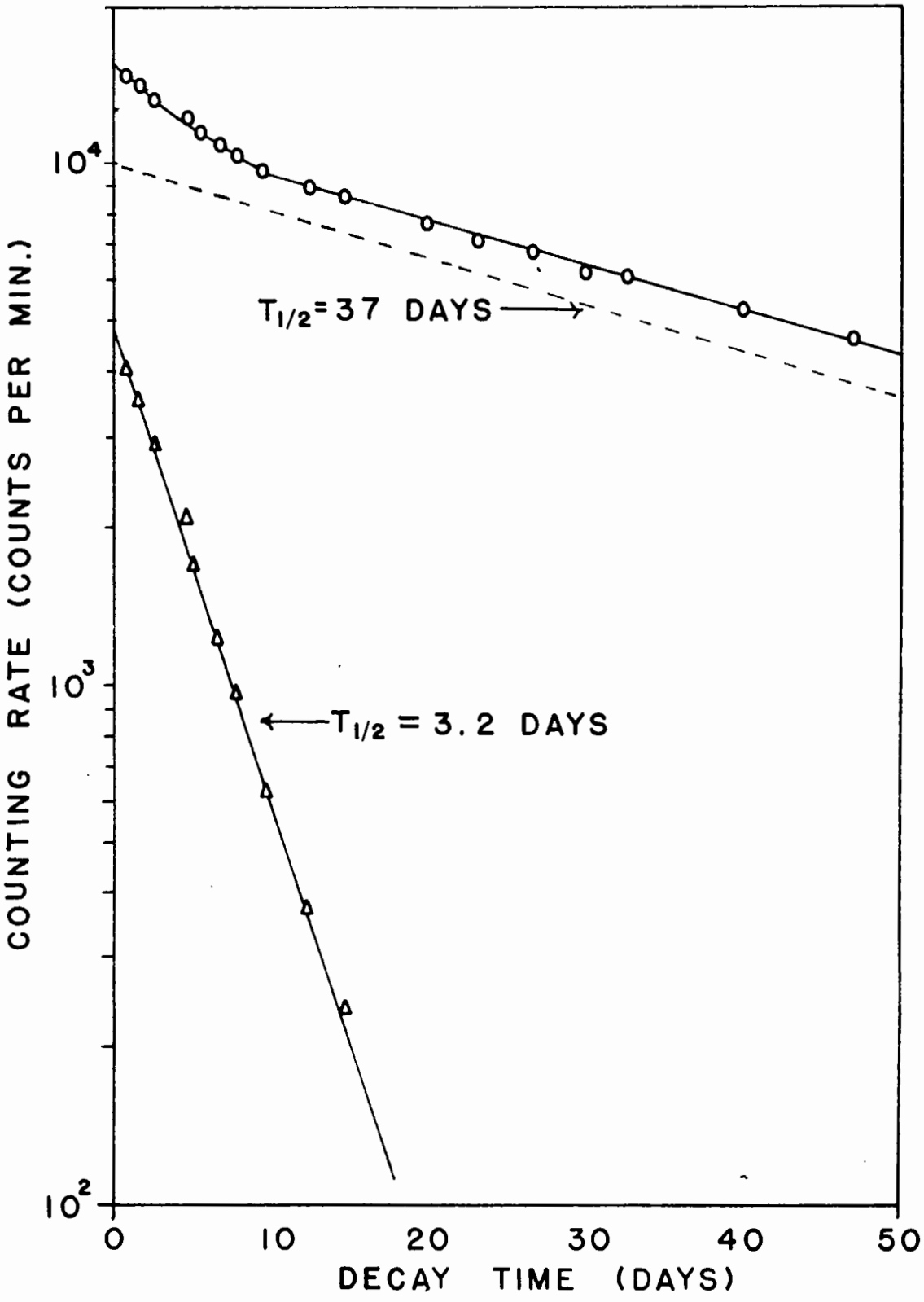
COUNTING RATE (COUNTS PER MIN.)
10^4
10^3
10^2
$T_{1/2}$=37 DAYS
$T_{1/2}$ = 3.2 DAYS
0
10
20
30
40
50
DECAY TIME (DAYS)

Figure 41

γ Spectrum of a Tellurium Separation

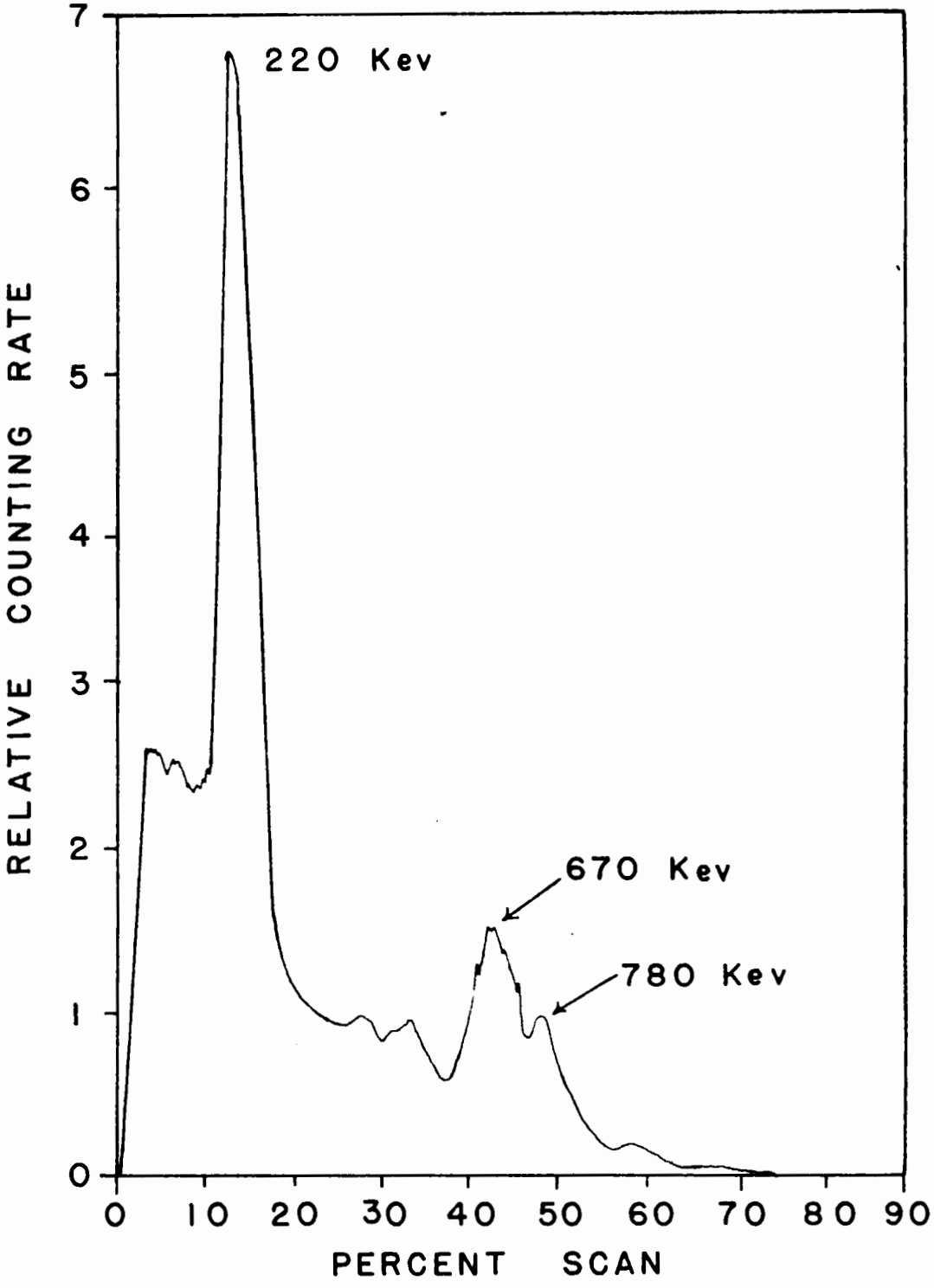
220 Kev
670 Kev
780 Kev
RELATIVE COUNTING RATE
PERCENT SCAN
0
1
2
3
4
5
6
7
0
10
20
30
40
50
60
70
80
90

Figure 42

γ Growth and Decay Curves Observed

in a Tellurium Separation

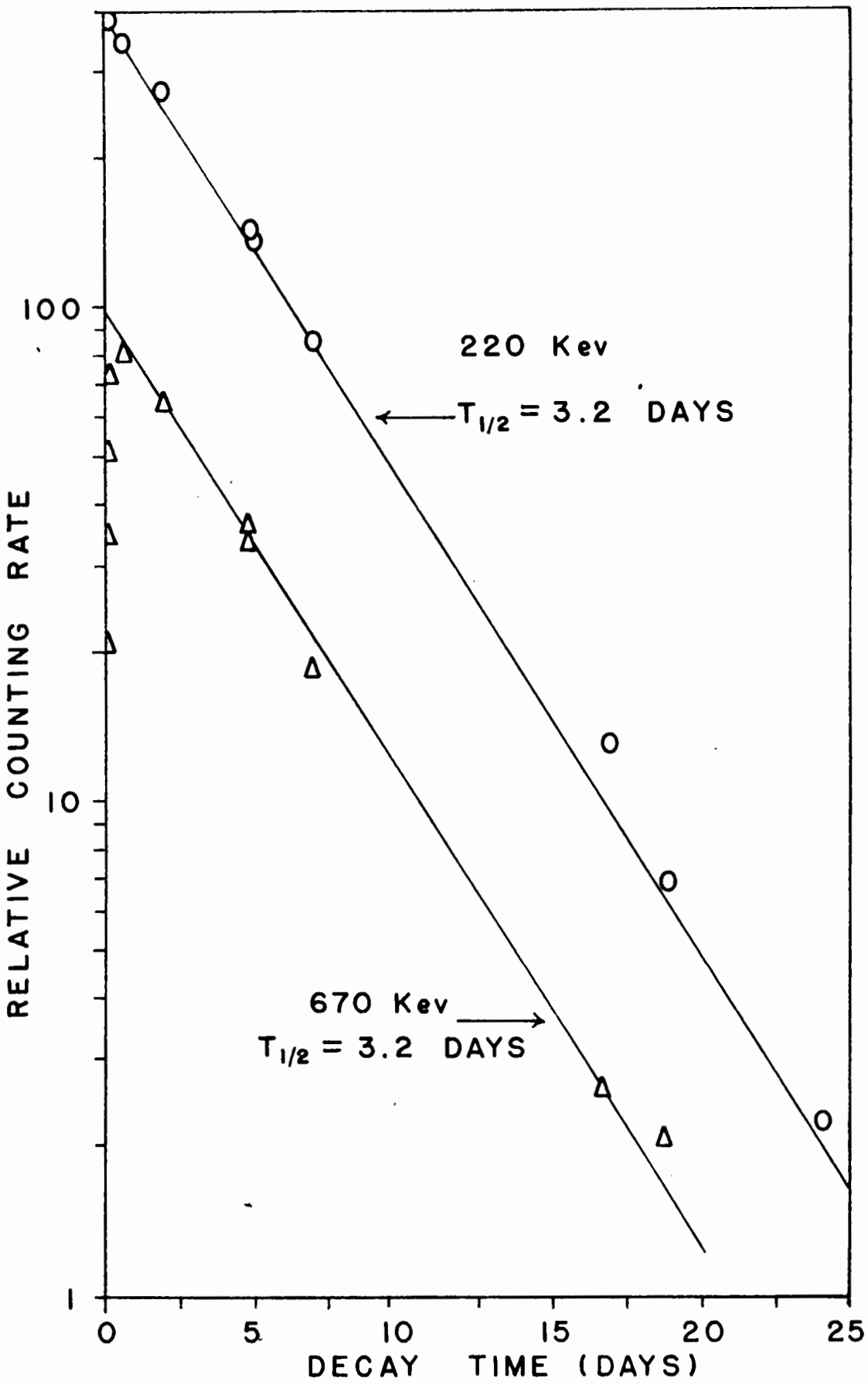
100
10
1
RELATIVE COUNTING RATE
220 Kev
$T_{1/2}$ = 3.2 DAYS
670 Kev
$T_{1/2}$ = 3.2 DAYS
0
5
10
15
20
25
DECAY TIME (DAYS)

The observed 220 Kev γ peak is characteristic of Te^{132}. The daughter activity of this nuclide is I^{132}, a short-lived activity, which gives rise to the 670 and 780 Kev peaks in Figures 41 and 42. The decay chains for the nuclides of interest are

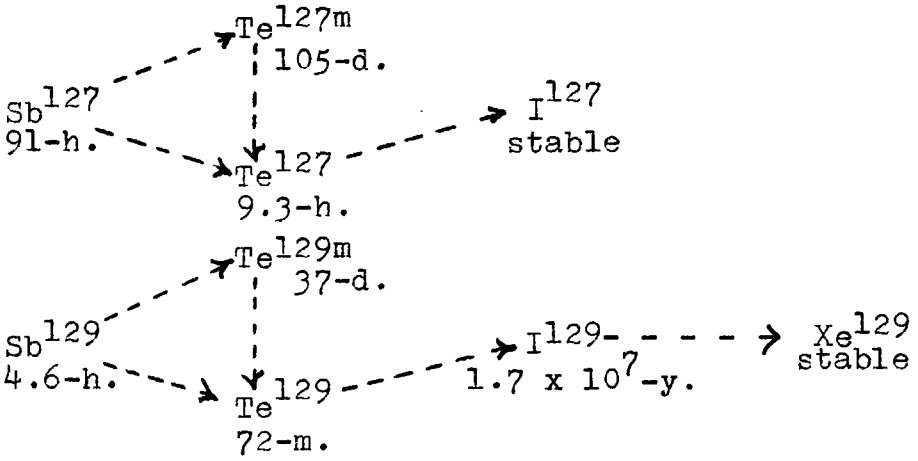

short-lived → Te^{132} (77-h.) - - → I^{132} (2.3-h.) - - - → Xe^{132} stable

The calculation of a fission yield for Te^{132} is not complicated and the data involved are given in Table 20. An additional yield measurement for Te^{132} was obtained by separating and measuring 2.3-hour Ag^{132}. Data for the latter measurements are listed in Table 21. Both Te^{127m} and Te^{129m} decay by γ emission, which involves internal conversion. No accurate measurements have yet been reported for the conversion coefficient of each isomer. For this reason it was impossible to calculate accurate fission yields for these nuclides. When such information becomes available, a yield for each isomer can then be calculated.

TABLE 20

FISSION YIELD DATA FOR 77-HOUR Te^{132}

Irradiation number	A 1	C 1
Observed activity	2365 c/m	53520
Self-absorption factor	0.990	0.984
Source-mount Absorption factor	1.000	1.000
Aliquot factor	2500	2500
Chemical yield	49 %	36. %
Time after irradiation	28.65 days	16.84 days
Decay factor	0.0020	0.0263
Time in reactor	24 hours	24 hours
Saturation factor	0.1943	0.1943
Activity at saturation	5.227×10^8 d/s	1.215×10^8
Fission rate		2.885×10^9 f/s
Fission yield	(4.70 ± 0.94) %	(4.21 ± 0.63) %

TABLE 21

FISSION YIELD DATA FOR 77-HOUR Te^{132}

(Determined from the Daughter 2.3-Hour I^{132})

Irradiation number	A 3	B 1
Observed activity	15600 c/m	145000 c/m
Self-absorption factor	0.89	0.93
Source-mount Absorption factor	1.000	1.000
Aliquot factor	1250	25000
Chemical yield	36.2 %	74.3 %
Time after irradiation	15.76 hours	87.01 hours
Decay factor	0.00994	0.4743
Time in reactor	24 hours	24 hours
Saturation factor	0.1927	0.1927
Activity at saturation	5.266×10^{8} d/s	9.56×10^{8} d/s
Fission rate	Relative yield	2.270×10^{10} f/s
Fission yield	(4.71 ± 0.14) %	(4.21 ± 0.13) %

TABLE 21 (Continued)

FISSION YIELD DATA FOR 77-HOUR Te^{132}

(Determined from the Daughter 2.3-Hour I^{132})

Irradiation number	C 1	F 1
Observed activity	60800 c/m	3300 c/m
Self-absorption factor	0.955	0.905
Source-mouht Absorption factor	1.000	1.000
Aliquot factor	12500	25000
Chemical yield	74.7 %	33.8 %
Time after irradiation	301.9 hours	433.4 hours
Decay factor	0.0698	0.0216
Time in reactor	24 hours	24.16 hours
Saturation factor	0.1927	0.1938
Activity at saturation	1.3198×10^9 d/s	1.073×10^8 d/s
Fission rate	2.885×10^{10} f/s	2.587×10^{10} f/s
Fission yield	(4.57 ± 0.16) %	(4.15 ± 0.05) %

(1) Iodine

A rapid solvent extraction method for the separation of iodine has been reported by Glendenin and Metcalf (111) and has been used in this work. Iodide carrier was added and preliminary steps were taken to ensure complete interchange between active iodine and carrier iodine. The carrier was reduced to I_2 with $NH_2OH.HCl$, and the I_2 was extracted with CCl_4. The iodine was removed from the CCl_4 by a back extraction using water containing $NaHSO_3$. Another CCl_4 extraction cycle was performed in which $NaNO_2$ was used to oxidize I^- to I_2 and a water solution of SO_2 was used for the reduction of I_2 to I^-. To the iodine in the form of I^- was added a small amount of LiOH. The solution was then diluted to a volume of 10 or 25 ml.

Chemical yields were determined by heating aliquots of the iodide solution and adding HNO_3-$AgNO_3$ to precipitate silver iodide. After it was digested, the precipitate was filtered, washed with water and alcohol and dried at 110°C. for 20 minutes. The solid was weighed as AgI.

The method used for source preparation was that suggested by Bartholomew et al. (112), in which the iodide solution was added to a drop of very dilute silver nitrate already present on the prepared VYNS film. The purpose of the silver is to prohibit the oxidation and subsequent volatilization of iodine. Prior to counting, each iodine source was heated for 15 minutes under an infra-red lamp. This technique was used to remove

xenon decay products formed from iodine. The half-lives observed for iodine by 4π- counting were 2.3 hours, 20.9 hours and 8.0 days (Figures 43 and 44). All γ photopeaks observed on the scintillation spectrometer decayed with similar half-lives (Figures 45, 46, 47, and 48). Peaks at 670, 780, 980 and 1400 Kev decayed with a half-life of 2.2 hours. The 520 Kev peak decayed with a half-life of 20.3 hours and the 360 and 640 Kev peaks with a half-life of 8.4 days. No attempt was made to remove xenon decay products from the sources used on the scintillation spectrometer. The nuclides observed were identified as I^{131}, and I^{133}. The decay chains for these nuclides are

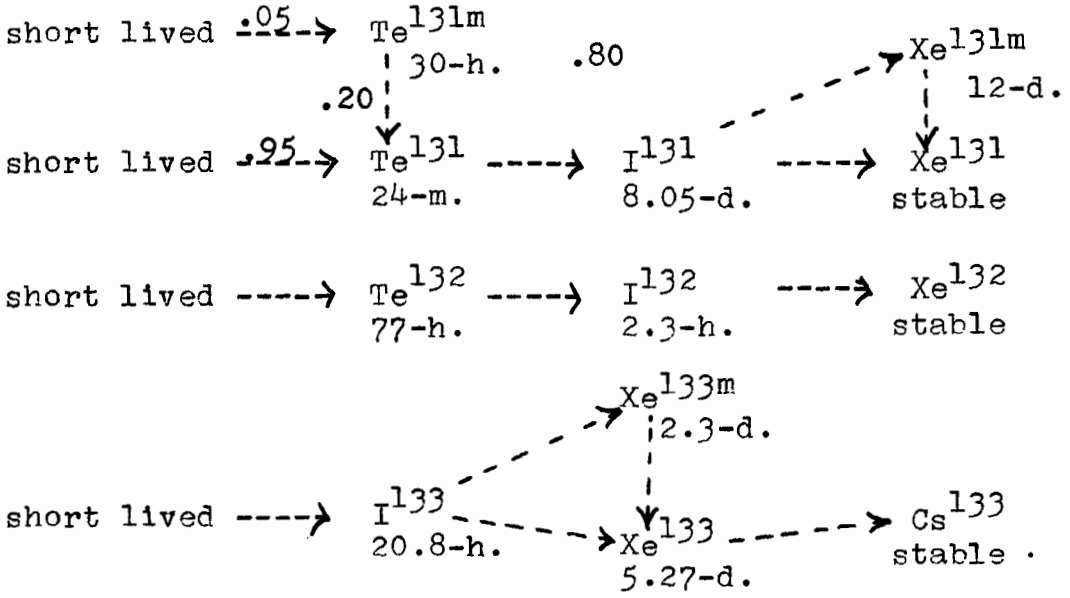

In Table 22 are listed the decay characteristics for these nuclides.

Figure 43

β Decay Curves of 2.3-Hour I^{132}

and 20.9-Hour I^{133}

O Experimental Points

▲ Longer-Lived Component Subtracted

□ 20.9-Hour Activity Subtracted

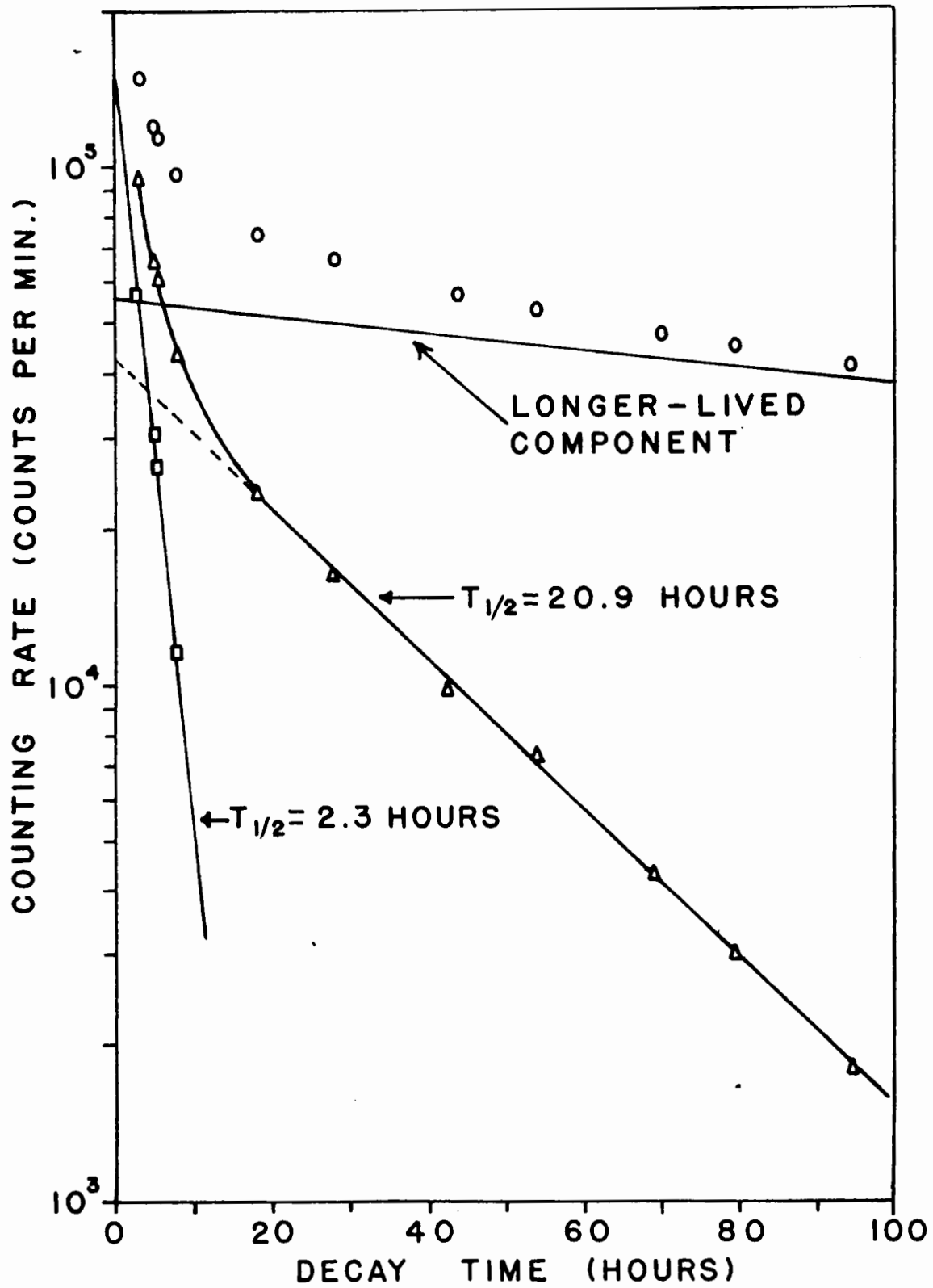
COUNTING RATE (COUNTS PER MIN.)
10^5
10^4
10^3
LONGER-LIVED COMPONENT
$T_{1/2}$= 20.9 HOURS
$T_{1/2}$= 2.3 HOURS
0
20
40
60
80
100
DECAY TIME (HOURS)

Figure 44

β Decay Curve of 8.05-Day I^{131}

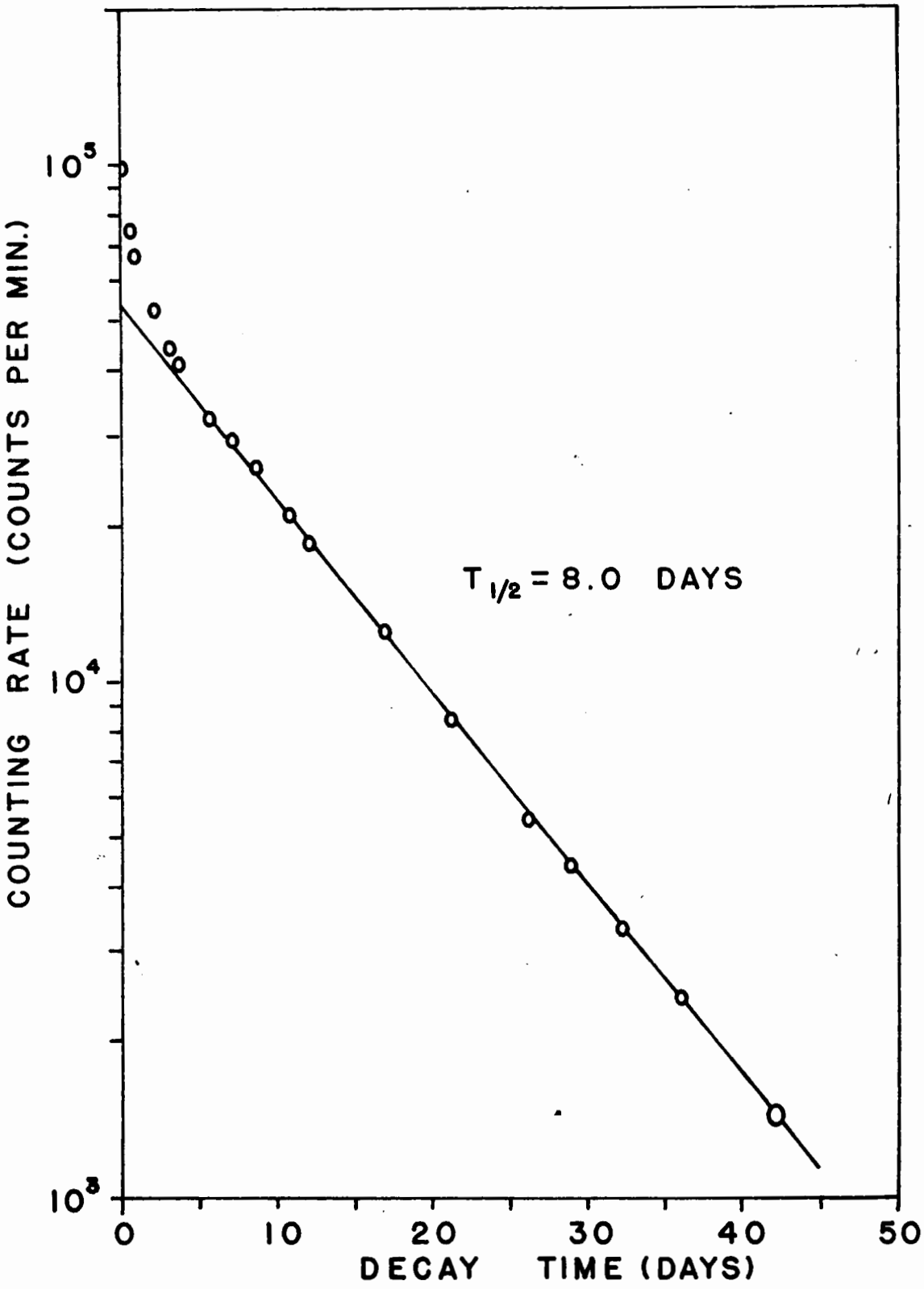
COUNTING RATE (COUNTS PER MIN.)
10^5
10^4
10^3
$T_{1/2}$ = 8.0 DAYS
0
10
20
30
40
50
DECAY TIME (DAYS)

Figure 45

γ Spectrum Obtained from an Iodine Separation

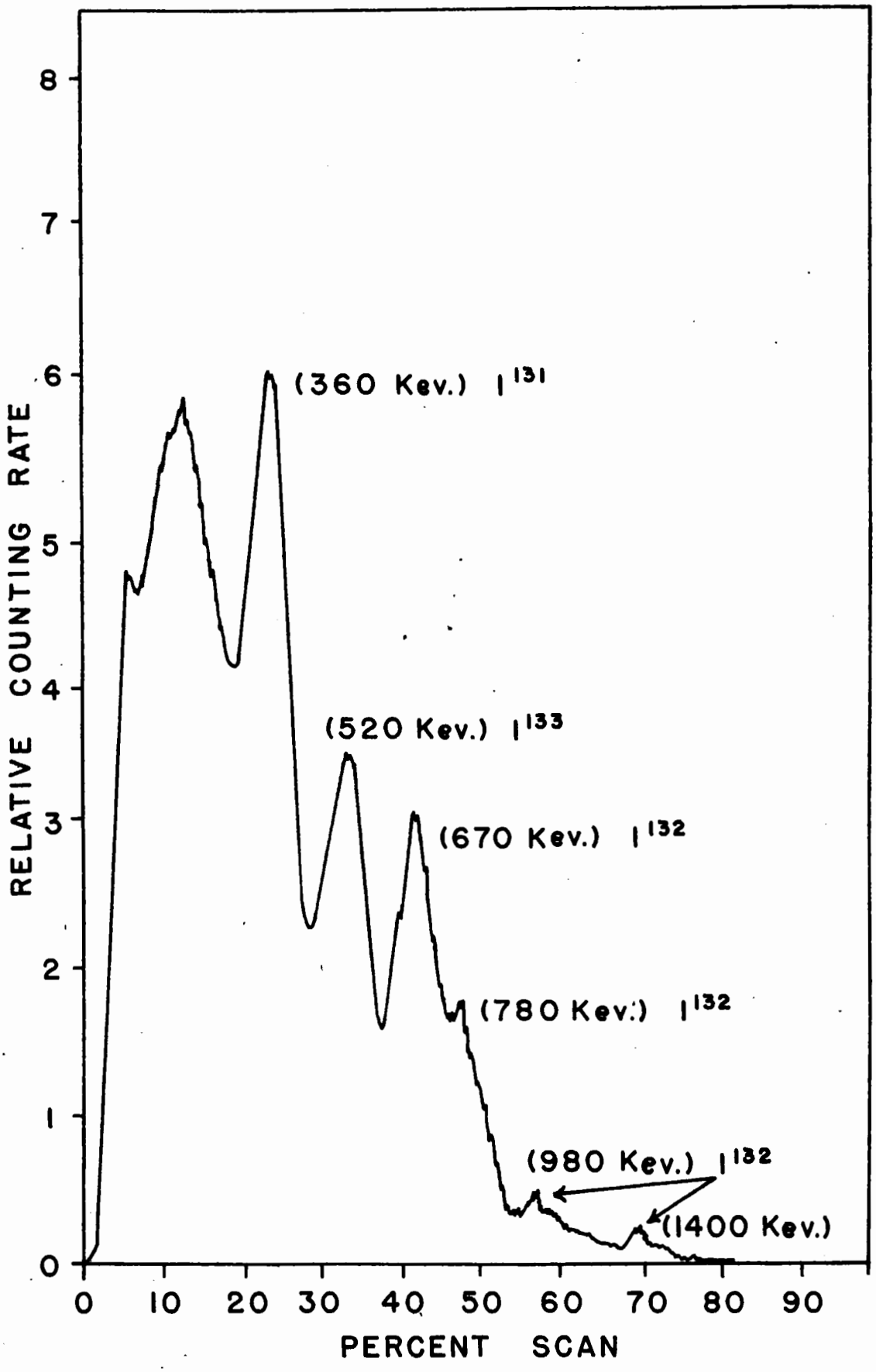
RELATIVE COUNTING RATE
0
1
2
3
4
5
6
7
8
0
10
20
30
40
50
60
70
80
90
PERCENT SCAN
(360 Kev.) I 131
(520 Kev.) I 133
(670 Kev.) I 132
(780 Kev.) I 132
(980 Kev.) I 132
(1400 Kev.)

Figure 46

γ Spectrum of an Iodine Sample after the

Decay of Shorter-Lived Members

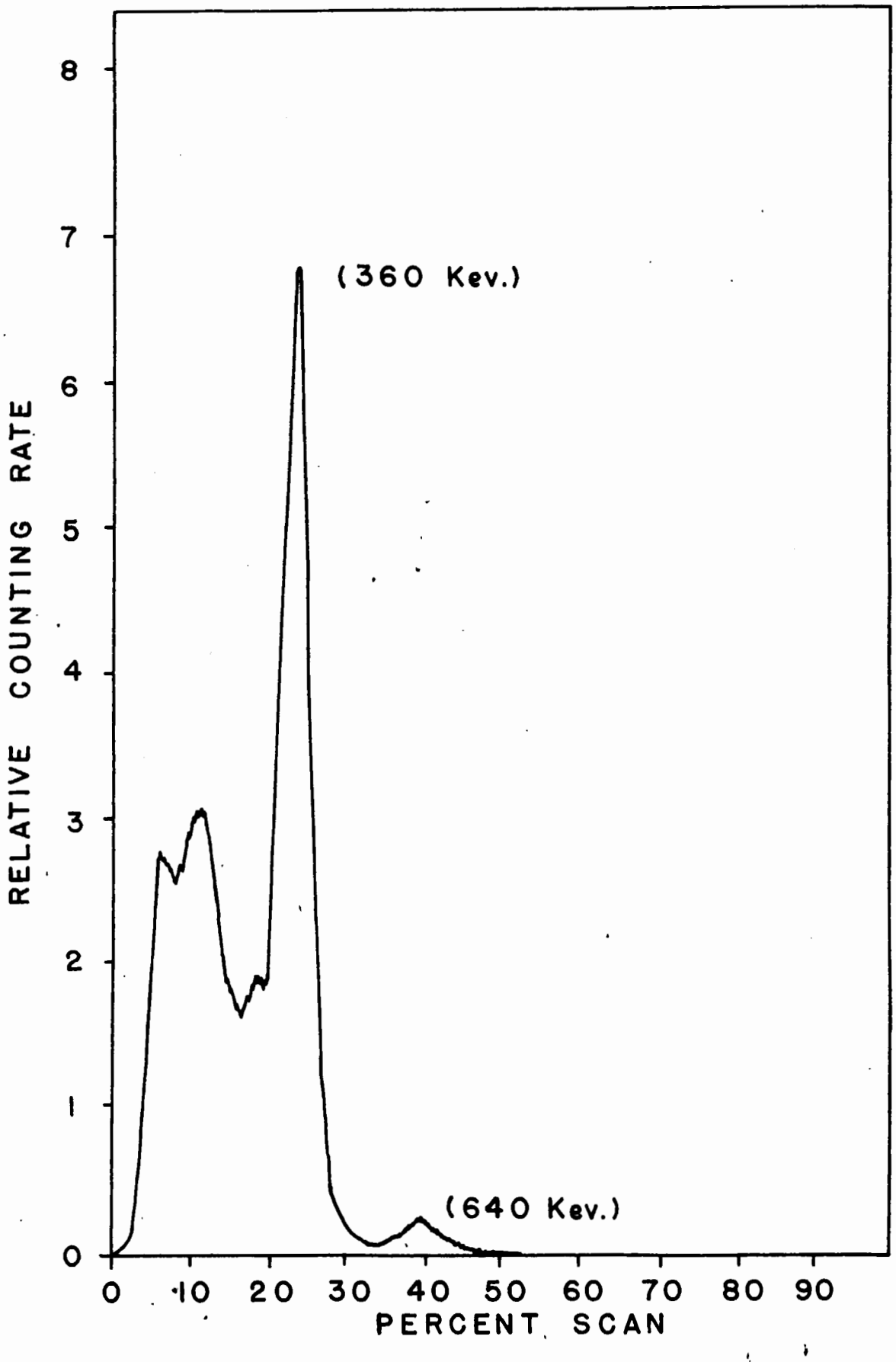
RELATIVE COUNTING RATE
0
1
2
3
4
5
6
7
8
(360 Kev.)
(640 Kev.)
0
10
20
30
40
50
60
70
80
90
PERCENT SCAN

Figure 47

γ Decay Curves of I^{133} 520 Kev

and I^{132} 670 Kev Photopeaks

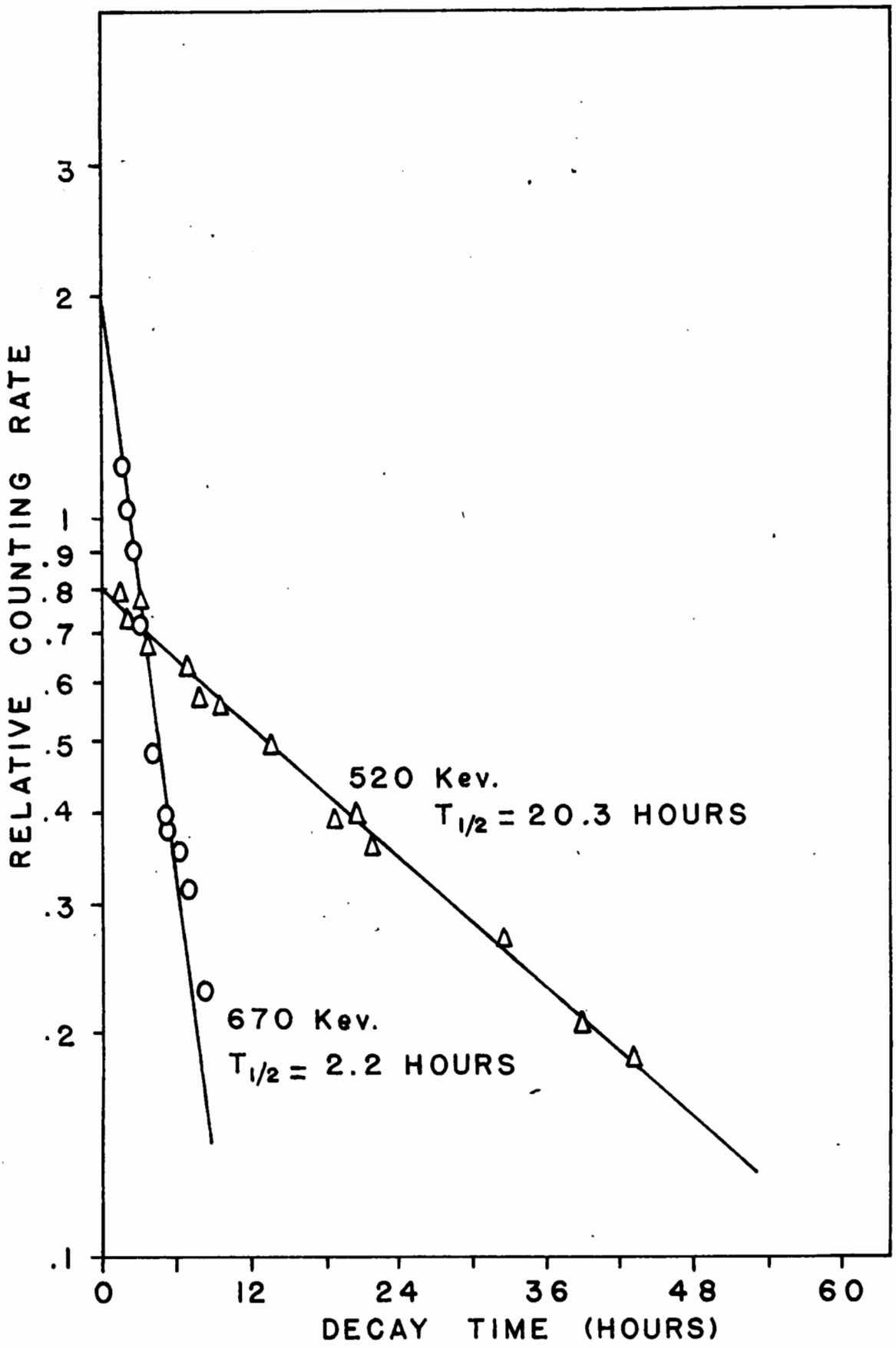
RELATIVE COUNTING RATE
3
2
1
.9
.8
.7
.6
.5
.4
.3
.2
.1
0
12
24
36
48
60
DECAY TIME (HOURS)
520 Kev.
T1/2 = 20.3 HOURS
670 Kev.
T1/2 = 2.2 HOURS

Figure 48

Decay Curve of I^{131} 360 Kev Photopeak

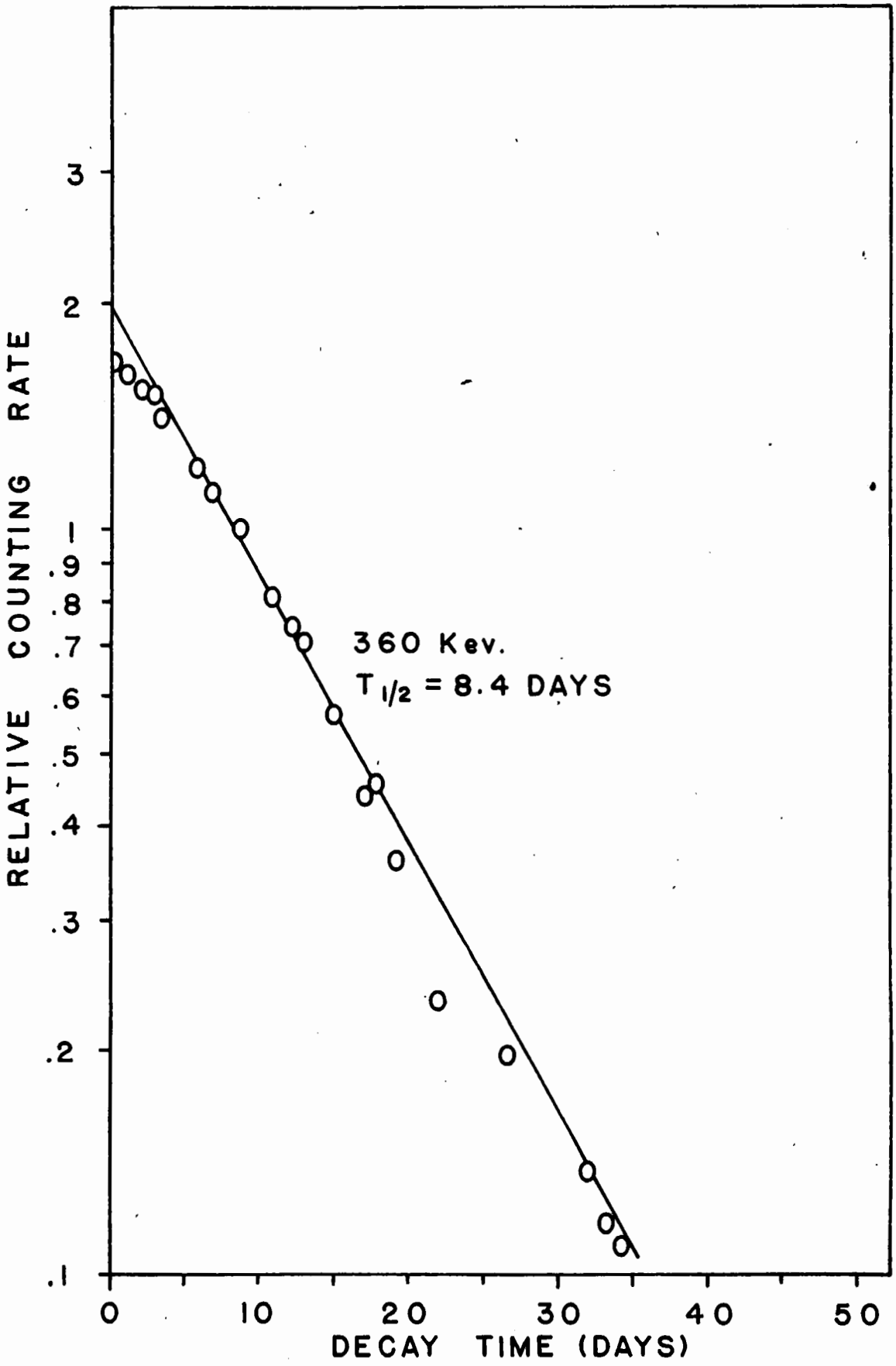
RELATIVE COUNTING RATE
3
2
1
.9
.8
.7
.6
.5
.4
.3
.2
.1
360 Kev.
$T_{1/2}$ = 8.4 DAYS
0
10
20
30
40
50
DECAY TIME (DAYS)

TABLE 22

REPORTED DECAY CHARACTERISTICS FOR IODINE ISOTOPES

Nuclide	Half-life	β^- Energies (Kev)		γ Energies (Kev)
I^{131}	8.05-day (112)	800 - 0.8 %		722
		600 - 80 %	(113)	638
		315 - 14 %		364
		244 - 5 %		
I^{132}	2.30-hour (114)	2120 - 18 %		1400
		1530 - 24 %		960
		1160 - 23 %		777
		900 - 20 %		673
		730 - 15 %		528
I^{133}	20.9-hour (114)	1400 - 94 %	(117)	850
		500 - 6 %		530

Iodine separations were performed at a time after the irradiation when any independently formed I^{132} had completely decayed. The observed I^{132} activity resulted from the decay of Te^{132} and consequently its disintegration rate was used to calculate the yield of Te^{132} (Table 21). The fission yields of I^{131} and I^{132} are given in Tables 23 and 24.

TABLE 23

FISSION YIELD DATA FOR 8.05-DAY I^{131}

Irradiation A 3

Observed activity	66000 counts per minute
Self-absorption factor	0.52
Source-mount Absorption factor	1.000
Aliquot factor	1250
Chemical yield	36.2 %
Time after irradiation	15.81 days
Decay factor	0.2579
Time in reactor	24 hours
Saturation factor	0.0828
Activity at saturation	3.420×10^8 dis. per second
Fission rate	relative yield
Fission yield	(3.06 ± 0.10) %

TABLE 23 (Continued)

FISSION YIELD DATA FOR 8.05-DAY I^{131}

Irradiation number	B 1	C 1
Observed activity	55500 c/m	74970 c/m
Self-absorption factor	0.75	0.84
Source-mount Absorption factor	1.000	1.000
Aliquot factor	25000	12500
Chemical yield	74.3 %	74.7 %
Time after irradiation	88 hours	12.6 days
Decay factor	0.7301	0.3403
Time in reactor	24 hours	24 hours
Saturation factor	0.0828	0.0828
Activity at saturation	6.866×10^{8} d/s	8.833×10^{8} d/s
Fission rate	2.270×10^{10} f/s	2.885×10^{10} f/s
Fission yield	(3.02 ± 0.09) %	(3.06 ± 0.09) %

TABLE 24

FISSION YIELD DATA FOR 20.9-HOUR I^{133}

Irradiation number	B 1	D 1
Observed activity	42000 c/m	40800 c/m
Self-absorption factor	0.925	0.910
Source-mount Absorption factor	1.000	1.000
Aliquot factor	25000	12500
Chemical yield	74.3 %	34.3 %
Time after irradiation	87.01 hours	62.6 hours
Decay factor	0.0558	0.1242
Time in reactor	24 hours	18.5 hours
Saturation factor	0.5488	o.486
Activity at saturation	8.31×10^8 d/s	4.504×10^8 d/s
Fission rate	2.270×10^{10} f/s	1.464×10^{10} f/s
Fission yield	(3.66 ± 0.10) %	(3.08 ± 0.10) %

(m) Cesium

The procedure used for the isolation of cesium activity from other fission products was that given by Glendenin and Nelson (117). A preliminary precipitation of cesium with silicotungstic acid was followed by a precipitation of $CsClO_4$ from $HClO_4$ with absolute ethanol. After dissolving the cesium, contaminants were removed by ferric hydroxide scavenging. The cesium was finally precipitated as the perchlorate and washed with absolute ethanol. Enough water was then added to dissolve the cesium and give a total volume of 10 ml.

Aliquots of cesium were precipitated with chloroplatinic acid and alcohol. The precipitates were filtered and dried at 110°C. for 20 minutes. Chemical yields were determined by weighing the solids as Cs_2PtCl_6.

The decay of cesium activity was followed by counting 20 and 50 λ sources in the 4π-proportional counter. The observed activity of 13 days (see Figure 49) was taken to be that of Cs^{136}. This nuclide has a reported half-life of 12.9 days (118) and decays by the emission of β^- particles with a maximum energy of 341 Kev (92.6 %) and 657 Kev (7.4 %). Cs^{136} is a shielded nuclide and is therefore produced directly in fission as a primary fragment. After 80 days of counting, the cesium activity remained constant at a value well above the background counting rate for the counter. It was thought that this activity might be due to the presence of long-lived

Figure 49

Decay Curve of 13-Day Cs^{136}

O Experimental Points

Δ Longer-Lived Component Subtracted

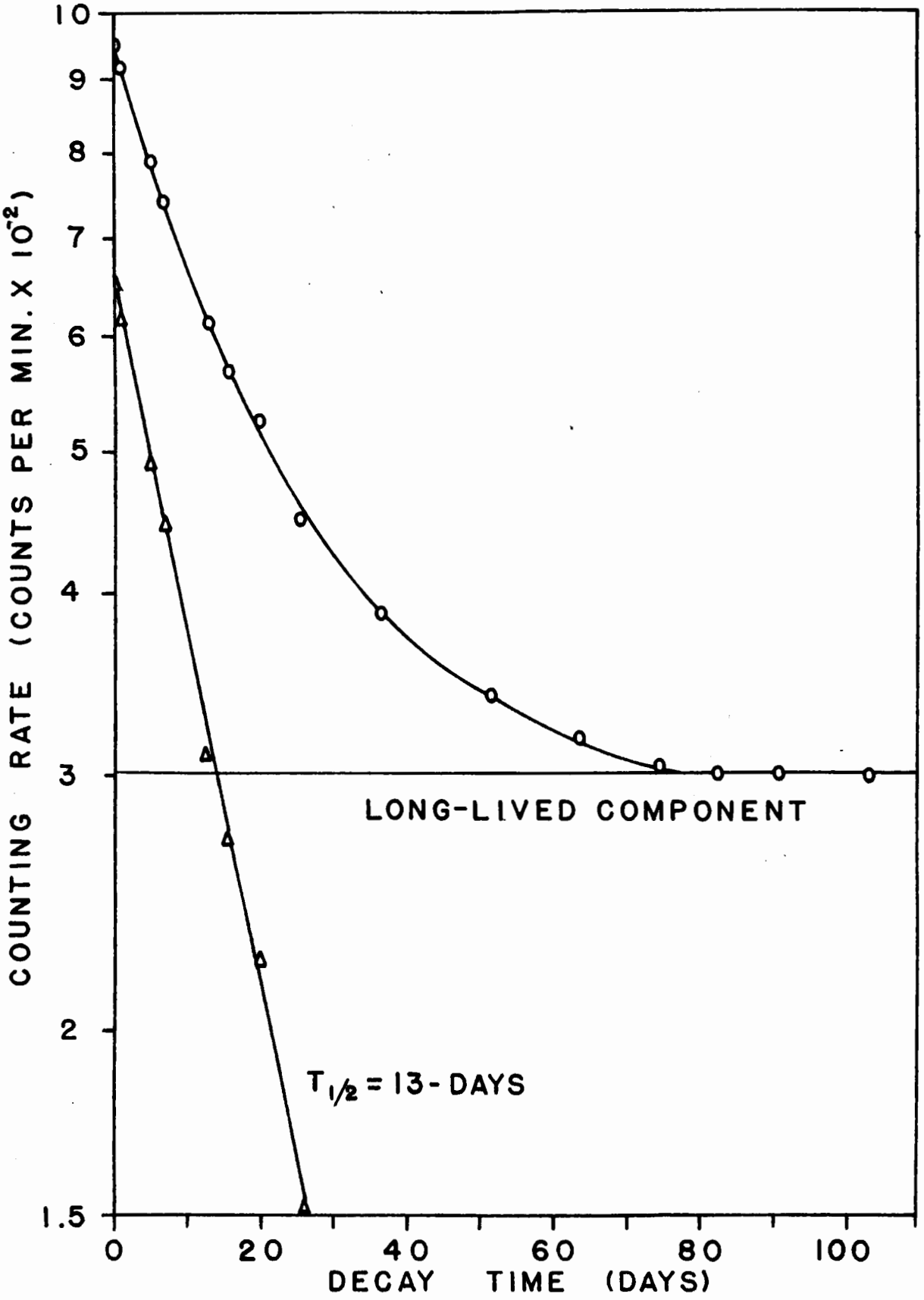
10
9
8
7
6
5
4
3
2
1.5
COUNTING RATE (COUNTS PER MIN. X 10^{-2})
LONG-LIVED COMPONENT
$T_{1/2}$ = 13-DAYS
0
20
40
60
80
100
DECAY TIME (DAYS)

Cs^{137} which is known to be produced in fission (119). The γ spectrum obtained for the cesium sample showed several very low intensity γ peaks which were not resolved. The data for the independent fission yield of Cs^{136} are given in Table 25. By assuming that the residual cesium activity was due to the presence of Cs^{137}, calculations were made for the fission yield of mass number 137. Cs^{137} decays by the emission of 1.2 Mev (5 %) and 0.523 Mev (95 %) β^- particles. The latter β^- emission leads to the formation of a metastable state, Ba^{137m} (2.6-minute). The isomer, in decaying to the ground state, contributes to the counting rate observed for Cs^{137}. Yaffe (120) has determined that the observed counting rate should be divided by 1.102 to obtain the true Cs^{137} counting rate. This correction factor is in agreement with the value of 1.100 calculated by Brown (121). The half-life of Cs^{137} has recently been reported as 30.0 years (121) and 26.6 years (122). Since no preference could be given to either value, the fission yield is given for Cs^{137} in Table 26 using both half-lives.

(n) Barium

The method used for the separation of barium was similar to that used for strontium (69). After the separation of barium from strontium by a chromate precipitation, the barium was dissolved and reprecipitated twice by means of a cold HCl-ether mixture. The final $BaCl_2$ precipitate was washed with ethanol before being dissolved in water and made up to a volume

TABLE 25

FISSION YIELD DATA FOR 12.9-DAY Cs^{136}

Irradiation D 1

Observed activity	650 counts per minute
Self-absorption factor	0.975
Source-mount Absorption factor	0.998
Aliquot factor	5000
Chemical yield	60.3 %
Time after irradiation	31.3 days
Decay factor	0.18611
Time in reactor	18.5 hours
Saturation factor	0.03985
Activity at saturation	1.244×10^{7} dis. per second
Fission rate	1.464×10^{10} fissions per second
Fission yield	(0.0849 ± 0.0022) %

TABLE 26

FISSION YIELD DATA FOR Cs^{137}

Irradiation D 1

Reported half-life	30.0 years	26.6 years
Observed activity	300 c/m	300 c/m
Self-absorption factor	0.980	0.980
Source-mount Absorption factor	0.999	0.999
Aliquot factor	5000	5000
Chemical yield	60.3 %	60.3 %
Time after irradiation	31.3 days	31.3 days
Decay factor	0.9980	0.9978
Time in reactor	18.5 hours	18.5 hours
Saturation factor	4.878×10^{-5}	5.42×10^{-5}
Activity at saturation	7.887×10^{8} d/s	7.100×10^{8} d/s
Fission rate	1.464×10^{10} f/s	1.464×10^{10} f/s
Fission yield	(5.39 ± 0.11) %	(4.85 ± 0.10) %

No natural cesium was detected in a spectrographic analysis of the uranium 233 sample used.

of either 10 or 25 ml.

Chemical yields were determined by precipitating barium as the sulphate. The precipitate was dried at 110°C. for 20 minutes and weighed as $BaSO_4$.

Barium sources were mounted and counted as soon after the end of a separation as possible. The counting rate, as measured by the 4π-proportional counter, increased with time reaching a maximum value of about 4 days, and then decreased with a half-life of 12.8 days (Figure 50). This activity was assigned to the presence of 12.8-day Ba^{140} (123) which decays to 40-hour La^{140},

$$\text{short lived} \longrightarrow \underset{12.8\text{-d.}}{Ba^{140}} \longrightarrow \underset{40\text{-h.}}{La^{140}} \longrightarrow \underset{\text{stable}}{Ce^{140}} .$$

For the first few hours after a barium separation the growth of lanthanum is linear with respect to time. Therefore, a plot of Ba plus La counting rates vs. time can be accurately extrapolated back to the time at which barium was separated (Figure 51). By using growth and decay equations it is also possible to calculate the amount of Ba present initially from a measured Ba plus La counting rate at a known time after the separation. The calculated values agreed with those obtained by back extrapolating the initial portions of the growth and decay curves.

Barium sources counted were about 30 μgm/cm^2 thick. A decrease in the thickness by a factor of 100 showed no change in the source specific activity. This observation together with the agreement between calculated and observed growth

Figure 50

Growth and Decay Curve for Ba^{140} La^{140}

O Experimental Points

□ Calculated Points

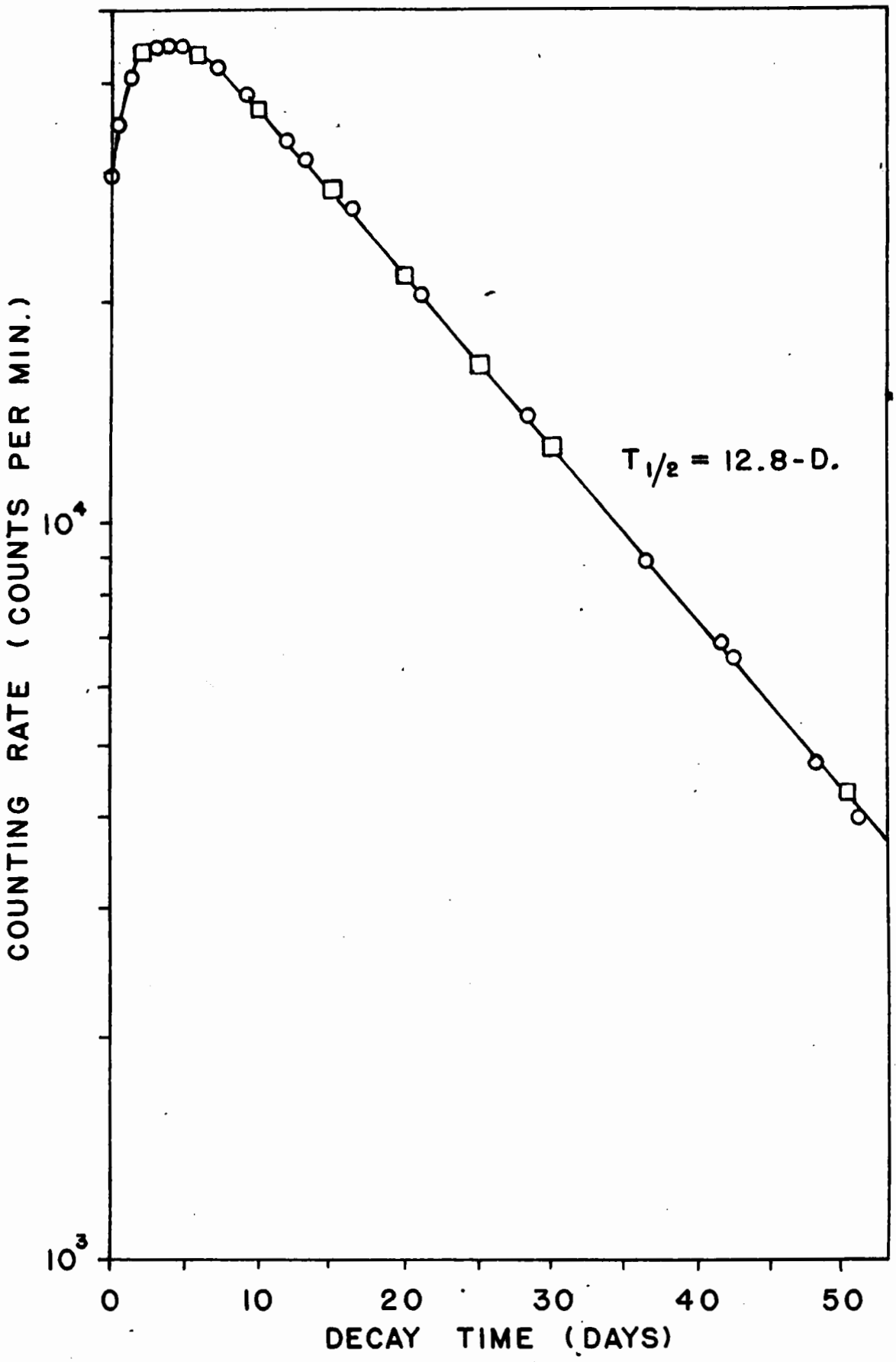
COUNTING RATE (COUNTS PER MIN.)
10^4
10^3
$T_{1/2}$ = 12.8-D.
0
10
20
30
40
50
DECAY TIME (DAYS)

Figure 51

Linear Growth Curve of La^{140} from Ba^{140}

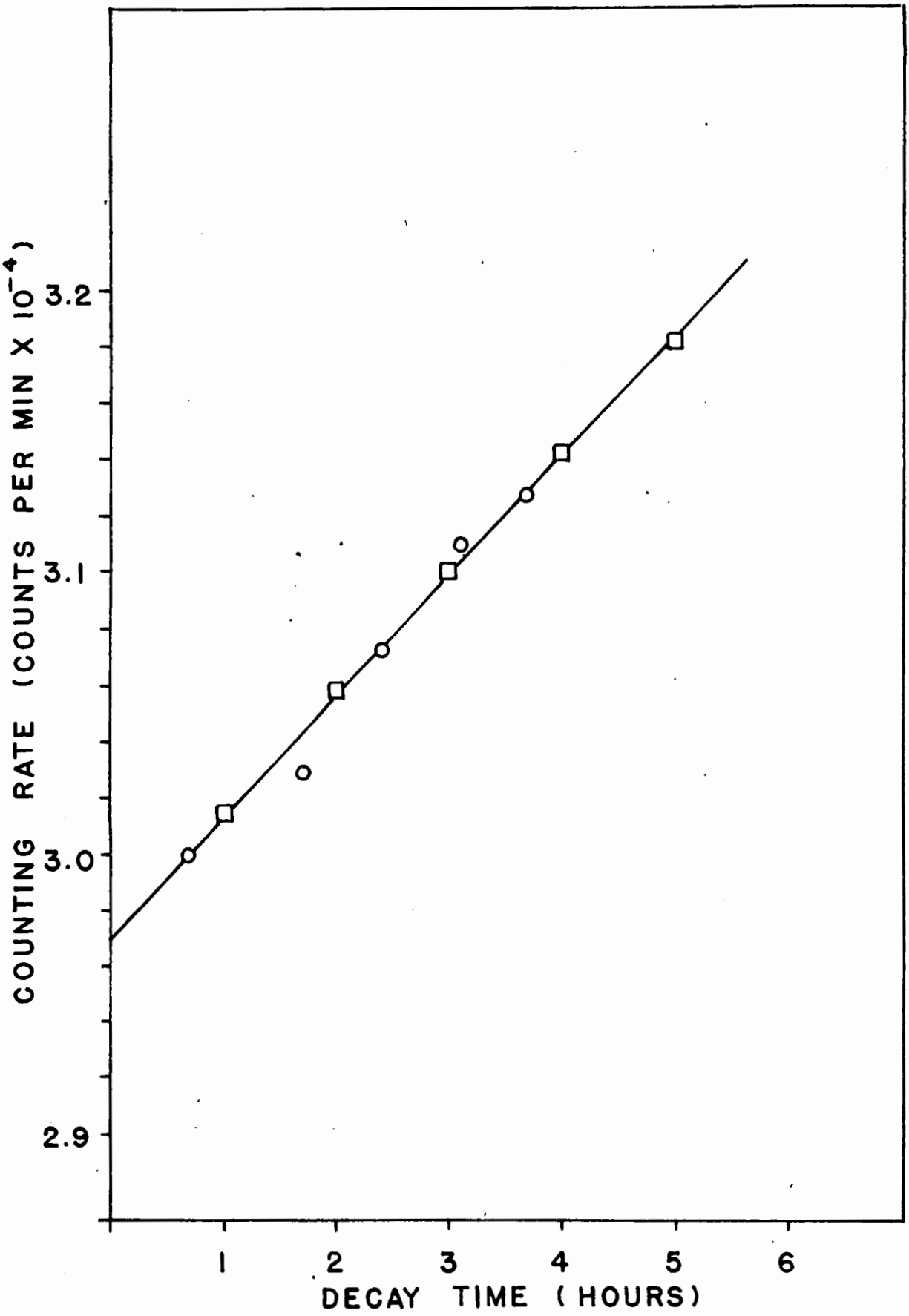
COUNTING RATE (COUNTS PER MIN X 10^{-4})
3.2
3.1
3.0
2.9
1
2
3
4
5
6
DECAY TIME (HOURS)

and decay curves indicatd that self-absorption effects, as described by Grummitt et al. (124), were not significant in this work.

Decay schemes given for Ba^{140} indicate that the nuclide decays to La^{140} by the emission of β^- particles of maximum energies 480 (40%), and 1022 (60 %). In coincidence with the β^- emission were reported (125) γ rays of energies 162, 304 and 537 Kev. The daughter activity, La^{140}, undergoes β^- emission with energies 1.34 (45 %), 1.67 (10 %) and 2.15 (7 %) Mev. Reported γ energies for the La decay were 328, 486, 815, 893, 1597 and 2570 Kev (126).

Each barium separation was analyzed on the scintillation spectrometer. The γ spectrum obtained 0.5 hours after the end of a separation is shown in Figure 52. Photopeaks were observed at energies of 305, 410 and 530 Kev. As the lanthanum activity grew in the position of the initial peaks shifted. At the same time the height of the peaks increased. In Figure 53 is shown a γ spectrum of barium and lanthanum decaying in equilibrium. The observed 320 Kev peak corresponds to the unresolved Ba^{140} 305 peak and the La^{140} 328 Kev peak. The La^{140} 490 peak now masks the Ba^{140} 510 Kev peak. The 820, 1250 and 1600 Kev peaks are due entirely to lanthanum daughter. A plot of peak height against time (Figure 54) produces a curve similar to the net growth and decay as shown in Figure 50.

The observed activity in irradiation E was caused by the presence of fast neutrons. The fissile material had been

Figure 52

γ Spectrum Observed for a Barium Sample

0.5 Hours after the End of a Separation

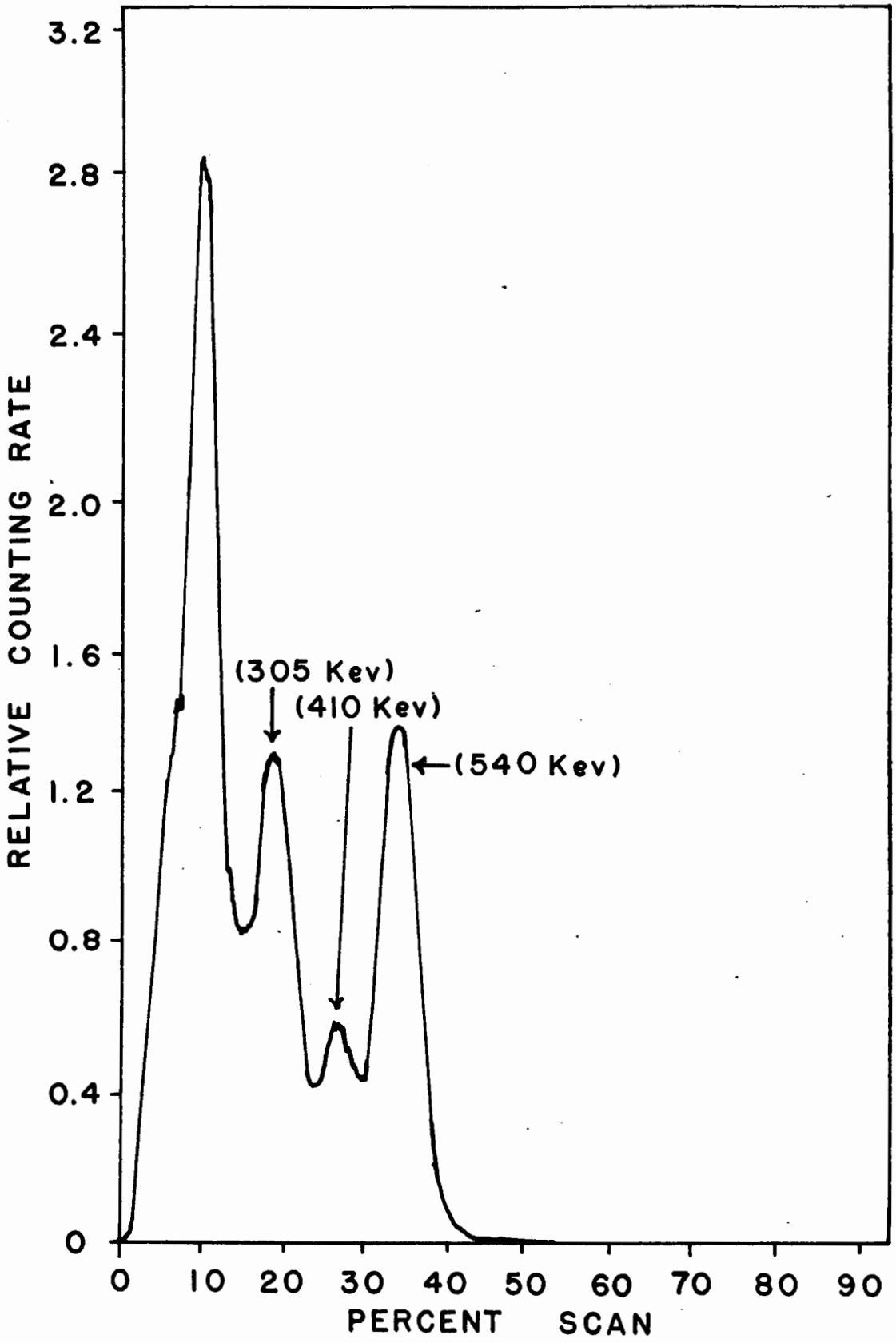
3.2
2.8
2.4
2.0
1.6
1.2
0.8
0.4
0
RELATIVE COUNTING RATE
(305 Kev)
(410 Kev)
(540 Kev)
0
10
20
30
40
50
60
70
80
90
PERCENT SCAN

Figure 53

γ Spectrum Observed for a Barium Sample

5 Days after the End of a Separation

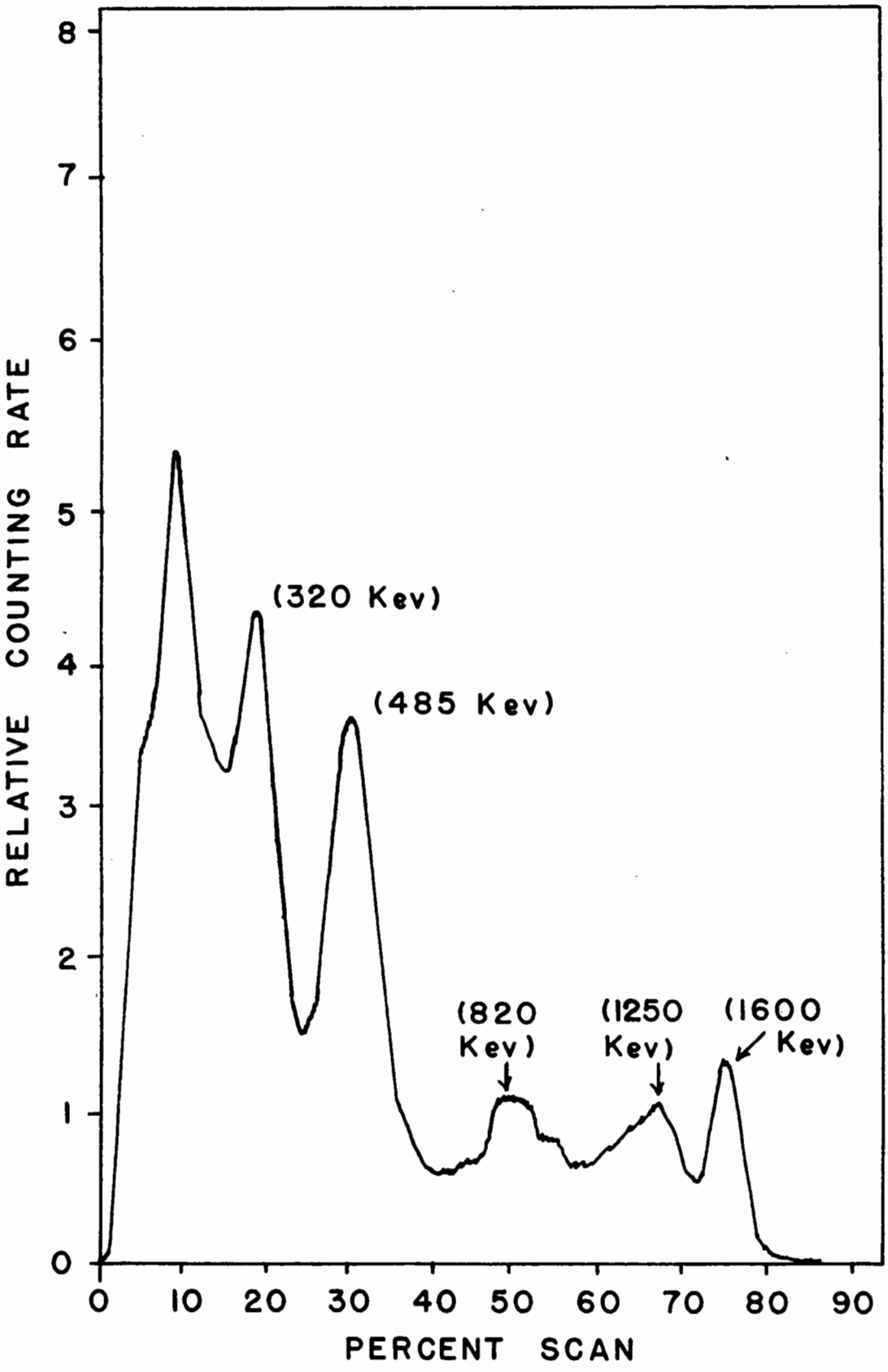
RELATIVE COUNTING RATE
PERCENT SCAN
0
1
2
3
4
5
6
7
8
0
10
20
30
40
50
60
70
80
90
(320 Kev)
(485 Kev)
(820 Kev)
(1250 Kev)
(1600 Kev)

Figure 54

Growth and Decay Curves for the

Observed Ba^{140} -La^{140} Photopeaks

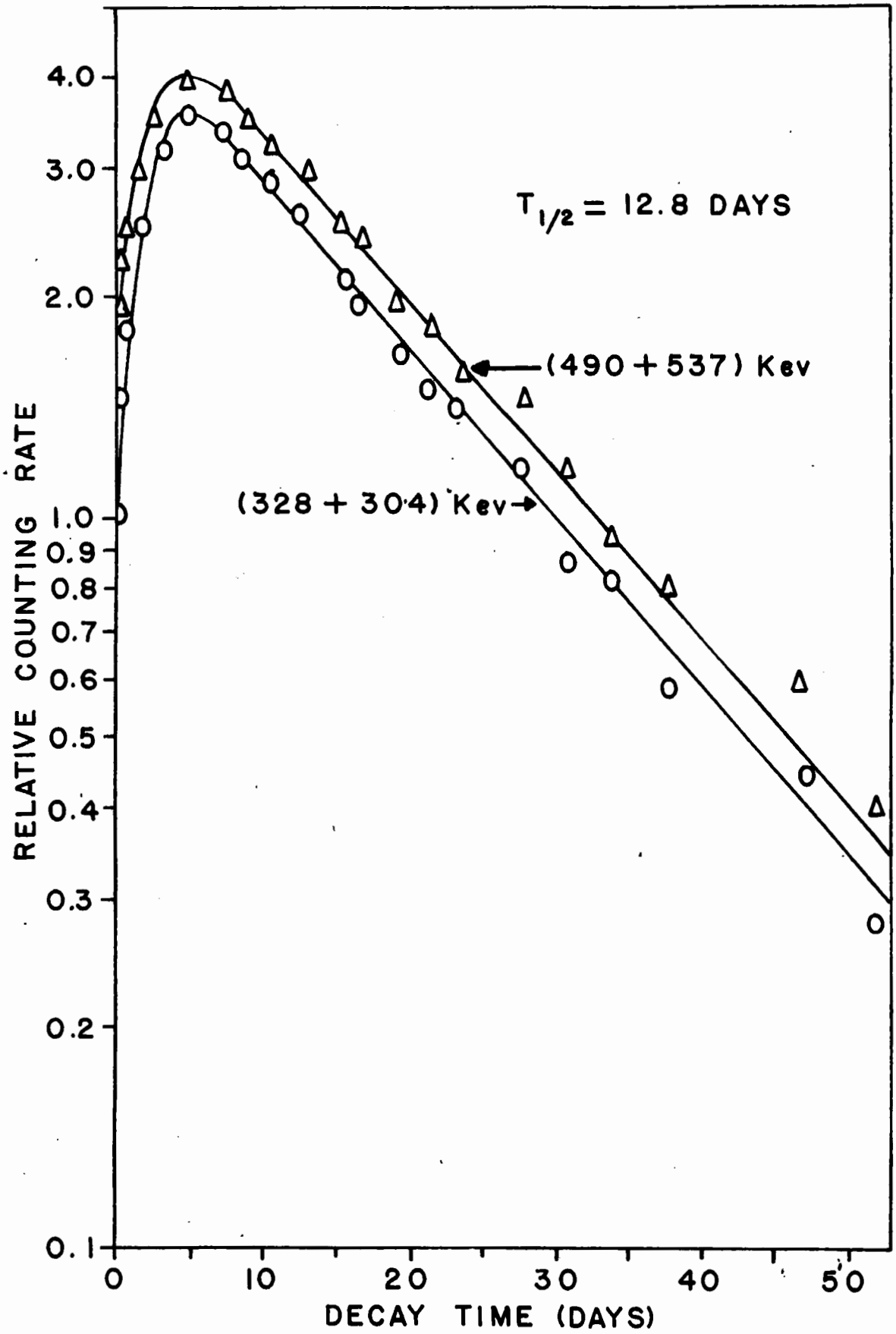
4.0
3.0
2.0
1.0
0.9
0.8
0.7
0.6
0.5
0.4
0.3
0.2
0.1
RELATIVE COUNTING RATE
$T_{1/2}$ = 12.8 DAYS
(490 + 537) Kev
(328 + 304) Kev
0
10
20
30
40
50
DECAY TIME (DAYS)

surrounded with cadmium, which absorbs low-energy neutrons. A comparison was made of the barium activity obtained in a shielded and an unshielded uranium sample to determine the number of epi-cadmium neutrons which were causing fast fission. In irradiation C the barium saturation activity per mgm. of sample was 2.983×10^{8} disintegrations per second, for a flux value of 5.05×10^{12} n/cm.^{2} per second. The barium saturation activity per mgm. of sample for irradiation E (shielded) was 6.237×10^{6} disintegrations per second when normalized to the same flux value as in C. Therefore, the percentage of barium activity produced by the presence of epi-cadmium neutrons was 2.09 %. A similar measurement, discussed earlier, for strontium in the light-mass peak gave a value of 2.10 %.

Spectrographic analysis of the original uranium sample revealed that no barium was present before the irradiation. The limit of detection of this analysis was 0.02 % of the U^{233} content. Consequently, less than 1.58×10^{15} atoms of barium could have been present as an impurity. The formation of Ba^{140} from such an impurity would involve a double neutron capture reaction. The heaviest stable isotope of barium found in nature is Ba^{138} (71.66 %) which has a thermal-neutron capture cross section of 4.9 barns. The result of a neutron capture reaction involving Ba^{138} is the production of 85-m. Ba^{139}. The thermal-neutron capture cross section for this unstable nuclide has been measured and is given as 0.5 barns (127).

TABLE 27

FISSION YIELD DATA FOR 12.8-DAY Ba^{140}

Irradiation number	A 1	A 2
Observed activity	8.30×10^4 c/m	6.37×10^4 c/m
Self-absorption factor	0.974	0.974
Source-mount Absorption factor	1.000	1.000
Aliquot factor	5000	5000
Chemical yield	63.8 %	63.5 %
Time after irradiation	17.0 days	23.83 days
Decay factor	0.3984	0.02753
Time in reactor	24 hours	24 hours
Saturation factor	0.05272	0.05272
Activity at saturation	5.300×10^8 d/s	5.913×10^8 d/s
Fission rate	Relative yield	
Fission yield	(4.76 ± 0.66) %	(5.31 ± 0.13) %

TABLE 27 (Continued)

FISSION YIELD DATA FOR 12.8-DAY Ba^{140}

Irradiation number	B 1	B 2
Observed activity	1.10×10^5 c/m	94000 c/m
Self-absorption factor	0.99	0.99
Source-mount Absorption factor	1.000	1.000
Aliquot factor	12500	12500
Chemical yield	46.6 %	59.7 %
Time after irradiation	4.69 days	10.69 days
Decay factor	0.7758	0.5606
Time in reactor	24 hours	24 hours
Saturation factor	0.05272	0.05272
Activity at saturation	1.214×10^9 d/s	1.121×10^9 d/s
Fission rate	2.2695×10^{10} f/s	2.269×10^{10} f/s
Fission yield	(5.35 ± 0.23) %	(4.94 ± 0.16) %

TABLE 27 (Continued)

FISSION YIELD DATA FOR 12.8-DAY Ba^{140}

Irradiation number	C 1	C 2
Observed activity	6.36×10^4 c/m	9400
Self-absorption factor	1.000	0.99
Source-mount Absorption factor	1.000	1.000
Aliquot factor	31250	12500
Chemical yield	49.2 %	51.9 %
Time after irradiation	3.56 days	56.71 days
Decay factor	0.8247	0.04641
Time in reactor	24 hours	24 hours
Saturation factor	0.05272	0.5272
Activity at saturation	1.548×10^9 d/s	1.567×10^9 d/s
Fission rate	2.8847×10^{10} f/s	2.8847×10^{10} f/s
Fission yield	5.37 ± 0.16) %	(5.43 ± 0.22) %

TABLE 27 (Continued)

FISSION YIELD DATA FOR 12.8-DAY Ba^{140}

Irradiation number	D_a 1	D_a 2
Observed activity	30535	4800
Self-absorption factor	0.99	0.99
Source-mount Absorption factor	1.000	1.000
Aliquot factor	12500	6250
Chemical yield	52.1 %	62.3 %
Time after irradiation	16.01 days	67.06 days
Decay factor	0.4203	0.0265
Time in reactor	18.5 hours	18.5 hours
Saturation factor	0.04049	0.04049
Activity at saturation	7.247×10^8 d/s	7.5517×10^8 d/s
Fission rate	1.4644×10^{10} f/s	1.464×10^{10} f/s
Fission yield	(4.95 ± 0.05) %	(5.16 ± 0.11) %

TABLE 27 (Continued)

FISSION YIELD DATA FOR 12.8-DAY Ba^{140}

Irradiation number	E 2	F 1
Observed activity	4400	29700
Self-absorption factor	0.99	0.99
Source-mount Absorption factor	1.000	1.000
Aliquot factor	2500	25000
Chemical yield	38.1 %	36.3 %
Time after irradiation	5.0 days	13.08 days
Decay factor	0.7628	0.4926
Time in reactor	23.8 hours	24.16 hours
Saturation factor	0.0523	0.05305
Activity at saturation	1.217×10^7 d/s	1.318×10^9 d/s
Fission rate	Fast fission	2.587×10^{10} f/s
Fission yield		(5.09 ± 0.05) %

Both Katcoff (128) and Rubinson (129) have given the general equations for calculating the number of atoms formed by a combination of decays and captures. The disintegration rate of Ba^{140} produced by a double neutron capture of Ba^{138} gives less than one count per second.

Fission yield data for Ba^{140} are given in Table 27.

(c) Cerium

Two procedures were used for the separation of cerium activity. The first was similar to that used for the separation of yttrium (76). After isolating Ce, Y and the rare earths from other fission products, cerium was oxidized and precipitated twice as the iodate. The precipitate was dissolved in HNO_3-H_2O_2 and further purified by $Zr(IO_3)_4$ scavenging. Precipitations of ceric hydroxide, cerous hydroxide and cerous oxalate produced radiochemically pure cerium. The final precipitate was washed with water, dissolved in a minimum of nitric acid and made up to a known volume.

The second method used for the separation of cerium was described by Glendenin et.al. (130). Cerium carrier and sodium bromate were added to an aliquot of the fission product stock solution. Cerium was extracted into methylisobutyl ketone (MIK). The organic layer was separated and washed with dilute nitric acid containing sodium bromate. Cerium was back extracted into water containing a little 30 % H_2O_2. An oxalate precipitation was used to recover cerium from the aqueous layer. The cerium was then dissolved in dilute nitric acid, diluted and reprecipitated with oxalic

acid. After washing, the final oxalate precipitate was dissolved and made up to a volume of 10 ml.

The amount of cerium recovered was determined by precipitating and weighing cerium oxalate which had been dried by vacuum desiccation after an alcohol-ether washing.

Cerium activities detected in this work were 33-day Ce^{141}, 33-hour Ce^{143} and 285-day Ce^{144}. The decay curves, as obtained in the 4π -proportional counter, are given in Figures 55 and 56. The presence of Ce^{143} was also observed on the scintillation spectrometer. A 290 Kev photopeak was observed to decay with a 33-hour half-life (Figures 57 and 58). The decay chains for the nuclides studied are

short lived ----> Ce^{141} (33-d.) ----> Pr^{141} (stable)

short lived ----> Ce^{143} (33-h.) ----> Pr^{143} (13.8-d.) ----> Nd^{143} (stable)

short lived ----> Ce^{144} (285-d.) ----> Pr^{144} (2.5-m.) ----> Nd^{144} (stable)

In Table 28 are listed the reported decay characteristics for the cerium isotopes.

4. Errors

The errors involved in fission yields measured in this work may be divided into three sections.

(a) Systematic Errors

Such errors occur in weighing, diluting solutions, pipeting volumes of solutions, and in chemical analysis. It

Figure 55

β Decay Curves of 285-Day Ce^{144}

and 33-Day Ce^{142}

O Experimental Points

Δ 285-Day Activity Subtracted

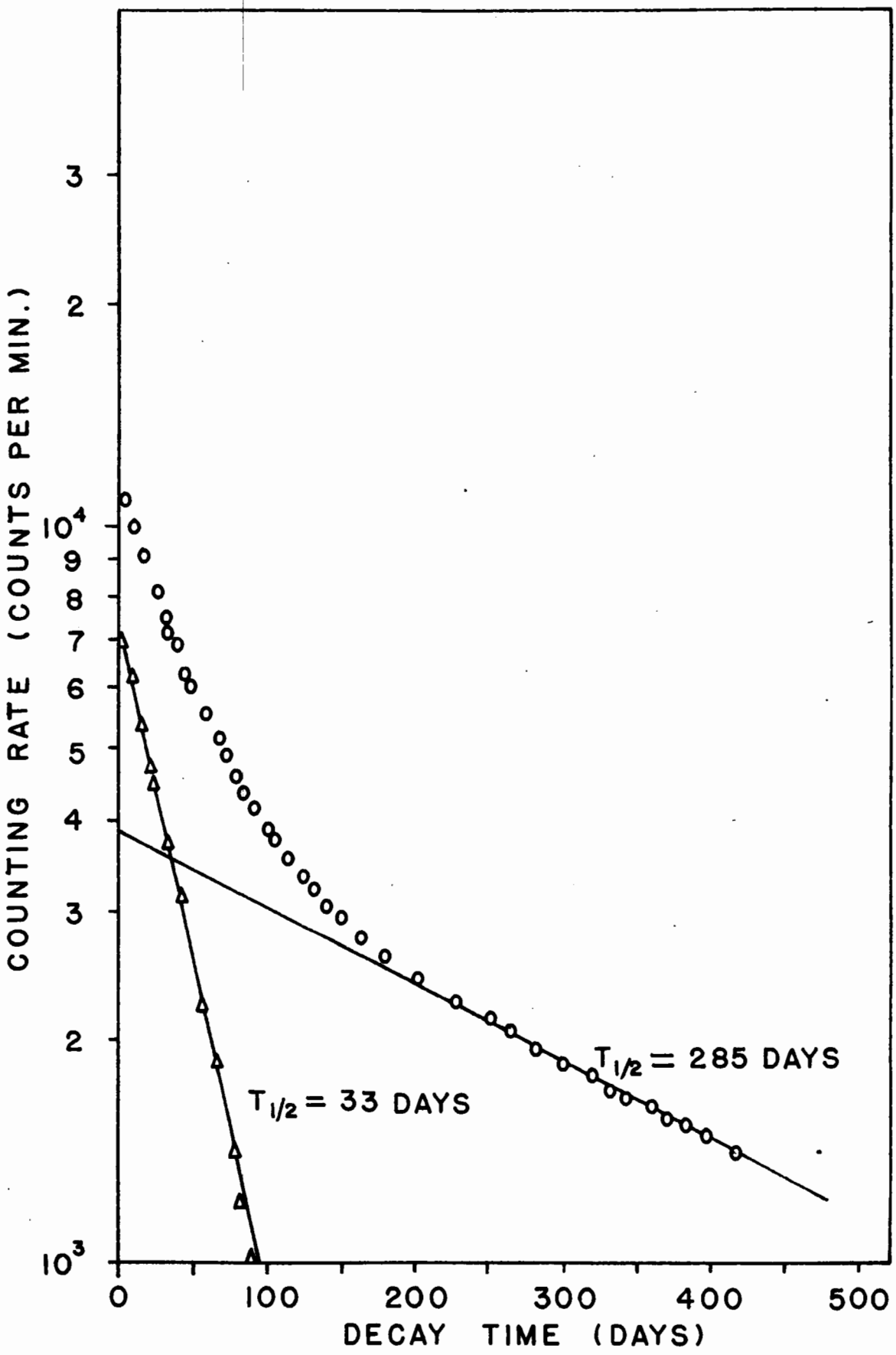
COUNTING RATE (COUNTS PER MIN.)
3
2
10^4
9
8
7
6
5
4
3
2
10^3
0
100
200
300
400
500
DECAY TIME (DAYS)
T1/2 = 285 DAYS
T1/2 = 33 DAYS

Figure 56

β Decay Curve of 33-Hour Ce^{143}

O Experimental Points

Δ Longer-Lived Components Subtracted

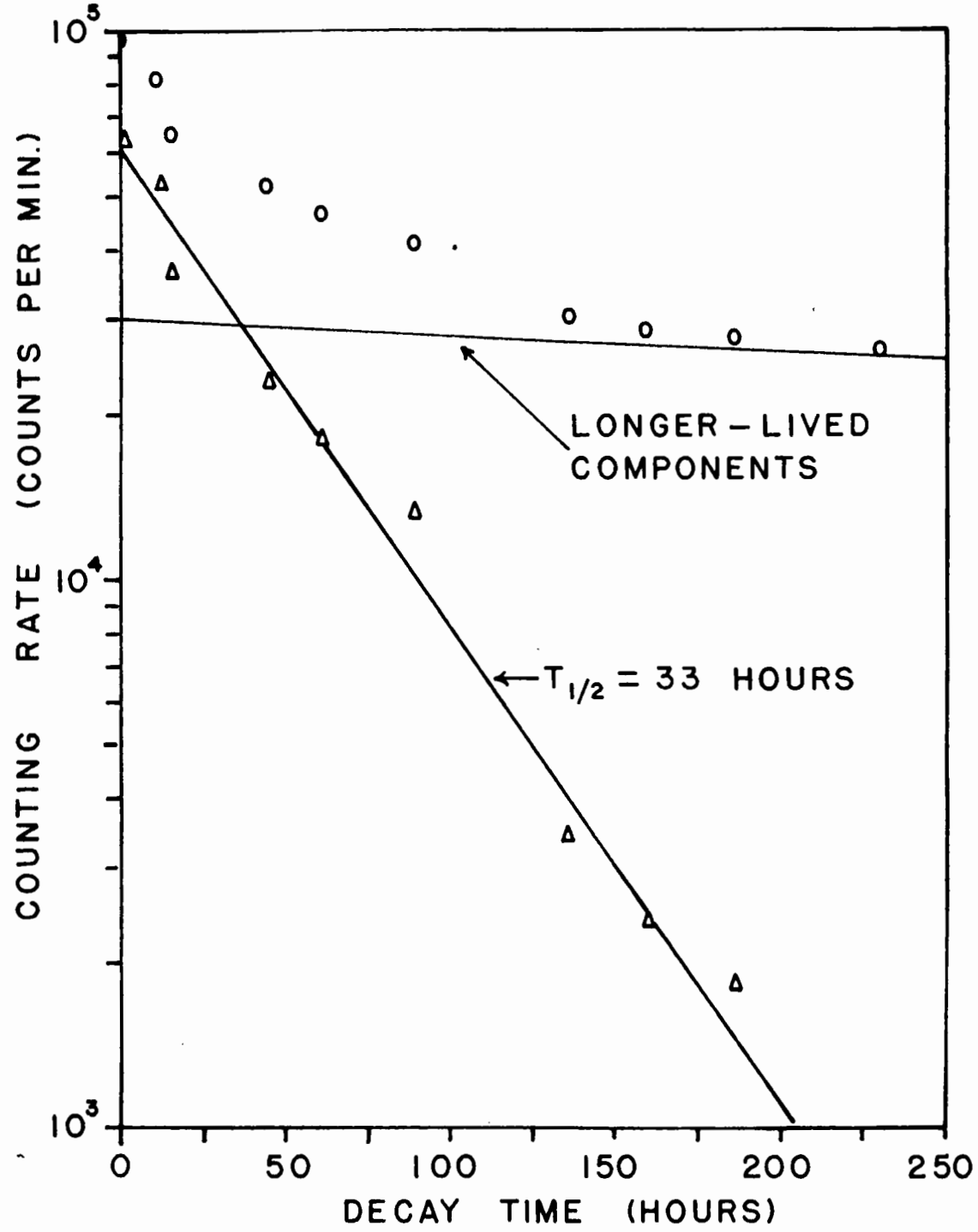
COUNTING RATE (COUNTS PER MIN.)
10^5
10^4
10^3
LONGER – LIVED COMPONENTS
$T_{1/2}$ = 33 HOURS
0
50
100
150
200
250
DECAY TIME (HOURS)

Figure 57

γ Spectrum of Ce^{143}

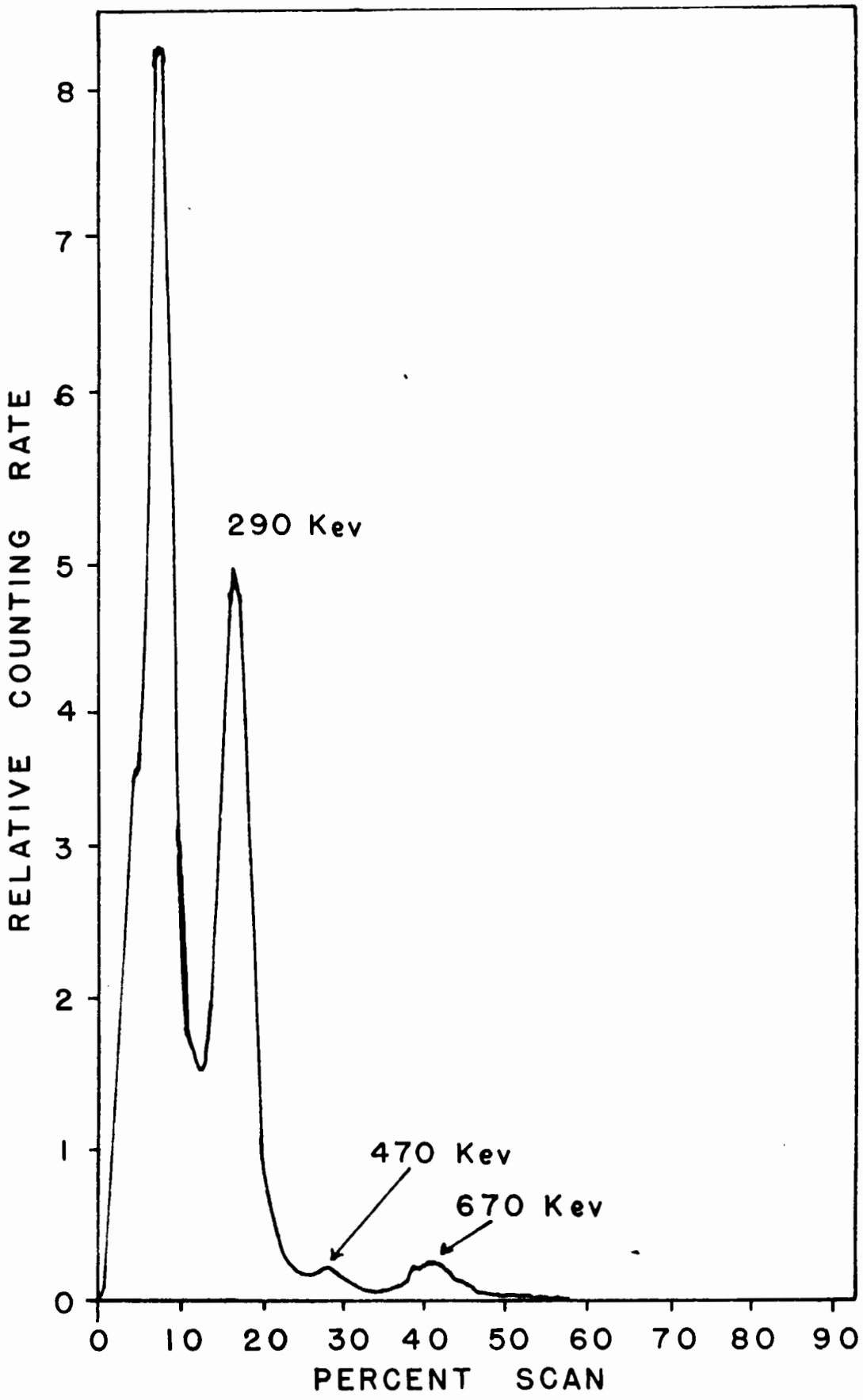
RELATIVE COUNTING RATE
0
1
2
3
4
5
6
7
8
290 Kev
470 Kev
670 Kev
0
10
20
30
40
50
60
70
80
90
PERCENT SCAN

Figure 58

Decay of Ce^{143} -290 Kev Photopeak

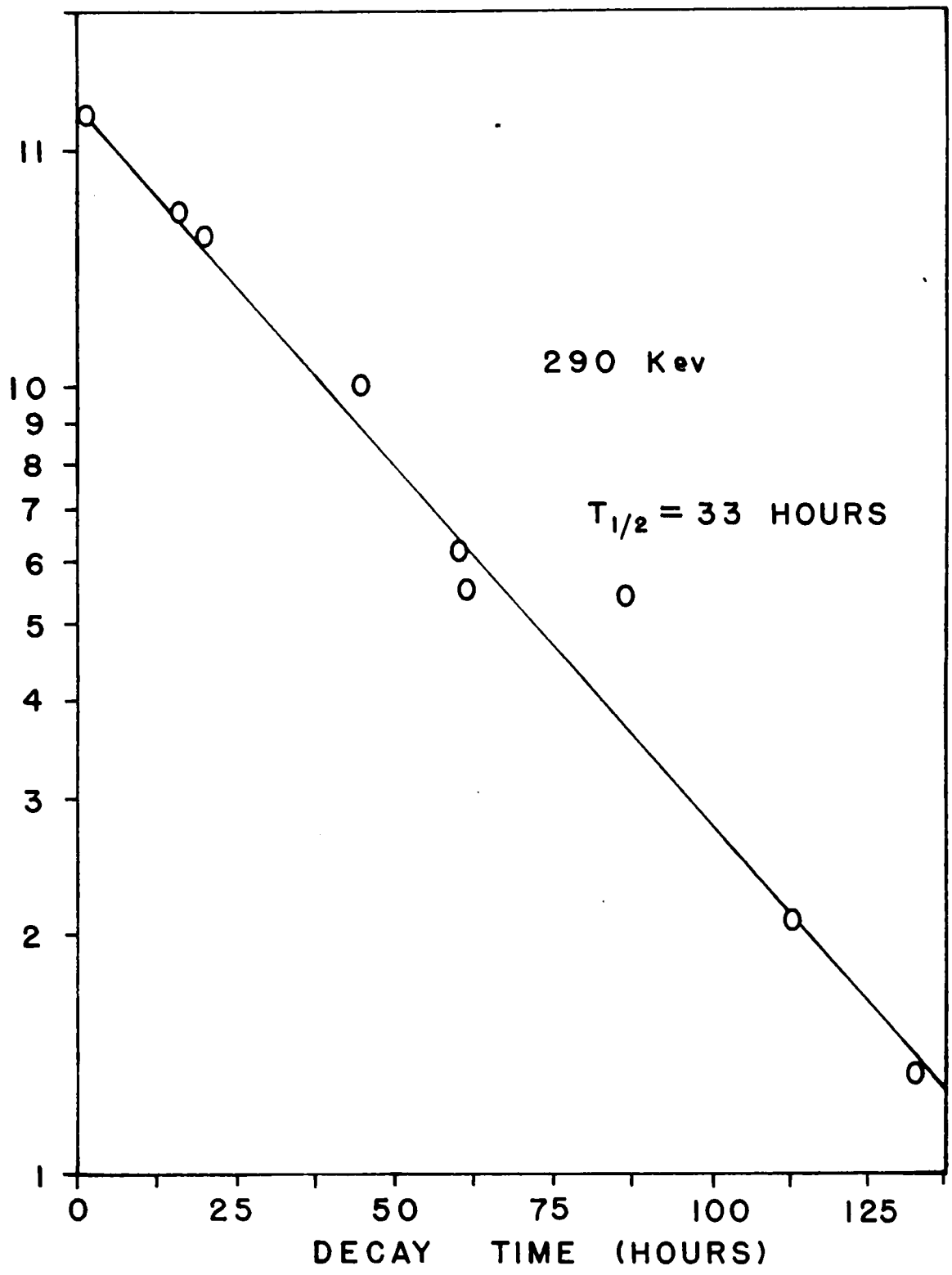
290 Kev
$T_{1/2}$ = 33 HOURS
11
10
9
8
7
6
5
4
3
2
1
0
25
50
75
100
125
DECAY TIME (HOURS)

TABLE 28

REPORTED DECAY CHARACTERISTICS FOR CERIUM ISOTOPES

Nuclide	Half-life	β Energies (Kev)		γ Energies (Kev)
Ce^{141}	33-day (131)	432 - 75 %	(132)	145
		574 - 25 %		
Ce^{143}	33.4-hour (133)	1400 - 37 %		294
		1125 - 40 %	(133)	others
		740 - 5 %		130 to 720
		500 - 12 %		
		220 - 6 %		
Ce^{144}	285-day (89)	309 - 76 %	(134)	34 to 134
		175 - 24 %		

The data from which the fission yields for Ce^{141}, Ce^{143} and Ce^{144} were calculated are given in Tables 29, 30 and 31 respectively.

TABLE 29

FISSION YIELD DATA FOR 33-DAY Ce^{141}

Irradiation number	A 1	B 2
Observed activity	7300 c/m	25100
Self-absorption factor	0.94	0.98
Source-mount Absorption factor	1.000	1.000
Aliquot factor	5000	12500
Chemical yield	37.8 %	43.7 %
Time after irradiation	61.0 days	35.51 days
Decay factor	0.2778	0.4744
Time in reactor	24 hours	24 hours
Saturation factor	0.0208	0.0208
Activity at saturation	2.966×10^8 d/s	1.236×10^9 d/s
Fission rate	relative yield	2.270×10^{10} f/s
Fission yield	(5.22 ± 0.04) %	$(5.44 \pm 0.16($ %

TABLE 29 (Continued)

FISSION YIELD DATA FOR 33-DAY Ce^{141}

Irradiation number	C 1	C 2
Observed activity	25700 c/m	11400 c/m
Self-absorption factor	0.98	0.98
Source-mount Absorption factor	1.000	1.000
Aliquot factor	12500	4166
Chemical yield	18.8 %	33.8 %
Time after irradiation	5.0 days	124.1 days
Decay factor	0.9003	0.0738
Time in reactor	24 hours	24 hours
Saturation factor	0.0208	0.0208
Activity at saturation	1.553×10^9 d/s	1.555×10^9 d/s
Fission rate	2.885×10^{10} f/s	2.885×10^{10} f/s
Fission yield	(5.38 ± 0.23) %	(5.39 ± 0.48) %

TABLE 30

FISSION YIELD DATA FOR 33-HOUR Ce^{143}

Irradiation number	C 1
Observed activity	56700 counts per minute
Self-absorption factor	0.980
Source-mount Absorption factor	1.000
Aliquot factor	12500
Chemical yield	18.8 %
Time after irradiation	5.0 days
Decay factor	0.0804
Time in reactor	24 hours
Saturation factor	0.3959
Activity at saturation	2.0184×10^{8} dis. per second
Fission rate	2.885×10^{10} fissions per second
Fission yield	(6.99 ± 0.35) %

TABLE 31

FISSION YIELD DATA FOR 285-DAY Ce^{144}

Irradiation number	B 2	C 1
Observed activity	8000 c/m	4280 c/m
Self-absorption factor	0.980	0.989
Source-mount Absorption factor	1.00	1.00
Aliquot factor	6250	6250
Chemical yield	43.7 %	18.8 %
Time after irradiation	35.51 days	5.0 days
Decay factor	0.9173	0.9879
Time in reactor	24 hours	24 hours
Saturation factor	0.00243	0.00243
Activity at saturation	8.724×10^9 d/s	9.999×10^8 d/s
Fission rate	2.2695×10^{10} f/s	2.8848×10^{10} f/s
Fission yield	(3.84 ± 0.11) %	(3.47 ± 0.15) %

was possible to keep most of these errors below 0.5 % by using a sensitive microbalance and calibrated volumetric glassware. By far the largest error in radiochemical studies of fission yields now appears to be caused in the determination of chemical yields. In general, the more carrier used, the greater is the accuracy obtainable in chemical analysis. However, the more carrier used, the greater are self-absorption losses in counting activities. The smaller the self-absorption effect, the greater the accuracy in measuring a disintegration rate. Optimum conditions were obtained in this work by recovering about 15 mgm. of cation or anion in a final volume of 10 ml. of solution. Three 2.0 ml. aliquots were used to determine chemical yields and an average value of the three measurements was used. Under these conditions, chemical recovery was reproducible up to a value of three percent. Occasionally, if the amount of carrier recovered was low, the error in chemical yields increased to as much as 20 %. Larger quantities of carrier were used in standardizing the carrier solutions so that an accuracy of between 0.5 and 1.0 % was obtained.

The fast fission correction measured was small ($\sim$2 %). The error in correcting for this effect is set at 0.2 %.

The loss of activity by fission recoil was kept to a minimum. An estimate maximum error for such a loss was 0.2 %.

By using very thin films the loss of activity by source-mount absorption was small. The error in the correction

factors used was never greater than 0.3 %. The error in the self-absorption correction depended on the value of the correction factor itself. For a factor greater than 0.95 an estimated error was set at 0.5 % while for a factor of about 0.75 the error was about 4 %.

(b) Statistical Errors

In all disintegration rate determinations more than 10^4 counts were recorded per measurement, giving a statistical error or standard deviation of 1 % or less. In practice, several sources were counted and an average value obtained from the results.

(c) External Errors

These are errors not associated with measurements made but which occur in calculations.

Errors in reported decay schemes and decay constants may greatly affect the measured fission yields. For this reason the yields are quoted together with the half-life of the nuclide for which the yield was measured. For simple decay schemes and accurately known half-lives the errors in calculating saturation activities are probably quite small.

The saturation factors calculated assume that irradiations were carried out in a constant neutron flux. In the operation of the nuclear reactor the pile power, which is proportional to the neutron flux, was observed to be constant

over all irradiation periods except one. In irradiation D several "shut-downs" occurred, i.e., short decay periods were intermixed with the irradiation. Saturation factors for this irradiation were calculated on an analog computer*. Saturation values calculated in this manner are accurate to one percent if the decay schemes involved are accurately known.

The thermal-neutron cross sections for cobalt (σ_c) and uranium 233 (σ_f) were obtained from the literature. Again it is necessary to quote the measured fission yields with reference to the value of σ_f / σ_c used. If a better value for this ratio is determined later, then the results of this work need only be corrected by the ratio of the new value to the old.

When several determinations were made for one nuclide, an average fission yield was calculated by "weighting" each individual value according to the reciprocal of its own experimental error, The error quoted for the average fission yield is a root mean square deviation.

---

* We are grateful to Dr. J.G. Bayly, Reactor Physics Branch, Atomic Energy of Canada Ltd., for performing these calculations.

DISCUSSION

The absolute fission yields measured radiochemically in this work for the thermal-neutron fission of U^{233} are presented in Table 32. Included in this table are values previously measured for the same nuclides by other investigators. Most of the yields for U^{233} fission measured earlier were determined relative to Ba^{140} which had a measured absolute yield of 6.0 % (137). In column 5 of Table 32 all yields which had been quoted relative to a value of 6.0 % for Ba^{140} have been renormalized to the more accurate value of 5.21 % obtained in this work. The normalized values compare favorably with those determined in this work. The yield for Sr^{90}, recently reported by Anikina and Ershler (136), was not normalized in this fashion since it represents an absolute measurement. However, the value was corrected by using a half-life of 27.7 years instead of 19.9 years. All yields listed above do not necessarily represent total chain yields. They merely refer to the cumulative yield for the nuclide given. No attempt was made to correct any of the values for delayed-neutron emission. No known corrections were required for neutron capture among the fission products themselves.

The same fast-fission correction has been applied to all values determined. This correction will certainly apply to values on or near the peaks of the yield-mass curve. The effect on the mass distribution of increasing the neutron

TABLE 32

ABSOLUTE THERMAL-NEUTRON FISSION YIELDS OF U^{233}

Nuclide	Half-life		Thermal-neutron fission yields (%)		
			Previously measured		Determined In this work
	Reported	Observed	Reported	Normalized*	
Br^{82}	36-h.	34.5-h.	---	---	0.000746 ±0.000017
Sr^{89}	50.4-d.	50-d.	6.5	5.64	5.56±0.15
Sr^{90}	27.7-y.	long	6.34	6.34	6.19±0.03
Y^{90}	64.3-h.	65-h.	---	---	(see Sr^{90})
Sr^{91}	9.7-h.	9.7-h.	---	---	4.82±0.25
Y^{91}	58.3-d.	59-d.	---	---	3.55±0.06
Zr^{95}	65-d.	65-d.	5.9	5.11	5.01±0.56
Nb^{95}	35-d.	35-d.	---	---	5.16±0.64
Ru^{103}	40-d.	40-d.	1.6	1.38	2.02±0.08
Rh^{105}	36.5-h.	36-h.	---	---	0.146±0.037
Ru^{106}	1.02-y.	1.0-y.	0.28	0.24	0.259±0.030
Ag^{111}	7.6-d.	7.6-d.	0.025	0.0217	0.0187 ±0.0002
Pd^{112}	21-h.	21-h.	0.016	0.0139	0.0125 ±0.0004
Ag^{112}	3.2-h.	3.2-h.	---	---	(see Pd^{112})
$Sb^{(126)}$	---	75-d.	---	---	0.53±0.14
Sb^{127}	93-h.	91-h.	---	---	0.59±0.08

TABLE 32 (Continued)

ABSOLUTE THERMAL-NEUTRON FISSION YIELDS OF U^{233}

Nuclide	Half-life		Thermal-neutron fission yields (%)		
			Previously measured		Determined
	Reported	Observed	Reported	Normalized*	In this work
I^{131}	8.05-d.	8.0-d.	2.7	2.34	2.84 0.20
Te^{132}	78-h.	77-h.	---	---	4.32 0.25
I^{132}	2.3-h.	2.4-h.	---	---	(see Te^{132})
I^{133}	20.9-h.	21-h.	---	---	3.37 0.29
Cs^{136}	13-d.	13-d.	0.12	0.104	0.0849 0.0022
Cs^{137}	27-y.	long	7.16	6.2	4.85 0.10
Cs^{137}	30-y.	long	---	---	5.39 0.11
Ba^{140}	12.8-d.	12.8-d.	6.0	5.21	5.21 0.27
Ce^{141}	33-d.	33-d.	---	---	5.30 0.10
Ce^{143}	33-h.	33-h.	---	---	6.99 0.35
Ce^{144}	285-d.	287-d.	4.1	3.55	3.69 0.18

* Normalized to Ba^{140} = 5.21 %.

1 Steinberg, et. al. (137)
2 Anikina, and Ershler (136)
3 Fleming, et. al. (140)
4 Glendenin, and Steinberg (31)

energy above the thermal region is to increase the probability of symmetric fission. For this reason the yields of nuclides residing in the trough of the mass distribution curve (Ag^{111} and Pd^{112}) are to be considered maximum values. However, the position of the samples inside the reactor was such that the epi-cadmium neutrons detected could not have possessed high energy. Recent investigations on the fission of U^{235} with energies as high as 9.5 ev show no significant change in trough yields from that produced by thermal neutrons (138) so that not too much change in yields of nuclides in the trough is to be expected.

There appears to be a discrepancy between the observed 4.82 % yield of Sr^{91} and the 3.55 % yield of Y^{91}. Reported yields (47) on the fission of U^{235} show that the yield of Y^{91} is greater than that of Sr^{91}, as would be expected if some Y^{91} were formed independently. The reverse effect, as observed in this work, is difficult to explain. In calculating the yield of Sr^{91} it was shown that no appreciable contribution to the total counting rate was attributable to the decay of the daughter activity Y^{91m}. This observation is confirmed by the low internal conversion coefficient given for this isomer (85). In addition, the β^- decay of Y^{91m} to Zr^{91} has been reported to be small ($\sim$0.02 %) and has been observed to be small in this work. Therefore, all Sr^{91} would be expected to decay through Y^{91}. Although only one measurement was made for the yield of Sr^{91}, two measurements which

agreed were performed on Y^{91}. As yet no satisfactory explanation exists for the discrepancy in the yields of mass 91. The value for the Y^{91} yield was much lower than expected for a fission product in this region. The same observation was made by Steinberg, et. al., (143) for masses 91 and 92.

The data in Table 32 were used as the basis for constructing a mass-distribution curve for the thermal-neutron fission of U^{233}. It was first necessary to correct the observed nuclide yields to obtain cumulative mass yields. This was done by determining the most probable nuclear charge, Z_p, of a particular mass number from curves given by Katcoff (20). A chain correction factor is then obtained for a value of the displacement from the most probable charge $(Z-Z_p)$. The total cumulative chain yield can be estimated from the product of the actual fission yield of a nuclide and its cumulative fractional chain yield. As an example of the procedure used, consider the nuclide $_{53}Te^{132}$. For the mass number of 132 the most probable nuclear charge, Z_p, is 51.3. The charge displacement, $Z-Z_p$, is + 0.7 and the corresponding fractional chain yield is 0.93. The yield measured for Te^{132} was 4.32 %. Consequently, the cumulative yield for mass 132 is 4.32/0.93 or 4.64 %.

The values measured in this work were used together with those compiled recently by Katcoff to establish the yield-mass curve given in Figure 59. Those yield values which were determined relative to a Ba^{140} yield of 6.0 %

Figure 59

Yield - Mass Distribution

in the Thermal - Neutron

Fission of U^{233}

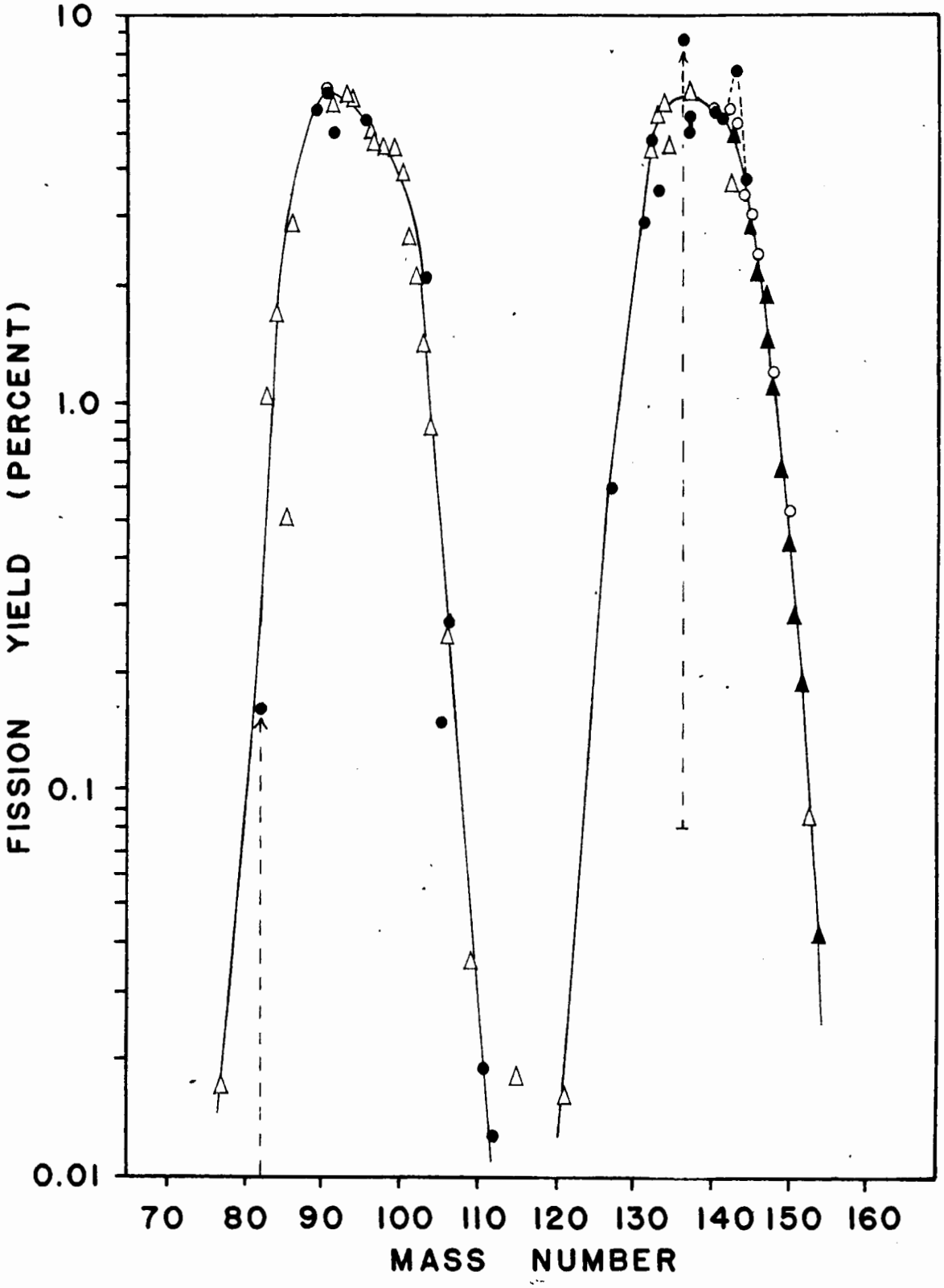
10
1.0
0.1
0.01
FISSION YIELD (PERCENT)
70
80
90
100
110
120
130
140
150
160
MASS NUMBER

were renormalized. The yields of Sr^{90} and the stable isotopes of cerium and neodymium were not normalized since they represent absolute yield measurements (136,56). The relative yields of Nd and Sm determined by Melaika,et. al., (139) have also been included. The Nd values were normalized to a yield value of 3.69 % for mass 144. The Nd values were then used to normalize their Sm yields.

The measured yields of Br^{82} and Cs^{136} have been corrected to chain yields as indicated by the broken arrows. Although the independent yields are accurate, the chain correction factors used may be in error. The Br^{82} yield lies on the smooth mass-distribution curve but the Cs^{136} yield is abnormally high. Fleming, et. al., (140) have reported a high yield ($\sim$8.9 %) for stable Xe^{136} in the thermal-neutron fission of U^{233}. Whether the observed fine structure at mass 136 is real or not cannot be decided on the basis of independent radiochemical yields unless a consistent and accurate charge distribution theory can be developed.

Two values for the yield of Cs^{137} have been included in Figure 59, one for each of the reported half-lives. The calculated yields appear to be too low to lie on the smooth mass-distribution curve. If no fine structure exists in this region, then a half-life for Cs^{137} calculated from yield measurements would be 34.4 years.

The low yield of I^{133} obtained in this work appeared real since I^{131} and Te^{132} yields calculated on the same

sample gave normal results. In the thermal-neutron fission of U^{235} a large peak was observed for mass 134 which was thought to be due to the preferential formation of 82 neutron fragments (37). The theories postulated to explain fine structure in fission also predict that a peak should be observed at mass 134 in the thermal-neutron fission of U^{233}. The presence of such a peak would require a corresponding decrease in yield of the neighboring mass numbers 133 or 135. A decrease in yield has been observed at mass 135 by Fleming, et. al., (140). However, they observed no increase in yield at mass 134 nor a decrease in yield at mass 133. It would appear as if a re-investigation of masses 134 and 135 should be performed radiochemically to determine the yields of the short-lived members of these chains.

The high yield at mass 143 was based on one measurement and has not been confirmed. The calculation of a Ce^{141} yield on the same samples gave a normal result.

The sum of the fission yields for each mass number was determined from Figure 59. The sum for the light-mass peak equalled 89 % while that for the heavy-mass peak equalled 94 %. Theoretically, the sum of both peaks should equal 200 %. The difference between the theoretical value and that determined from the mass-distribution curve may be due to several factors. The value of the Ba^{140} yield to which most of the previously measured values have been normalized, may be low. Such a probability is possible but seems unlikely

since the chain yield for mass 140 calculated in this work (5.48 %) agrees favorably with a recently measured absolute yield of 5.6 % for Ce^{140} (56). A more likely possibility is that enhanced yields at certain mass numbers have not yet been measured. A comparison of yield-mass curves for the thermal-neutron fission of U^{233} and U^{235} shows that the former is displaced about one mass unit lower in both the light and heavy mass peaks.

On the basis of its calculated fission yield the observed 75-day antimony activity was assigned the mass number 126. The formation of Sb^{126} as a fission product is to be expected since both Sb^{125} and Sb^{127} have been identified in the products of neutron fission. No reliable data have yet been published on the identification of Sb^{126} (141,142). A confirmation of the mass assignment may perhaps be made by studying the decay characteristics of Sb^{126} produced by the reaction $Te^{126}(n,p)Sb^{126}$ using enriched isotopes.

The yields measured in this work involve a knowledge of the thermal-neutron fission cross section of U^{233} and the thermal-neutron capture cross section of Co^{59}. An error in either or both values used would produce an error in an observed fission yield. The resulting error is such that a decrease in the fission cross section (σ_f) or an increase in the capture cross section (σ_c) of uranium and cobalt respectively tends to decrease the observed fission yield. Reported absolute yields on Sr^{90} and Ce^{140} were not dependent

on these cross section values and agreed with the results of this work. Therefore, the value of σ_f/σ_c used appears to be correct.

The use of 4π-proportional counting techniques was shown to be a very sensitive method for accurate fission yield measurements of most radioactive nuclides. With these the accuracy is dependent mainly on chemical analysis of the element. Nuclides which undergo β emission or β - γ emission to a ground state can be accurately measured in this fashion. However, a 4π-proportional counter has been observed to be sensitive to the emission of conversion electrons. Those nuclides which are directly or indirectly involved in isomeric transitions can thus be determined less accurately due to lack of information on the transition characteristics.

SUMMARY

The absolute fission yields of twenty-one nuclides formed in the thermal-neutron fission of U^{233} have been measured radiochemically. Disintegration rates and half-lives were determined very accurately by means of 4π-proportional counting techniques. The identity of each nuclide emitting γ radiation was confirmed by γ-ray scintillation spectrometry.

Irradiations were performed in the NRX reactor at Chalk River, Ontario. Neutron fluxes of about 5×10^{12} neutrons per $cm.^2$ per second were accurately measured by means of a Co^{59} flux monitor. The rate at which the uranium sample underwent fission was determined in terms of the thermal-neutron capture cross section of Co^{59} (36.3 barns) and the thermal-neutron fission cross section of U^{233} (524 barns). Corrections were made for fissions caused by epi-cadmium neutrons.

All relative yields had been previously normalized to one absolute yield measurement which possessed large experimental errors. Absolute yield values have been measured in this work for nuclides at various positions along the mass-distribution curve. The results obtained will serve as the basis for the normalization of any future relative yields.

Abnormal yields were observed at mass numbers 91, 133, 136 and 143. Further studies on nuclides of adjacent mass

numbers would complete a description of fine structure in fission.

REFERENCES

1. Tsien, S. T., Ho, Z. W., Chastel, R., and Vigneron, L., J. phys. radium, 8, 165,200 (1947).

2. Hahn, O., and Strassmann, F., Naturwiss. 27, 11 (1939).

3. Dessauer, G., and Hafner, E. M., Phys. Rev. 59, 840 (1941).

4. Gant, D. H., Nature, 144, 707 (1939).

5. Fermi, E., and Segre, E., Phys. Rev. 59, 680 (1941).

6. Brown, F., Price, M. R., and Willis, H. H., J. Inorg. Nuc. Chem. 3, 9 (1956).

7. Haxby, R. O., Shoupp, W. E., Stephens, W. E., and Wells, W. H., Phys. Rev. 59, 57 (1941).

8. Al-Salam, S. G., Phys. Rev. 84, 254 (1951).

9. Perfilov, N. A., and Ivanova, N. S., Soviet Physics, J. E. T. P. 2, 433 (1956).

10. Perlman, I., Goeckermann, R. H., Templeton, D. H., and Howland, J. J., Phys. Rev. 72, 352 (1947).

11. Flerov, G. N., and Petrzhak, K. A., Acad. Sci. U. S. S. R. 28, 500 (1940). J. Gen. Phys. 3, 275 (1940).

12. Segre, E., Phys. Rev. 86, 21 (1952).

13. Turner, L. A., Rev. Mod. Phys. 12, 1 (1940).

14. Whitehouse, W. J., " Progress in Nuclear Physics ", Vol. II, p. 120 (1952); Pergamon Press, London.

15. Coryell, C. D., and Sugarman, N., (Editors), " Radiochemical Studies : The Fission Products ". National Nuclear Energy Series, Div. IV, 9, McGraw-Hill Co., Inc., New York (1951).

16. Spence, R. W., and Ford, G. P., Ann. Rev. Nuc. Sci. 2, 399 (1953).

17. Glendenin, L. E., and Steinberg, E. P., Ann. Rev. Nuc. Sci. 4, 69 (1954).

18. Seaborg, G. T., Gofman, J. W., and Stoughton, R. W., Phys. Rev. 71, 378 (1947).

19. Jentschke, W., Zeit. f. Physik, 120, 165 (1943).

20. Katcoff, S., Low-Energy Induced Fission, " Handbook of Nuclear Engineering ", Addison-Wesly, Inc., Cambridge, Mass. (1956).

21. Glendenin, L. E., Technical Report No. 35, Laboratory for Nuclear Research, Massachusetts Institute of Technology (1949).

22. Glendenin, L. E., Coryell, C. D., and Edwards, R. R., Reference 15, N. N. E. S., paper 52.

23. Pappas, A. C., Technical Report No. 63, Laboratory for Nuclear Research, Massachusetts Institute of Technology (1953).

24. Wilson, R. R., Phys. Rev. 72, 189 (1947).

25. Coryell, C. D., Brighsten, R. A., and Pappas, A. C., Phys. Rev. 85, 732 (1952).

26. Coryell, C. D., Ann. Rev. Nuc. Sci. 2, 305 (1953).

27. Kennett, T. J., and Thode, H. G., Phys. Rev. 103, 323 (1956).

28. Cameron, A. G. W., Private Communication, as given in Reference 29.

29. Grummitt, W. E., and Milton, G. M., J. Inorg. Nuc. Chem. 5, 93 (1957).

30. Coryell, C. D., and Sugarman, N., Reference 15, N. N. E. S., Appendix B.

31. Glendenin, L. E., and Steinberg, E. P., International Conference on the Peaceful Uses of Atomic Energy, Vol. 7, p. 3, United Nations, New York (1956).

32. Keepin, G. R., and Wimmett, T. F., International Conference on the Peaceful Uses of Atomic Energy, Vol. 4, p. 162, United Nations, New York (1956).

33. Snell, A. H., Nedzel, V. A., Ibser, H. W., Sevinger, J. S., Wilkinson, R. G., and Sampson, M. B., Phys. Rev. 72, 541 (1947).

34. Mayer, M. G., and Jensen, J. H. D., " Elementary Theory of Nuclear Shell Structure ", John Wiley and Sons, New York (1955).

35. Turkevich, A., and Kohman, T. P., American Report CN-1044, Nov. 1943, Quoted in Reference 15, N. N. E. S., p. 539.

36. Coryell, C. D., American Report CC-1112, Dec., 1943, Quoted in Reference 15, N. N. E. S., p. 539.

37. Thode, H. G., and Graham, R. L., Can. J. Res. 25A, 1 (1947).

38. Stanley, C. W., and Katcoff, S., J. Chem. Phys. 17, 653 (1949).

39. Wiles, D. R., Ph. D. Thesis, Massachusetts Institute of Technology, Cambridge, Massachusetts, 1953.

40. Flammersfeld, A., Jensen, P., and Gentner, W., Zeit. f. Physik, 120, 450 (1943).

41. Deutsch, M., and Ramsey, M., Los Alamos Scientific Report, MDDC-945 (January 1946).

42. Freedman, M. S., and Steinberg, E. P., Reference 15, N. N. E. S., paper 200.

43. Engelkemeir, D. W., Novey, T. B., and Schrover, D. S., Reference 15, N. N. E. S., paper 205.

44. Anderson, H. L., Fermi, E., and Grosse, A. V., Phys. Rev. 59, 52 (1941).

45. Yaffe, L., Thode, H. G., Merritt, W. F., Hawkings, R. C., Brown, F. and Bartholomew, R. M., Can. J. Chem. 32, 1017 (1954).

46. Inghram, M. G., Ann. Rev. Nuc. Sci. 4, 81 (1954).

47. Baerg, A. P., and Bartholomew, R. M., Can. J. Chem. 35, 980 (1957).

48. Pate, B. D., and Yaffe, L., Can. J. Chem. 33, 15 (1955).

49. Pate, B. D., and Yaffe, L., Can. J. Chem. 33, 610 (1955).

50. Pate, B. D., and Yaffe, L., Can. J. Chem. 33, 929 (1955).

51. Pate, B. D., and Yaffe, L., Can. J. Chem. 33, 1656 (1955).

52. Pate, B. D., and Yaffe, L., Can. J. Chem. 34, 265 (1956).

53. Pate, B. D., Ph. D. Thesis, McGill University, Montreal (1955).

54. Flemimg, W. F., Tomlinson, R. H., and Thode, H. G., Can. J. Phys. 32, 522 (1954).

55. Tomlinson, W. F., Proceedings of the Symposium on the Physics of Fission Held at Chalk River, Ontario. CRP-642-A, paper C3, p. 262 (1956).

56. Kukavadze, G. M., Anikina, M. P., Goldin, L. L. and Ershler, B. V., Conference of the Academy of Sciences of the S. S. S. R. on Peaceful Uses of Atomic Energy, p. 125 (1955).

57. Yaffe, L., Hawkings, R. C., Merritt, W. F., and Craven, J. A., Phys. Rev. 82, 553 (1951).

58. Carter, R. S., Palevsky, H., Myers, V. W., and Hughes, D. J., Phys. Rev. 92, 716 (1953).

59. Fishman, J. B., And Yaffe, L., Private Communication.

60. Sugarman, N., J. Chem. Phys. 15, 544 (1947).

61. Rutherford, E., Chadwick, J., and Ellis, C. D., Theory of Successive Transformations - Radiations from Radioactive Substances, University Press, Cambridge, 1930.

62. Deutsch, M., Elliott, L. G., and Roberts, A., Phys. Rev. 68, 193 (1945).

63. Geiger, K. W., Phys. Rev. 105, 1539 (1957).

64. Charpie, R. A., Horowitz, J., Hughes, D. J., and Littler, D. J., (Editors), " Progress in Nuclear Energy " - Physics and Mathematics, Volume 1.,p. 1.

65. Glendenin, L. E., Edwards, R. R., and Gest, H., Reference 15, N. N. E. S., paper 232.

66. Feldman, M. E., Glendenin, L. E., and Edwards, R. R., Reference 15, N. N. E. S., paper 62.

67. Dubey, V. S., Mandeville, C. E., and Rothman, M. A., Phys. Rev. 103, 1430 (1956).

68. Benczer, N., and Wu, C. S., Bul. Am. Phys. Soc. 1, No. 1, 41, K1 (1956).

69. Glendenin, L. E., Reference 15, N. N. E. S., paper 236.

70. Herrmann, G. V., and Strassmann, F., Z. Naturf. 10a, 146 (1955).

71. Nottorf, R. W., Reference 15, N. N. E. S., paper 77.

72. Wiles, D. M., and Tomlinson, R. H., Can. J. Phys. 33, 133 (1955).

73. Bisi, A., Terrani, L., and Zappa, L., Nuovo Cim. 2, 11297 (1955).

74. Nainan, T. D., Deware, H. G., and Mukerji, A., Proc. Indian Acad. Sci. 44A, 111 (1956).

75. Ames, D. P., Bunker, M. E., Langer, L. M., and Sorenson, B. M., Phys. Rev. 91, 68 (1953).

76. Ballou, N. E., Reference 15, N. N. E. S., paper 292.

77. Herrmann, G. V., and Strassmann, F., Z. Naturf. 11a, 946 (1956).

78. Johnson, O. E., Johnson, R. G., and Langer, L. M., Phys. Rev. 98, 1517 (1955).

79. Kahn, B., and Lyon, W. S., Phys. Rev. 98, 58 (1955).

80. Hume, N. D., Reference 15, N. N. E. S., paper 245.

81. Moore, F. L., Anal. Chem. 28, 997 (1956).

82. Brady, E. L., Engelkemeir, D. W., and Steinberg, E. P., Reference 15, N. N. E. S., paper 85.

83. Drabkin, G. M., Orlov, V. I., and Rusinov, L. I., Izvest. Akad. Nauk. Ser. Fiz. S. S. S. R. 19, 324 (1955), Columbia Tech. Translation, p. 294.

84. Glendenin, L. E., Reference 15, N. N. E. S., paper 253.

85. Goldhaber, M., and Sunyar, A. W.,
Phys. Rev. 83, 906 (1951).

86. Fine, S., and Hendee, C. F.,
Nucleonics, 13, March, 36, (1955).

87. Glendenin, L. E., Reference 15, N. N. E. S., paper 260.

88. Saraf, B., Phys. Rev. 97, 715 (1955).
J. Franklin Inst. 258, 517A (1954).

89. Merritt, W. F., Campion, P. J., and Hawkings, R. C.,
Can. J. Phys. 35, 16 (1957).

90. Agnew, H. M., Phys. Rev. 77, 655 (1950).

91. Avignon, P., Michalowicz, A., and Bouchez, R.,
J. phys. radium 16, 404 (1955).

92. Peacock, W. L., Phys. Rev. 72, 1049 (1947).

93. Ballou, N. E., Reference 15, N. N. E. S., paper 263.

94. Levi, C., and Papineau, L.,
Compt. rend. 238, 1407 (1954).

95. Glendenin, L. E., Reference 15, N. N. E. S., paper 267.

96. Steinberg, E. P., and Glendenin, L. E.,
Reference 15, N. N. E. S., paper 123.

97. Johansson, S., Phys. Rev. 79, 896 (1950).

98. Pool, M. L., Phys. Rev. 53, 116 (1938).

99. Nussbaum, R. H., Physica, 19, 385 (1953).

100. Seiler, J. A., Reference 15, N. N. E. S., paper 119.

101. Glendenin, L. E., Reference 15, N. N. E. S., paper 265.

102. Boldridge, W. F., and Hume, D. N.,
Reference 15, N. N. E. S., paper 272.

103. Bosch, H., and Munczek, H., Phys. Rev. 106, 983 (1957).

104. Day, M. C., and Voigt, A. F.,
Phys. Rev. 101, 1784 (1956).

105. Campbell, G. W., Sleight, N. R., and Sullivan, W. H.,
Reference 15, N. N. E. S., paper 132.

106. Grummitt, W. E., and Wilkinson, G.,
Nature, 158, 163 (1946).

107. Glendenin, L. E., Reference 15, N. N. E. S., paper 274.

108. Knight, J. D., Mize, J. P., Starner, J. W., and
Barnes, J. W., Phys. Rev. 102, 1592 (1956).

109. Pappas, A. C., and Coryell, C. D.,
Phys. Rev. 81, 329 (1951).

110. Abelson, P. H., Phys. Rev. 56, 1 (1939).

111. Glendenin, L. E., and Metcalf, R. R.,
Reference 15, N. N. E. S., paper 278.

112. Bartholomew, R. M., Brown, F., Hawkings, R. C., and
Yaffe, L., Can. J. Chem. 31, 120 (1953).

113. Emery, E. W., Phys. Rev. 83, 679 (1951).

114. Wahl, A. C., Phys. Rev. 99, 730 (1955).

115. Finston, H. L., and Bernstein, W.,
Phys. Rev. 96, 71 (1954).

116. Brosi, A. R., and Gross, P. M.,
O. R. N. L. Report No. 499 (1947).

117. Glendenin, L. E., and Nelson, C. M.,
Reference 15, N. N. E. S., paper 283.

118. Olsen, J. L., and O'Kelly, G. D.,
Phys. Rev. 95, 1539 (1954).

119. Turkevich, A., Steinberg, E. P., Finkle, B., and
Sugarman, N., Reference 15, N. N. E. S., paper 153.

120. Yaffe, L., Private Communication.

121. Brown, F., Hall, G. R., and Walters, A. J.,
J. Inorg. Nuclear Chem. 1, 241 (1955).

122. Wiles, D. M., and Tomlinson, R. H.,
Phys. Rev. 99, 188 (1955).

123. Engelkemeir, D. W., Freedman, M. S., Glendenin, L. E.,
and Metcalf, R. P., Reference 15, N. N. E. S.,
paper 163.

124. Grummitt, W. E., Gueron, J., Wilkinson, G., and Yaffe, L., Can. J. Res. B25, 357 (1947).

125. Beach, L. A., Peacock, C. L., and Wilkinson, G., Phys. Rev. 76, 1624 (1949).

126. Peacock, C. L., Quinn, J. F., and Oser, A. W., Phys. Rev. 94, 372 (1954).

127. Hughes, D. J., and Harvey, J. A., B. N. L. Report 325 (1955).

128. Katcoff, S., Reference 15, N. N. E. S., paper 220.

129. Rubinson, W., J. Chem. Phys. 17, 542 (1949).

130. Glendenin, L. E., Flynn, K. F., Buchanan, R. F., and Steinberg, E. P., Anal. Chem. 27, 59 (1955).

131. Sugarman, N., Ballou, N. E., Engelkemeir, D. W., and Burgus, W. H., Reference 15, N. N. E. S. , paper 175.

132. Jones, J. T., and Jensen, E. N., Phys. Rev. 97, 1031 (1955).

133. Martin, D. W., Brice, M. K., Cork, J. M., and Burson, S. B., Phys. Rev. 101, 182 (1956).

134. Pullman, I., and Axel, P., Phys. Rev. 102, 1366 (1956).

135. Kukavadze, G. M., Goldin, L. L., Anikina, M. P., and Ershler, B. V., International Conference on the Peaceful Uses of Atomic Energy, Vol. 4, p. 230, United Nations, New York (1956).

136. Anikina, M. P., and Ershler, B. V., J. Nuclear Energy, 6, 169 (1957).

137. Steinberg, E. P., Seiler, J. A., Goldstein, A., and Dudley, A., Report MDDC-1632 (1948).

138. Nasuhoglu, R., Raboy, S., Ringo, G. R., Glendenin, L. E., and Steinberg, E. P., Phys. Rev. 108, 1522 (1957).

139. Melaika, E. A., Parker, M. J., Petruska, J. A., and Tomlinson, R. H., Can. J. Chem. 33, 830 (1955).

140. Fleming, W., Tomlinson, R. H., and Thode, H. G., Can. J. Phys. 32, 522 (1954).

141. De Fraenz, I. G., Rodriguez, J., and Carminatti, H., International Conference on the Peaceful Uses of Atomic Energy, Vol. 7, p. 180, United Nations, New York (1956).

142. Barnes, J. W., and Freedman, A. J., Phys. Rev. 84, 365 (1951).

143. Steinberg, E. P., Glendenin, L. E., Inghram, M. G., and Hayden, R. J., Phys. Rev. 95, 867 (1954).